

Characterization of the \tilde{X}^1A' state of isocyanic acid

Allan L. L. East, Christopher S. Johnson, and Wesley D. Allen
Department of Chemistry, Stanford University, Stanford, California 94305

(Received 6 July 1992; accepted 24 September 1992)

Characteristics of the ground electronic state of HNCO have been investigated theoretically in a series of eight *ab initio* analyses involving qualitative features of the electronic structure, the barrier to linearity, the $\text{NH}(^3\Sigma^-) + \text{CO}$ fragmentation energy, the H–NCO bond dissociation energy, heats of formation of isomers of HNCO, fundamental vibrational frequencies and anharmonic force fields, the rovibrational spectrum of DNCO, and the precise R_e structure of isocyanic acid. Sundry state-of-the-art electronic structure methods were employed in the study, including restricted and unrestricted Hartree–Fock (RHF and UHF), complete-active-space self-consistent-field (CASSCF), configuration interaction singles and doubles (CISD), Møller–Plesset perturbation theory through fourth and occasionally fifth order (MP2–MP5), coupled-cluster singles and doubles (CCSD), and CCSD augmented by a perturbative contribution from connected triple excitations [CCSD(T)]. The one-particle basis sets ranged in quality from (9s5p1d/4s2p1d) to (13s8p3d2f/6s5p3d2f) on the heavy atoms and from (4s1p/2s1p) to (6s2p1d/4s2p1d) on hydrogen. Several revisions of thermochemical data are proposed, in particular, a larger barrier to linearity of 5.7(3) kcal mol⁻¹, an enhanced bond energy of 85.4(10) kcal mol⁻¹ for $D_0(\text{NH–CO})$, and more reliable relative energies for the isomers of HNCO, viz., $\gamma_e(\text{HOCN})=25.5(10)$, $\gamma_e(\text{HCNO})=70(2)$, and $\gamma_e(\text{HONC})=84.5(15)$ kcal mol⁻¹. In addition, the experimental value $D_0(\text{H–NCO})=113.0(2)$ kcal mol⁻¹ is confirmed. These results lead to several new proposals for heats of formation ($\Delta H_{f,0}^\circ$, kcal mol⁻¹): HNCO (–26.1), HOCN (–0.7), HCNO (+43.0), HONC (+57.6), and NCO (+35.3). A complete quartic force field has been constructed for HNCO by combining RHF third- and fourth-derivative predictions with CCSD quadratic force constants subjected to the scaled quantum mechanical (SQM) optimization scheme. This force field yields a set of ω_i and χ_{ij} vibrational constants which gives the following fundamental frequencies (with total anharmonicities in parentheses): $\nu_1=3534(-186)$, $\nu_2=2268(-45)$, $\nu_3=1330(-9)$, $\nu_4=778(-50)$, $\nu_5=576(+9)$, and $\nu_6=657(+21)$ cm⁻¹, thus reproducing the observed band origins to 4 cm⁻¹ or less. For DNCO the theoretical force field reveals misassignments of the low-frequency bending vibrations and predicts $\nu_4(a')=727$, $\nu_5(a')=458$, and $\nu_6(a'')=633$ cm⁻¹. Finally, the theoretical vibration–rotation interaction constants (α_i) for five isotopic species of HNCO have been used in conjunction with empirical rotational constants and the Kraitchman equations to determine $r_e(\text{N–H})=1.0030(20)$ Å, $r_e(\text{N–C})=1.2145(6)$ Å, $r_e(\text{C–O})=1.1634(4)$ Å, $\theta_e(\text{H–N–C})=123.34(20)^\circ$, and $\theta_e(\text{N–C–O})=172.22(20)^\circ$.

I. INTRODUCTION

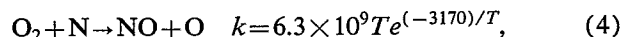
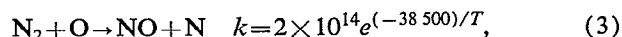
A. Combustion chemistry of HNCO

In the summer of 1970 a study of critical environmental problems was convened in which the effect of supersonic transport exhausts on the chemistry of the stratosphere was considered for the first time.¹ Preliminary results suggested that nitric oxide emissions were innocuous, posing even less of a threat to the stratospheric ozone layer than H₂O. In a 1971 article, Johnston² dispelled this conclusion by showing that “the projected increase in stratospheric oxides of nitrogen [due to SST exhausts] could reduce the ozone shield by about a factor of 2, thus permitting the harsh radiation below 300 nanometers to permeate the lower atmosphere.” Johnston emphasized the following catalytic cycle in his analysis:



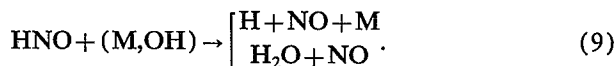
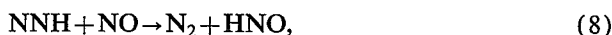
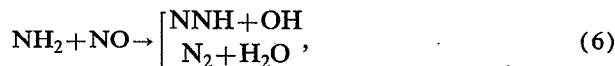
thus heightening awareness of the effects of NO_x pollutants in the stratosphere. Indeed, as evidence for the deleterious role of elevated atmospheric NO_x concentrations in photochemical smog formation, ozone depletion, and acid rain production has burgeoned, stringent emission standards for these combustion by-products have been established.^{3–5}

The literature on NO_x formation in combustion devices and on control of NO_x emissions in exhaust streams is vast and can only be given a cursory review here. The main source of NO species in combustion effluents is generally considered to be the Zeldovich mechanism,^{5,6}



whose high sensitivity to temperature is apparent from the observed values of the rate coefficients, which are given in cm³ mol⁻¹ s⁻¹. Accordingly, a simple technique for preventing NO_x formation is the addition of water vapor to

the combustion system, which acts not only to reduce the combustion temperature and but also to scavenge O atoms.⁵ An alternate technique for reducing NO_x emissions involves the injection of NH₃ into exhaust streams,⁷ which is effective in removing NO_x by-products after their formation under conditions within a narrow temperature range of $T=1250\pm 75$ K.⁸ It has been proposed that the rudiments of the NO reduction sequence in this thermal De-NO_x process are^{9,10}



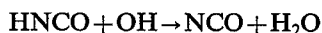
However, recent theoretical work by Walch and co-workers¹¹⁻¹³ has confirmed earlier predictions that NNH is not a stable intermediate, thus necessitating some revision of the thermal De-NO_x mechanism.

In 1986 Perry and Siebers¹⁴ introduced the RAPRENO_x (RAPid REDuction of Nitrogen Oxides) process, which involves the removal of NO_x combustion products by the injection of cyanuric acid, (HOCN)₃, into exhaust streams. In the initial study of the RAPRENO_x process, the removal of NO in a stainless steel flow reactor at relatively low temperatures between 600 and 700 K was reported to be almost complete, although it was later discovered¹⁵⁻¹⁸ that the metal surface of the apparatus was responsible for initiation of the observed NO reduction. Nonetheless, in more recent experiments involving quartz flow reactors,^{19,20} temperature windows for NO removal were established within the 1000-1400 K region, the precise location depending on the composition of the gas stream. In order to understand these observations, the RAPRENO_x reaction scheme and its kinetics have been pursued via shock-tube experiments, chemical kinetic modeling, and thermal rate studies.^{10,21,22} It is well known that above 600 K cyanuric acid sublimates and decomposes into isocyanic acid^{10,23}

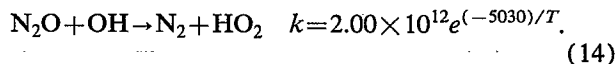
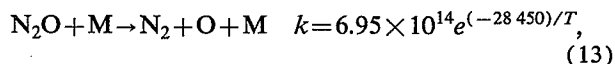
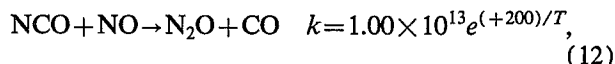


Several recent studies have focused on the ensuing elementary reactions of HNCO with prevalent free radicals such as O,^{24,25} H,²⁶ and OH;²⁴ other recent investigations have probed the subsequent thermal pyrolysis reactions of HNCO.^{27,28}

The most recent computer simulation of the RAPRENO_x process by Miller and Bowman¹⁰ involved a chemical kinetic model comprised of 105 elementary reactions, which indicated that several reactions of HNCO with O, H, and OH are important and that the product channels for NO reduction are not unique. Nevertheless, when CO, H₂O, and O₂ are present initially, the dominant channel appears to consist of the following steps:



$$k = 1.99 \times 10^{12} e^{(-2790)/T}, \quad (11)$$



At higher temperatures a pair of inhibiting reactions becomes effective, giving rise to the observed temperature boundary,



The initiation steps proposed by Perry and Siebers,¹⁴ namely, HNCO → NH + CO and NH + NO → N₂O + H, appear to be less significant. Further modifications of the kinetic model of the RAPRENO_x process are likely, as exemplified by a very recent suggestion that the bimolecular reaction 2 HNCO → CO₂ + HNCNH be included to account for observed reaction rates and high yields of CO₂.²⁸

B. Thermochemistry and spectroscopy of HNCO

Much of the recent attention afforded the HNCO molecule is a consequence of its central role in the RAPRENO_x process, but the thermochemistry and spectroscopy of isocyanic acid (and related isomers) is a rich topic of study with an extensive history. Of the four isomers with the molecular formula CHNO, isocyanic acid is the most stable thermodynamically, but it must be stored as a liquid below -30 °C to prevent polymerization.²³ Fulminic acid (HCNO) is liberated upon acidification of aqueous sodium fulminate with dilute H₂SO₄ and can be condensed as colorless crystals in a liquid nitrogen trap;^{29,30} sublimation below -20 °C at reduced pressures yields gaseous HCNO, which has been characterized by infrared,²⁹⁻³¹ far infrared,³² and microwave spectroscopy.³³⁻³⁵ Cyanic acid (HOCN) has only been produced in matrix-isolation experiments via the uv irradiation of either isocyanic or fulminic acid; no gas-phase synthesis is currently known.³⁶ Isofulminic acid (HONC) is the least stable of the four CHNO isomers, and its isolation in an argon matrix at 13 K was not achieved until 1988.³⁶

The relative energies of the isomers of HNCO have not been determined experimentally, but several *ab initio* studies have addressed this issue. In 1977 Poppinger, Radom, and Pople³⁷ performed an extensive investigation of local minima and transition states on the CHNO surface and found HOCN, HCNO, and HONC to lie 21.1, 79.7, and 81.3 kcal mol⁻¹, respectively, above HNCO at the 6-31G* RHF//4-31G RHF level. Earlier that year McLean and co-workers³⁸ had reported DZ SCF results in which HONC was predicted to be lower in energy than HCNO. In 1989 Teles *et al.*³⁶ reported the relative energies of HOCN, HCNO, and HONC to be 21.2, 73.6, and 81.3 kcal mol⁻¹, respectively, at the 6-31G** CCD level,

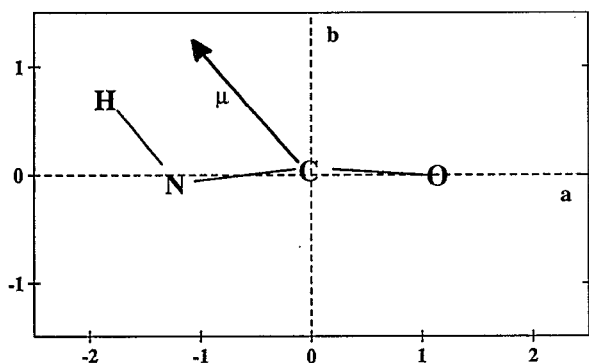


FIG. 1. A plot of the equilibrium nuclear positions for HNCO in the center-of-mass, principal-axis coordinate system. The direction vector for the molecular dipole moment is also depicted. The Cartesian position vectors (a,b) in Å are H $(-1.8607, 0.6975)$, N $(-1.2301, -0.0825)$, C $(-0.0214, 0.0397)$, O $(1.1412, -0.0057)$.

whereas Yokoyama, Takane, and Fueno³⁹ have very recently determined values of 22.9, 79.1, and 91.3 kcal mol⁻¹ with 6-31G** MRD-CI wave functions. Substantial uncertainties in the heats of formation of fulminic and isofulminic acid are apparent from the variations in the predicted relative energies of these compounds.

The fragmentation energies of HNCO have been the subject of several experimental and theoretical investigations,^{37,39-45} although certain thermochemical issues have not yet been resolved. In 1970 Okabe⁴¹ photolyzed HNCO at various wavelengths in the vacuum ultraviolet and observed thresholds for emission from the systems $\text{NCO}(\tilde{A}^2\Sigma^+ \rightarrow \tilde{X}^2\Pi)$, $\text{NH}(\tilde{c}^1\Pi \rightarrow \tilde{a}^1\Delta)$, and $\text{NH}(\tilde{A}^3\Pi \rightarrow \tilde{X}^3\Sigma^-)$, subsequently arriving at dissociation energies for the fragmentation of isocyanic acid to the ground electronic states of H+NCO and NH+CO. Specifically, $D_0(\text{H-NCO})=113.0\pm 0.2$ kcal mol⁻¹ and $D_0(\text{HN-CO})=78\pm 2$ kcal mol⁻¹ were ascertained. In 1986 Spiglanin, Perry, and Chandler⁴⁰ performed photodissociation studies of HNCO in which nascent NH($\tilde{a}^1\Delta$) and NCO($\tilde{X}^2\Pi$) products were detected via laser induced fluorescence. A threshold energy of 118.7 kcal mol⁻¹ was deduced for production of NH($\tilde{a}^1\Delta$), from which revised values of $D_0(\text{HN-CO})=82.9$ kcal mol⁻¹ and $\Delta H_{f,298}^\circ(\text{HNCO})=-24.9_{-2.8}^{+0.7}$ kcal mol⁻¹ were derived. The branching ratio for NCO/NH production from photolysis at 193 nm was found to be significant but within an upper limit of 0.10.

The infrared absorption spectrum of isocyanic acid exhibits many challenging features—to quote Yamada, Winnewisser, and Johns,⁴⁶ “fascinating anomalies [are] observed almost everywhere in the spectrum.” Although the equilibrium H-N-C angle in isocyanic acid is near 123° (Fig. 1), the barrier to linearity is only ca. 6 kcal mol⁻¹ (*vide infra*). The broad, flat H-N-C bending potential gives rise to quasilinear behavior in the low-frequency bending vibrations and engenders sizeable Coriolis coupling and centrifugal distortion effects. Numerous mathematical forms for the rovibrational Hamiltonian of HNCO have been invoked to account for these phenomena.⁴⁶⁻⁵⁶

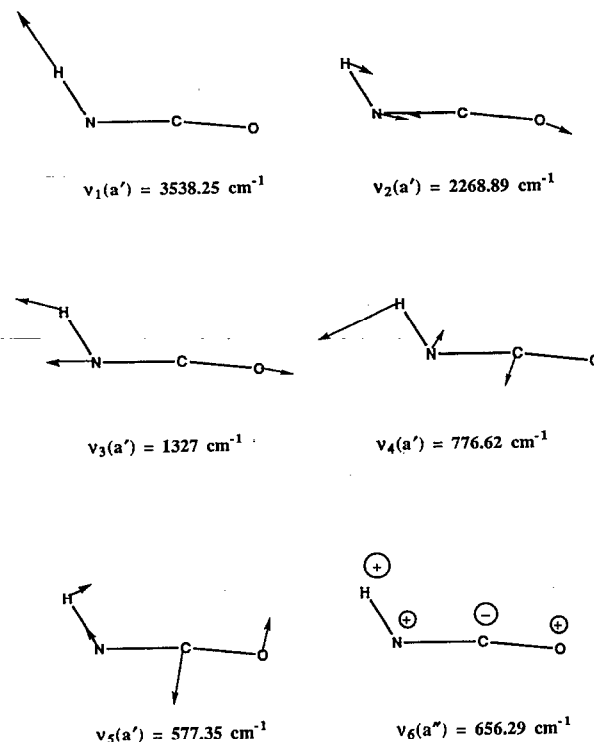


FIG. 2. A depiction of the normal modes of vibration of HNCO. The arrows define the directions of positive displacement of the normal modes, as assumed in the anharmonic force field tabulations in Tables XI and XII.

The large Coriolis coupling among the three fundamental bending vibrations in the 500–800 cm⁻¹ region (Fig. 2) contributed to a considerable debate over the original assignments made by Herzberg and Reid in 1950.⁵⁷ This issue was not resolved definitively until the work of Yamada⁵⁴ in 1977 and Steiner and co-workers⁵¹ in 1979, the latter study involving the observation and analysis of over 1200 rovibrational transitions in the infrared spectrum between 465 and 1100 cm⁻¹. The currently accepted values for the band origins of the bending fundamentals are $\nu_4(a')=776.623$ cm⁻¹, $\nu_5(a')=577.346$ cm⁻¹, and $\nu_6(a'')=656.287$ cm⁻¹. Difficulties attend the reproduction of these results via *ab initio* techniques, as evidenced by the 2.2% and 5.9% underestimations of ν_5 and ν_6 by the 6-31G** MP2 method,³⁶ an uncharacteristic occurrence at this level of theory. In fact, early predictions obtained at the RHF level with a small basis set supported an incorrect assignment of the low-frequency vibrations,⁵⁸ and reliable data for the force field of isocyanic acid are still meager. Moreover, confusion remains as to the location of the bending fundamentals of the deuterated isotopomer of HNCO. The stretching fundamentals of HNCO and its isotopomers have generated less controversy, and discussion of these assignments is reserved for Secs. III F and III G below.

The detection of interstellar isocyanic acid in the galactic radiation source Sgr B2⁵⁹⁻⁶² stimulated renewed interest in the microwave and millimeter wave spectra of HNCO. The pure rotational spectra of the HNCO mole-

cule are characteristic of a prolate near-symmetric top with a Wang asymmetry parameter of only -8.9×10^{-5} .⁵¹ In 1975 Hocking *et al.*⁶² determined high-precision values for the effective moments of inertia of six isotopomers and obtained an R_e structure for isocyanic acid by the method of Kraitchman⁶³ and Costain.⁶⁴ The quasilinearity of HNCO leads to a large rotational constant, $A_0 \approx 30 \text{ cm}^{-1}$, which ineffectuates the separation of molecular vibration and rotation in zeroth order and adds complexity to the extraction of geometrical structures from I_a^0 , I_b^0 , and I_c^0 values. In 1980 Yamada⁵² was able to circumvent such problems in determining an improved R_e structure of HNCO. No precise experimental R_e structure is known, although Fusina and Mills⁵⁵ reported R_z parameters for HNCO in 1981.

The goal of our current study is to obtain an exhaustive *ab initio* characterization of the ground and excited electronic states of isocyanic acid in view of the importance of this molecule to combustion chemistry and other areas of investigation. This paper focuses on the key issues highlighted above pertaining to the ground-state surface of HNCO, viz. the barrier to linearity, the HN-CO and H-NCO fragmentation energies, heats of formation of HNCO and related isomers, the anharmonic force field, fundamental vibrational frequencies, the equilibrium molecular structure, and vibration-rotation interaction. Eight theoretical analyses of these topics are presented, which in large part can be assimilated independently. The photochemistry and excited electronic states of HNCO are also topics of prime importance, as numerous experiments have probed the ultraviolet spectrum,^{65,66} flash photolysis reactions,^{44,67-72} nascent product state energy distributions,^{40,73,74} and dissociation and reaction dynamics of this system.^{41,43,45,75} The photochemistry of HNCO is examined extensively with the aid of *ab initio* methods in a forthcoming paper.

II. THEORETICAL METHODS

The atomic-orbital basis sets employed in this study are denoted as DZ(d,p), QZ($2d,2p$), QZ($2d1f,2p1d$), QZ(+)($2d1f,2p1d$), and PZ($3d2f,2p1d$), in which A in the designation $A(x,y)$ is descriptive of the underlying sp basis⁷⁶ and x and y indicate the sets of polarization functions appended to the (C,N,O) atoms and the H atom, respectively. These basis sets range in number of contracted Gaussian functions (CGFs) from 53 in the DZ(d,p) case to 175 in the PZ($3d2f,2p1d$) set. For carbon, nitrogen, and oxygen, the DZ sp basis involves the (9s5p) Gaussian primitives of Huzinaga⁷⁷ and the (4s2p) contractions of Dunning;⁷⁸ the analogous hydrogen basis is a (4s/2s) set in which the exponents are scaled by a factor of 1.2^2 as usual.⁷⁸ In the QZ case the heavy-atom sp sets are Huzinaga-Dunning (10s6p/5s4p) contractions,⁷⁹ whereas for hydrogen a (6s/4s) contraction of the unscaled exponents of Huzinaga⁷⁷ is used, as tabulated by Allen and Schaefer.⁸⁰ In considerations of the dissociation of HNCO to H^+ and the NCO^- anion, the QZ sp basis was augmented in an even-tempered manner with single sets of diffuse s and p functions⁸¹ on each heavy atom, giving

(11s7p/6s5p) contractions denoted as QZ(+). In the PZ basis the C, N, and O sp set consists of (13s8p/6s5p) contractions constructed from the primitives of Partridge⁸² according to (6,3,1,1,1,1) and (4,1,1,1,1) schemes for the s and p functions, respectively. The H(6s/4s) contraction in the PZ set is identical to that used in the QZ set.

The DZ(d,p) basis set was constructed from the DZ core by the addition of polarization functions to all atoms, the exponents being $\alpha_d(\text{C})=0.75$, $\alpha_d(\text{N})=0.80$, $\alpha_d(\text{O})=0.85$, and $\alpha_p(\text{H})=0.75$, which are representative optimal exponents for uncorrelated wave functions.⁸³ For all other basis sets, correlation-optimized polarization function exponents were utilized, as developed by Dunning.⁸⁴ For the $2p$ and $1d$ sets of hydrogen, the exponents are (0.388, 1.407) and 1.057, respectively. For the heavy atoms the exponents for the $2d$, $3d$, $1f$, and $2f$ sets are, in order: carbon, (0.318, 1.097), (0.228, 0.649, 1.848), 0.761, (0.485, 1.419); nitrogen, (0.469, 1.654), (0.335, 0.968, 2.837), 1.093, (0.685, 2.027); and oxygen, (0.645, 2.314), (0.444, 1.300, 3.775), 1.428, (0.859, 2.666). Unless otherwise noted the d sets were comprised of six Cartesian components, while the f sets involved real combinations of only the seven $l=3$ spherical harmonics.

Reference electronic wave functions were determined in this study by the single-configuration, self-consistent-field, restricted and unrestricted Hartree-Fock methods (RHF and UHF)⁸⁵⁻⁸⁸ and also by the complete-active-space self-consistent-field approach (CASSCF).⁸⁹ Dynamical electron correlation was accounted for by the single-reference, configuration interaction singles and doubles method (CISD),⁹⁰⁻⁹³ by Møller-Plesset perturbation theory through fourth⁹⁴⁻⁹⁷ and occasionally fifth^{98,99} order [MP2, MP3, MP4(SDTQ), and MP5(SDTQ)], and by the coupled-cluster singles and doubles method (CCSD),¹⁰⁰⁻¹⁰⁵ including in cases the addition of a perturbative correction for contributions from connected triple excitations [CCSD(T)].^{106,107} All CISD and CCSD wave functions were constructed from RHF orbitals. In some instances CISD+(Q) results were obtained by applying the Davidson correction⁹³ to CISD energies in order to gauge the unlinked cluster contribution from quadruple excitations. In other cases extrapolation of the MP n series was performed to estimate the correlation energy, E_{corr} , in the MP ∞ limit by means of the simple formula^{108,109}

$$E_{\text{corr}} = (E_2 + E_3)(1 - E_4/E_2)^{-1}, \quad (16a)$$

or the (shifted) [2,1] Padé approximant¹⁰⁹⁻¹¹¹

$$E_{\text{corr}} = \frac{E_2^2(E_4 - E_5) + 2E_2E_3(E_4 - E_3) + E_3^2(E_2 - E_3)}{(E_2 - E_3)(E_4 - E_5) - (E_3 - E_4)^2}, \quad (16b)$$

where E_n denotes the n th order perturbation correction to the electronic energy. For open-shell fragments, corrections for spin contamination in the UHF, UMP2, and UMP3 procedures were incorporated according to the approximate projection scheme of Schlegel,^{112,113} yielding electronic energies denoted as PUHF, PMP2, and PMP3, respectively. In this approach, successively higher spin multiplicities were projected out of the UHF reference

wave functions until the PUHF energy and the corresponding PMP n estimates were converged to 1 μ hartree. The electronic structure computations reported here were performed by various implementations of the program packages PSI,¹¹⁴ CADPAC,¹¹⁵ and GAUSSIAN (86, 88, 90, and 92).¹¹⁶

In all correlation treatments the 1s core orbital for each of the C, N, and O atoms was excluded from the active space. Likewise, the highest-lying 1s* virtual orbital for each heavy atom was frozen in the correlation procedures, all of these orbitals lying higher than 20 a.u. in the DZ and QZ computations and above 150 a.u. in the PZ studies. The only exception to these excitation restrictions involved the optimization of the geometric structure of HNCO at the DZ(d,p) CCSD level, in which no orbitals were frozen due to initial program limitations in the analytic derivative codes.

Analytic gradient techniques^{117–119} for the RHF,^{120,121} CASSCF,¹¹⁷ CISD,^{122,123} and CCSD^{105,124} methods were utilized in the determination of optimum geometric structures to 10^{-6} Å or rad in the internal coordinates. Quadratic force fields and dipole-moment derivatives were evaluated via analytic second-derivative techniques for RHF wave functions^{117,125,126} and by finite differences of analytic gradients in the CASSCF, CISD, and CCSD cases. All CISD and CCSD dipole moments were computed as energy derivatives with respect to an external electric field. In the numerical differentiation procedures, displacement sizes of ± 0.005 Å and ± 0.01 rad were employed for the various internal coordinates. The harmonic frequencies obtained from the resulting force constants are expected to differ from their analytic analogs by no more than 0.1 cm^{-1} .

In the harmonic vibrational analyses of HNCO, normal modes were characterized in internal coordinates by the total energy distribution (TED) method advocated by Pulay and Török,¹²⁷ and integrated infrared band intensities (A_i) were computed as usual within the double-harmonic approximation^{128,129} using the formula $A_i \approx 42.254 \cdot 72 |\partial\mu/\partial Q_i|^2$, where A_i is in km mol^{-1} , and μ is in $\text{D Å}^{-1} \text{ amu}^{-1/2}$. The anharmonicity of molecular vibrations was investigated by evaluating complete quartic force fields of isocyanic acid at the DZ(d,p) RHF level of theory using analytic third-derivative procedures.^{117,130,131} Specifically, cubic and lower-order force constants were evaluated analytically, while quartic force constants were found numerically from finite differences of analytic third derivatives using internal-coordinate displacements sizes of ± 0.005 Å or ± 0.01 rad as before. After transformation of the internal-coordinate quartic force fields to reduced normal coordinate representations, vibrational anharmonic constants (χ_{ij}), vibration-rotation interaction constants (α_i^B), and quartic centrifugal distortion constants were determined using formulas¹³² derived from second-order perturbation theory as applied to the standard vibration-rotation Hamiltonian^{132–136} for semirigid asymmetric top molecules. This procedure has been investigated extensively in the systematic studies of vibrational anharmonic-

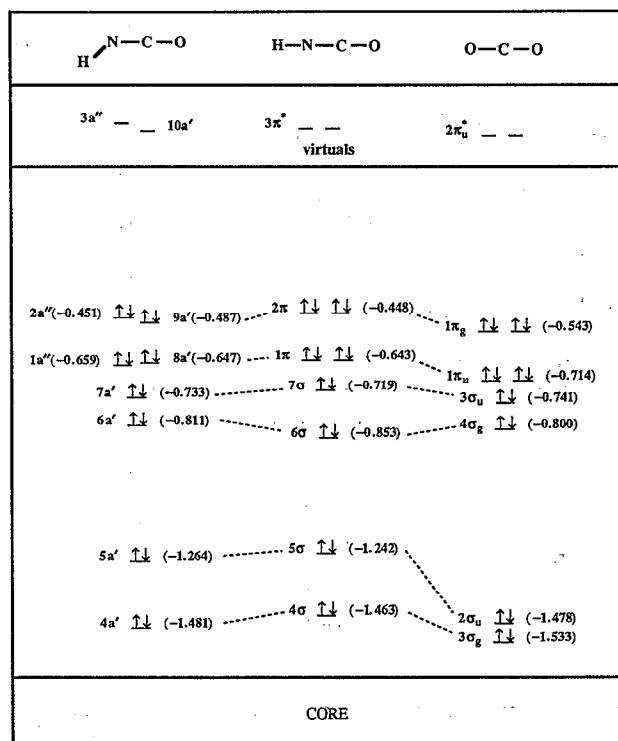


FIG. 3. DZ(d,p) RHF orbital energies (a.u.) for linear and bent, hockey-stick conformations of HNCO as compared to CO_2 . The H–N–C bond angle in the bent structure is 122° . Bond distances (in Å) were taken from the DZ(d,p) CISD optimum values in Table I and also Ref. 131: linear and bent HNCO, $r(\text{N–H})=1.0062$, $r(\text{N–C})=1.2206$, and $r(\text{C–O})=1.1691$; CO_2 , $r(\text{C–O})=1.1647$. Note that the ordering of the 7σ and 1π orbitals in linear HNCO differs from that given in a previous diagram by Dixon and Kirby (Ref. 66). The DZ(d,p) RHF orbital energy derivatives with respect to $\theta(\text{N–C–O})$ in the hockey-stick structure are (in mH rad^{-1}): valence orbitals, $4a'$ (8.268), $5a'$ (–8.124), $6a'$ (–6.646), $7a'$ (12.754), $1a''$ (6.704), $8a'$ (4.824), $9a'$ (–14.811), and $2a''$ (–5.202); core orbitals, $1a'$ (8.972), $2a'$ (–15.097), and $3a'$ (8.892). In these results a positive angle displacement refers to bending in the *trans* direction.

ity in linear and asymmetric top molecules by Allen and co-workers.^{137,138}

In several instances throughout this paper, particularly in cases of relative energy predictions, error bars are affixed to final theoretical proposals. These estimates are to be interpreted as confidence intervals analogous to those arising from one standard deviation in a statistical analysis. Without question the quantification of uncertainties in *ab initio* predictions can be treacherous, but reporting reasonable error bounds based on computational experience with numerous benchmarks is deemed worthwhile here.

III. THEORETICAL ANALYSES

A. Qualitative features of the electronic structure of HNCO

The electronic structure of isocyanic acid is elucidated by comparisons of the linear configuration ($\tilde{X}^1\Sigma^+$) of HNCO with the isoelectronic molecule CO_2 , as illustrated in Fig. 3. Relative to carbon dioxide the valence molecular orbitals of $\tilde{X}^1\Sigma^+$ HNCO are uniformly shifted to higher

TABLE I. Geometric structures (R_e) for HNCO and associated fragmentation products.^a

	Total energy	$r(\text{N-H})$	$r(\text{N-C})$	$r(\text{C-O})$	$\theta(\text{H-N-C})$	$\theta(\text{N-C-O})$
\tilde{X}^1A' HNCO, <i>trans</i> -bent						
DZ(d,p) RHF	-167.799 178	0.9970	1.2036	1.1499	123.93	174.38
DZ(d,p) CASSCF ^b	-167.876 897	0.9956	1.2148	1.1621	125.54	170.65
DZ(d,p) CISD ^{c,d}	-168.213 908	1.0062	1.2206	1.1691	122.08	173.02
DZ(d,p) CCSD ^e	-168.306 617	1.0115	1.2285	1.1771	121.23	172.49
R_e (expt.) ^f	...	0.9946	1.2140	1.1664	123.9	172.6
R_e (expt.) ^g	...	1.0127	1.2175	1.1654	124.0	172.1
R_e (expt.) ^h I	...	1.0033	1.2150	1.1637	123.29	172.37
II	...	1.0030(20)	1.2145(6)	1.1634(4)	123.34(20)	172.22(20)
$\tilde{X}^1\Sigma^+$ HNCO, linear ⁱ						
DZ(d,p) RHF	-167.792 762	0.9824	1.1666	1.1614	180.0	180.0
DZ(d,p) CISD ^d	-168.205 394	0.9904	1.1828	1.1797	180.0	180.0
$\tilde{X}^3\Sigma^-$ NH + $\tilde{X}^1\Sigma^+$ CO						
DZ(d,p) RHF	-167.727 206	1.0251	∞	1.1174
DZ(d,p) CISD ^{d,j}	-168.102 357	1.0399	∞	1.1383
R_e (expt.) ^k	...	1.0362	∞	1.1283
\tilde{X}^2S H + $\tilde{X}^2\Pi$ NCO						
DZ(d,p) RHF	-167.649 130	∞	1.2331	1.1448	180.0	...
DZ(d,p) CISD ^{d,j}	-168.039 953	∞	1.2430	1.1711	180.0	...
$\text{H}^+ + \tilde{X}^1\Sigma^+ \text{NCO}^-$						
DZ(d,p) CISD ^j	-167.648 615	∞	1.1920	1.2345	180.0	...

^aBond distances in Å, bond angles in degrees, and total energies in hartrees.

^bActive space: eight electrons in six orbitals.

^cThree core and three virtual orbitals frozen, yielding 25 839 configuration state functions (CSFs) in C_s symmetry.

^dDZ(d,p) CISD+(Q)//DZ(d,p) CISD total energies: $^1A'$ HNCO (-168.259 884), $^1\Sigma^+$ HNCO (-168.250 387), NH+CO (-168.143 424), H+NCO (-168.084 302).

^eNo orbitals frozen in the correlation treatment.

^fReference 52.

^gReference 55.

^h R_e structures derived from the observed rotational constants of Ref. 52. See Sec. III H of the text for details.

ⁱTransition state for the interconversion of equivalent *trans*-bent minima. The corresponding DZ(d,p) RHF frequencies are given in the text.

^jSupermolecule results determined at an N-C separation of 1000 Å.

^kReference 152.

energies, except in the case of 6σ , which exhibits the most N-H sigma bonding character. The strong polarization of 6σ into the N-H bonding region which results from the presence of the hydrogen nucleus leads to a stabilization of ca. 0.05 a.u. relative to the $4\sigma_g$ counterpart in CO_2 . The sizeable polarization of the overall charge distribution is evident from the DZ(d,p) CISD value of 3.137 D for the molecular dipole moment. As shown in Table I, the theoretical N-C and C-O bond lengths for $\tilde{X}^1\Sigma^+$ HNCO differ by less than 0.006 Å and are elongated relative to the analogous bond distances in CO_2 by only 0.015–0.02 Å. The harmonic vibrational stretching frequencies of $\tilde{X}^1\Sigma^+$ HNCO obtained at the DZ(d,p) RHF level are $\omega_1(\sigma) = 4144 \text{ cm}^{-1}$ (N-H str.), $\omega_2(\sigma) = 2588 \text{ cm}^{-1}$ (N-C-O asym. str.), and $\omega_3(\sigma) = 1501 \text{ cm}^{-1}$ (N-C-O sym. str.), the latter two being remarkably close to the corresponding stretching frequencies of CO_2 , viz. 2590 and 1513 cm^{-1} ,¹³⁸ respectively, as predicted by the same level of theory. The DZ(d,p) RHF $\omega_4(\pi)$ frequency, which occurs at 723 cm^{-1} , corresponds almost exclusively to N-C-O bending according to the TED analysis, and thus it is comparable to the analogous theoretical frequency for linear bending (766 cm^{-1}) in CO_2 . These similarities with CO_2 notwithstanding, linear HNCO is actually a transition state, as shown by the DZ(d,p) RHF prediction of $\omega_5(\pi) = 468i$

cm^{-1} , which pertains to a *trans* deformational mode comprised of about 70% H-N-C bending and 30% N-C-O bending.

For a tetraatomic molecule which has bent stationary points lying below the optimum linear configuration, there are numerous possibilities for the general topography of the potential energy surface. Within the constraint of molecular planarity, some of the possible cases are (a) Only *cis* or *trans* minima exist, and the optimum linear structure is the transition state for interconversion of equivalent conformations, thereby displaying an in-plane Hessian index of 1.¹³⁹ (b) Both *cis* and *trans* minima occur, and the in-plane transition states for *cis*-*trans* isomerization are nonlinear; the *trans*-*trans* interconversion pathways pass through the *cis* minima, and vice versa. Characteristically the optimum linear structure has a Hessian index of 2 for in-plane deformations.¹⁴⁰ (c) Only *cis* or *trans* minima exist, but the transition state for interconversion is nonlinear; the Hessian index of the optimum linear structure is 2. (d) Both *cis* and *trans* minima occur, but the transition states for both *cis*-*trans* isomerization and the interconversion of equivalent *cis* and *trans* structures coincide with the optimum linear configuration. In this improbable case, a single linear, bifurcating transition state is present which has eigenvalues exactly equal to zero for both *cis*- and *trans*-

bending deformations.¹⁴¹ These four cases are certainly not exhaustive, and the consideration of torsional degrees of freedom further enhances the list of possibilities.

The HNCO molecule corresponds to case (a). Only *trans* minima are found, and these are connected via the linear transition state by displacements along the in-plane component of the $\omega_5(\pi)$ normal mode. The theoretical methods listed in Table I yield optimum geometric structures which are *trans* bent with an H–N–C angle in the range 121°–126° and an N–C–O framework which deviates from linearity by 6°–10°, in good agreement with experiment. These angle deformations from linearity have the effect of increasing the N–H and N–C bond lengths by 0.01–0.02 and 0.03–0.04 Å, respectively, presumably due to the rehybridization of the nitrogen atom; a concomitant 0.01–0.02 Å decrease occurs in the C–O distance. Further discussion of the equilibrium structure of \tilde{X}^1A' HNCO is reserved for Sec. III H.

The molecular orbital energy diagram for a particular bent configuration of HNCO is also given in Fig. 3 along with those of CO₂ and linear HNCO. The bent structure, which is slightly removed from the equilibrium geometry, is one in which the H–N–C angle is 122° but the N–C–O chain is constrained to be linear. In going from linear HNCO to this “hockey-stick” structure, all of the occupied valence molecular orbitals are stabilized by up to 0.04 a.u., except again in the case of the N–H sigma bonding orbital (6σ or $6a'$), which is destabilized by 0.042 a.u. The sum of the energy lowerings for the orbitals which are stabilized is clearly larger than the energy increase for 6σ , and thus the substantial bending of the H–N–C angle can be rationalized according to the principles of Walsh.^{142,143} However, the use of Walsh-type arguments is less successful in explaining the bending of the N–C–O framework in the *trans* direction. The first derivatives with respect to $\theta(\text{N–C–O})$ of the DZ(d,p) RHF molecular orbital energies of the hockey-stick structure appear in the caption to Fig. 3. Although N–C–O bending in the *trans* direction is predicted by the resulting negative sum of the first derivatives,¹⁴⁴ the extent of bending obtained by a quadratic extrapolation involving the net second derivative is only 0.3°. Thus the full deviation of the NCO unit from linearity cannot be explained by a simple decomposition based on molecular orbital energy variations alone.

The polarization of the charge density observed in linear HNCO appears to be diminished somewhat as the molecule adopts the *trans*-bent conformation. The net atomic charges given by Mulliken population analyses with the DZ(d,p) SCF density matrices at the optimum DZ(d,p) CISD geometries are $q(\text{O}) = -0.41$, $q(\text{C}) = 0.60$, $q(\text{N}) = -0.50$, and $q(\text{H}) = 0.31$ for the linear structure, as compared to $q(\text{O}) = -0.33$, $q(\text{C}) = 0.56$, $q(\text{N}) = -0.50$, and $q(\text{H}) = 0.28$ in the *trans*-bent case.¹⁴⁵ A more compelling indication of this charge redistribution is the reduction of the dipole moment by ca. 1 D in going to the bent geometry. In the molecule-fixed principal axis system in which the hydrogen atom is positioned in the $-a$ and $+b$ directions from the origin (see Fig. 1), the equilibrium DZ(d,p) CISD dipole moment vector has a magnitude of 2.184 D

and the components $\mu_a = -1.478$ and $\mu_b = 1.608$ D. Shifts in the magnitude of μ due to electron correlation and basis set enlargement appear to be only of the order of 0.1 D.¹⁴⁶ The DZ(d,p) CISD result is in excellent agreement with the 2.07 ± 0.10 D magnitude and the $|\mu_a| = 1.575 \pm 0.005$ D component deduced from Stark effect measurements by Hocking *et al.*,⁶² both of which include zero-point vibrational effects, however.¹⁴⁷

The degree of importance of nondynamical electron correlation in \tilde{X}^1A' HNCO was investigated here using CASSCF wave functions of modest size as well as a diagnostic based on the t_1 amplitudes given by the CCSD procedure.¹⁴⁸ The DZ(d,p) CASSCF results reported in Table I for \tilde{X}^1A' HNCO refer to wave functions involving eight electrons in six molecular orbitals, specifically the complete active space comprised of the $1a''$, $8a'$, $9a'$, $2a''$, $3a''$, and $10a'$ orbitals in Fig. 3. This active space is analogous to that of a full π -space, valence CASSCF procedure for either CO₂ or linear HNCO. In the representation of the wave function at the optimum structure in which the component orbitals are canonicalized as CASSCF natural orbitals, the reference coefficient is 0.969, and none of the remaining CI coefficients exceeds 0.10. The excited *determinants* of greatest importance are as follows: $(9a')^2 \rightarrow (10a')^2$, $C_2 = -0.097$; $(2a'')^2 \rightarrow (3a'')^2$, $C_3 = -0.096$; $(9a')(2a'') \rightarrow (10a')(3a'')$, $(C_4, C_5) = -0.073$, $(C_8, C_9) = -0.064$; $(8a')^2 \rightarrow (10a')^2$, $C_6 = -0.068$; and $(1a'')^2 \rightarrow (3a'')^2$, $C_7 = -0.064$. In brief, \tilde{X}^1A' HNCO does not exhibit a high degree of multireference character in its electronic structure for bond lengths near the equilibrium values. This assertion is supported by the favorable comparisons in Table I of the CASSCF geometrical parameters with the RHF, CISD, and CCSD results. Final support for this conclusion is seen in the Euclidean norms (\mathcal{S}_1) of the t_1 amplitudes of the DZ(d,p) CCSD wave functions, which are 0.0172 and 0.0186 for the linear and *trans*-bent optimum CCSD structures, respectively. These values are less than the 0.02 cutoff criterion proposed by Lee and Taylor¹⁴⁸ for determining the point at which the multireference character of electronic wave functions becomes substantial.

B. Barrier to linearity for \tilde{X}^1A' HNCO

A precise experimental determination of the barrier to linearity on the ground-state potential energy surface of isocyanic acid has not yet been achieved, although an early spectroscopic study by Neely⁵⁰ suggested a value of 10.3 ± 0.6 kcal mol⁻¹. In 1978 McLean *et al.*¹⁴⁹ investigated this barrier height theoretically via *ab initio* techniques and advanced an estimate of 4.8 ± 0.5 kcal mol⁻¹ on the basis of double-zeta plus polarization RHF and CISD predictions. Later Glidewell and Thomson¹⁵⁰ obtained 6–311G** MP2 and MP3 values of 5.22 and 5.01 kcal mol⁻¹, respectively, in good agreement with the earlier proposal. Nonetheless, the higher levels of theory applied here indicate that these prior predictions for the barrier height are too low by 0.5–1.0 kcal mol⁻¹.

In Table II results are tabulated for the classical barrier to linearity at several levels of theory, as determined from the total energies listed in Table III obtained at the

TABLE II. Energy differences (Δ , kcal mol⁻¹) between the linear and *trans*-bent structures on the ground-state surface of HNCO.^a

	DZ(<i>d,p</i>) ^b	QZ(2 <i>d</i> ,2 <i>p</i>)	QZ(2 <i>d</i> 1 <i>f</i> , 2 <i>p</i> 1 <i>d</i>)	PZ(3 <i>d</i> 2 <i>f</i> , 2 <i>p</i> 1 <i>d</i>)
Δ [RHF]	4.01	5.22	4.50	4.46
Δ [E_2]	+1.92	+1.11	+0.78	+0.74
Δ [E_3]	-0.34	-0.13	-0.23	...
Δ [E_4 (SDTQ)]	+1.22	+1.07	+1.05	...
Δ [MP3]	5.59	6.20	5.05	...
Δ [MP4(SDTQ)]	6.81	7.27	6.10	...
Δ [CCSD]	...	6.50	5.33	...
Δ [CCSD(T)]	...	7.00	5.77	...
Final prediction:	$\Delta E_e(^1\Sigma^+ - ^1A') = 5.7 \pm 0.3$ kcal mol ⁻¹			

^aBased on the optimum DZ(*d,p*) CISD structures in Table I. Zero-point vibrational contributions are not included. E_n denotes the *n*th-order perturbation correction to the electronic energy.

^bAdditional DZ(*d,p*) predictions for the barrier to linearity: CISD (5.34), CISD+(Q) (5.96), and MP5 (6.07).

optimum DZ(*d,p*) CISD structures. The DZ(*d,p*) RHF barrier of 4.01 kcal mol⁻¹ is very similar to previous uncorrelated predictions. Since the \mathcal{S}_1 diagnostic mentioned above for the *trans*-bent structure of HNCO exceeds that for the linear form, an increase in the barrier height upon the inclusion of electron correlation is expected. Indeed, the successive contributions to the barrier height due to the second-, third-, and fourth-order perturbation energies are +1.92, -0.34, and +1.22 kcal mol⁻¹, respectively, giving a net DZ(*d,p*) MP4(SDTQ) result of 6.81 kcal mol⁻¹. The apparent lack of convergence in the successive DZ(*d,p*) MP n predictions is conspicuous. Moreover, substantial changes in the various barrier height contributions

are observed as the basis set is enlarged from DZ(*d,p*) to PZ(3*d*2*f*,2*p*1*d*). Most notably, the RHF energy difference increases to over 5 kcal mol⁻¹ before converging to 4.46 kcal mol⁻¹, and the second-order contribution exhibits a striking decrease from +1.92 to +0.74 kcal mol⁻¹. Nevertheless, the partitioning of the energy barrier at each order appears to have stabilized once the basis set is improved to QZ(2*d*1*f*,2*p*1*d*) quality. While the resulting QZ(2*d*1*f*,2*p*1*d*) MP3 prediction of 5.05 kcal mol⁻¹ is in good agreement with the original estimate of McLean and co-workers,¹⁴⁹ the large fourth-order contribution of +1.05 kcal mol⁻¹ suggests that the barrier height be revised toward higher values. The Δ [E_4] shift is comprised predominantly of terms due to triple and single substitutions, +0.53 and +0.43 kcal mol⁻¹, respectively; the doubles term (+0.27 kcal mol⁻¹) largely cancels the quadruples plus renormalization contribution (-0.22 kcal mol⁻¹).

The CCSD and CCSD(T) barriers to linearity are intermediate between the corresponding MP3 and MP4 results; in particular, the CCSD(T) values lie ca. 0.3 kcal mol⁻¹ lower than the analogous MP4 predictions. The difference in the QZ(2*d*1*f*,2*p*1*d*) CCSD(T) and CCSD barrier heights (+0.44 kcal mol⁻¹), i.e., the contribution from connected triple excitations, compares favorably with the triples term in Δ [E_4]. In order to substantiate the preference of the QZ(2*d*1*f*,2*p*1*d*) CCSD(T) barrier over the analogous MP4 prediction, DZ(*d,p*) MP5 energies for linear and bent HNCO were determined along with the corresponding [2,1] Padé approximants of the MP ∞ limits [see Eq. 16(b)]. The barriers to linearity based on the DZ(*d,p*) MP5 data and the Padé approximants are 6.07

TABLE III. Total energies (hartree) for HNCO isomers.

	\tilde{X}^1A' HNCO ^a	$\tilde{X}^1\Sigma^+$ HNCO ^a	HOCN ^b	HCNO ^c	HONC ^b
DZ(<i>d,p</i>) RHF	-167.797 726	-167.791 331	-167.756 925	-167.662 433	-167.664 076
DZ(<i>d,p</i>) MP2	-168.256 947	-168.247 496	-168.219 534	-168.145 865	-168.118 611
DZ(<i>d,p</i>) MP3	-168.251 630	-168.242 727	-168.216 830	-168.132 065	-168.122 707
DZ(<i>d,p</i>) MP4	-168.285 835	-168.274 983	-168.246 802	-168.176 113	-168.153 416
DZ(<i>d,p</i>) MP5	-168.271 552	-168.261 871	...	-168.152 163	...
QZ(2 <i>d</i> ,2 <i>p</i>) RHF	-167.829 072	-167.820 752	-167.785 862	-167.691 925	-167.690 386
QZ(2 <i>d</i> ,2 <i>p</i>) MP2	-168.374 787	-168.364 698	-168.335 511	-168.263 647	-168.233 560
QZ(2 <i>d</i> ,2 <i>p</i>) MP3	-168.362 881	-168.353 000	-168.325 668	-168.242 126	-168.230 734
QZ(2 <i>d</i> ,2 <i>p</i>) MP4	-168.407 813	-168.396 224	-168.367 780	-168.298 730	-168.272 488
QZ(2 <i>d</i> ,2 <i>p</i>) CCSD	-168.371 058	-168.360 693	...	-168.251 002	...
QZ(2 <i>d</i> ,2 <i>p</i>) CCSD(T)	-168.398 588	-168.387 429	...	-168.284 808	...
QZ(2 <i>d</i> 1 <i>f</i> ,2 <i>p</i> 1 <i>d</i>) RHF	-167.835 206 ^d	-167.828 032	-167.791 310	-167.699 898	-167.696 971
QZ(2 <i>d</i> 1 <i>f</i> ,2 <i>p</i> 1 <i>d</i>) MP2	-168.423 617 ^d	-168.415 198	-168.383 580	-168.314 784	-168.282 114
QZ(2 <i>d</i> 1 <i>f</i> ,2 <i>p</i> 1 <i>d</i>) MP3	-168.413 575 ^d	-168.405 522	-168.375 397	-168.294 909	-168.280 515
QZ(2 <i>d</i> 1 <i>f</i> ,2 <i>p</i> 1 <i>d</i>) MP4	-168.459 037 ^d	-168.449 311	-168.418 098	-168.352 059	-168.322 641
QZ(2 <i>d</i> 1 <i>f</i> ,2 <i>p</i> 1 <i>d</i>)* RHF ^e	-167.834 651	-167.827 481	-167.790 751	-167.699 395	-167.696 577
QZ(2 <i>d</i> 1 <i>f</i> ,2 <i>p</i> 1 <i>d</i>)* CCSD ^c	-168.417 651	-168.409 162	-168.379 770	-168.301 836	-168.285 284
QZ(2 <i>d</i> 1 <i>f</i> ,2 <i>p</i> 1 <i>d</i>)* CCSD(T) ^c	-168.447 282	-168.438 082	-168.408 503	-168.335 617	-168.314 500
PZ(3 <i>d</i> 2 <i>f</i> ,2 <i>p</i> 1 <i>d</i>) RHF	-167.839 311	-167.832 207	-167.795 101	-167.704 101	-167.700 836
PZ(3 <i>d</i> 2 <i>f</i> ,2 <i>p</i> 1 <i>d</i>) MP2	-168.446 909	-168.438 622	-168.406 118	-168.338 418	-168.304 927

^aObtained at the DZ(*d,p*) CISD optimum geometries reported in Table I.

^bDetermined at the 6-31G** MP2 geometries of Ref. 36.

^cDetermined at the linear TZ2P CCSD(T) geometry of Ref. 184.

^dAnalogous QZ(+)(2*d*1*f*,2*p*1*d*) results for \tilde{X}^1A' HNCO: RHF(-167.835 667), MP2(-168.424 604), MP3(-168.414 376), and MP4(-168.459 976).

^eThe asterisk signifies the use of *d* sets of five components in the one-particle basis, that is, the exclusion of the supernumerary *s* orbitals.

and 6.40 kcal mol⁻¹, respectively, the latter MP_∞ result lying ca. 0.4 kcal mol⁻¹ below the DZ(*d,p*) MP4 prediction. Because the higher-order correlation contributions to the barrier height of HNCO appear to converge rapidly with respect to basis set enlargement, it is reasonable to surmise a barrier of about 6.1–0.4=5.7 kcal mol⁻¹ for the QZ(2*d1f*,2*p1d*) MP_∞ limit. Accordingly, the validity of the QZ(2*d1f*,2*p1d*) CCSD(T) prediction of 5.77 kcal mol⁻¹ is demonstrated. The final prediction of 5.7 kcal mol⁻¹ reported in Table II for the vibrationless barrier is based on the QZ(2*d1f*,2*p1d*) CCSD(T) result corrected by the QZ(2*d1f*,2*p1d*)→PZ(3*d2f*,2*p1d*) basis set shift observed at the MP2 level.

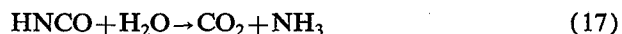
An appropriate benchmark for testing the accuracy of the coupled-cluster and MP_n predictions for HNCO is the classical inversion barrier in ammonia, which is also near 6 kcal mol⁻¹ and also involves a change of configuration about a nitrogen center. Lee and co-workers¹⁵¹ have previously reported total energies and molecular properties of planar and pyramidal NH₃ at the CISD, CISDT, and CISDTQ levels of theory using both DZ and DZP basis sets. The following inversion barriers (in kcal mol⁻¹) were obtained with the DZP basis at the optimum structures for each level of theory: RHF(4.788), CISD(5.910), CISDT(6.050), and CISDTQ(6.214). By comparison, the MP_n and coupled-cluster predictions determined here with the same basis set at the DZP CISDTQ geometries were MP2(5.715), MP3(5.915), MP4(6.176), MP5(6.192), CCSD(6.061), and CCSD(T) (6.217). The [2,1] Padé approximant based on the DZP MP_n energies gives an MP_∞ inversion barrier of 6.205 kcal mol⁻¹. The agreement of the CCSD(T) value with the CISDTQ result is remarkable; moreover, the CCSD(T) prediction is also supported by the MP_∞ extrapolation. The results of this calibration involving NH₃ are encouraging and bolster confidence in the final prediction for the barrier to linearity of HNCO as derived from the CCSD(T) method.

C. Fragmentation energy for \tilde{X}^1A' HNCO→ $\tilde{X}^3\Sigma^-$ NH + $\tilde{X}^1\Sigma^+$ CO

In previous work the energy required for the fragmentation of HNCO into imidogen (NH) and carbon monoxide has been the basis for establishing the heat of formation of isocyanic acid,^{40,41} a quantity of some importance in combustion studies. Three electronic states of the imidogen fragment appear below 25 000 cm⁻¹:¹⁵² $\tilde{X}^3\Sigma^-$ ($r_e=1.0362$ Å), $\tilde{a}^1\Delta$ ($T_e=12\,566$ cm⁻¹, $r_e=1.0341$ Å), and $\tilde{b}^1\Sigma^+$ ($T_e=21\,202$ cm⁻¹, $r_e=1.0360$ Å). Experimental data for the heat of formation of the triplet ground state of NH, with values ranging from 84 to over 90 kcal mol⁻¹ in the literature as of 1986, were re-evaluated by Anderson in 1989,¹⁵³ leading to a proposal of $\Delta H_{f,0}^\circ=85.3\pm 0.2$ kcal mol⁻¹. However, in 1987 Bauschlicher and Langhoff¹⁵⁴ determined $D_0(\text{N-H})=3.37\pm 0.03$ eV for triplet imidogen on the basis of high-level MR CI computations with a [5*s4p3d2f1g/4s3p2d*] basis set. This dissociation energy leads to $\Delta H_{f,0}^\circ(\text{NH})=86.5$ kcal mol⁻¹,¹⁵⁵ which is preferred in the thermochemical manipulations reported here. Hence, with the aid of the accepted heat of formation of

carbon monoxide, the value of $\Delta H_{f,0}^\circ(\text{HNCO})$ can be ascertained from the dissociation energy, $D_0(\text{NH-CO})$, for the spin-forbidden fragmentation \tilde{X}^1A' HNCO→ $\tilde{X}^3\Sigma^-$ NH + $\tilde{X}^1\Sigma^+$ CO. Previous photolysis experiments designed to ascertain $D_0(\text{NH-CO})$ were reviewed in Sec. I B.

In the current theoretical analysis, two independent methods (I and II) were used to determine $D_0(\text{NH-CO})$ and $\Delta H_{f,0}^\circ(\text{HNCO})$. In Method I, $D_e(\text{NH-CO})$ was evaluated directly via the *ab initio* prediction of reactant and fragment total energies, and a zero-point vibrational energy term was appended to give $D_0(\text{NH-CO})$, and subsequently $\Delta H_{f,0}^\circ(\text{HNCO})$. In Method II the reaction



was employed to extract $\Delta H_{f,0}^\circ(\text{HNCO})$ first, from which $D_0(\text{NH-CO})$ was in turn evaluated. Not only is reaction (17) isogyric, but it is also comprised of isoelectronic pairs of reactants and products so that differential correlation effects on the reaction energy are almost completely eliminated. The reference geometries for the total energy determinations of \tilde{X}^1A' HNCO, $\tilde{X}^3\Sigma^-$ NH, and $\tilde{X}^1\Sigma^+$ CO were the DZ(*d,p*) CISD optimum structures given in Table I. The corresponding bond lengths and bond angles deviate from the experimental R_e parameters by no more than 0.01 Å and 1.5°, respectively, and consequently the effects of further geometry relaxation on the total energy predictions should only be of the order of 0.1 kcal mol⁻¹. For the H₂O, NH₃, and CO₂ species, precisely known experimental R_e reference structures were employed.^{156–158}

The total energies at several levels of theory for \tilde{X}^1A' HNCO and the NH(³Σ⁻) and CO fragments are listed in Tables III, IV, and V, and the resulting dissociation energies given by Method I appear in Table VI. The spin contaminations in the UHF reference wave functions for NH(³Σ⁻) are small, as shown in footnote c of Table V, where the expectation values of S^2 differ by less than 0.02 units of \hbar^2 from the correct value of 2. Since only the imidogen fragment is an open-shell species, the PMP_n scheme is rigorously size extensive in addition to the UMP_n procedure, allowing the total energies of NH and CO to be determined separately. However, in obtaining the UMP_∞ estimates via Eq. (16a), the individual *n*th-order perturbation energies were summed to yield supermolecule values before extrapolation of the overall series. Dissociation energy predictions for the isoelectronic system \tilde{X}^1A_1 CH₂CO→ \tilde{X}^3B_1 CH₂+ $\tilde{X}^1\Sigma^+$ CO are also given in Table VI. In previous photolysis experiments, Chen, Green, and Moore¹⁵⁹ have determined a very precise dissociation energy (30 116.2±0.4 cm⁻¹) for the production of singlet methylene and carbon monoxide from ground-state CH₂CO. When combined with the observed singlet–triplet splitting in CH₂ ($T_0=9.02\pm 0.01$ kcal mol⁻¹)¹⁶⁰ and the known vibrational frequencies of the parent ketene molecule¹⁶¹ and its fragments,^{152,162,163} $D_e(\text{CH}_2\text{-CO})=83.0$ kcal mol⁻¹ is obtained for CH₂(³B₁) production. This result is used for calibration of the theoretical predictions for HNCO.

The application of the RHF method (Table VI) to determine $D_e(\text{NH-CO})$ via Method I reveals that about

TABLE IV. Total energies (hartree) for closed-shell fragments pertinent to HNCO thermochemistry.^{a,b}

	CO	CH ₄	NH ₃	H ₂ O	N ₂ O	CO ₂	NCO ⁻
DZ(<i>d,p</i>) RHF	-112.758 249	-40.206 283	-56.208 763	-76.046 481	-183.712 932	-187.675 210	-167.235 781
DZ(<i>d,p</i>) MP2	-113.039 505	-40.368 302	-56.396 489	-76.243 236	-184.226 918	-188.142 009	-167.696 651
DZ(<i>d,p</i>) MP3	-113.037 583	-40.388 118	-56.409 449	-76.249 099	-184.201 030	-188.128 370	-167.687 201
DZ(<i>d,p</i>) MP4	-113.061 293	-40.393 727	-56.415 093	-76.255 138	-184.251 120	-188.164 954	-167.720 875
QZ(2 <i>d,2p</i>) RHF	-112.780 222	-40.214 198	-56.220 142	-76.060 574	-183.747 297	-187.707 726	-167.268 909
QZ(2 <i>d,2p</i>) MP2	-113.118 790	-40.399 724	-56.441 134	-76.306 712	-184.356 145	-188.275 271	-167.820 595
QZ(2 <i>d,2p</i>) MP3	-113.112 939	-40.418 184	-56.451 525	-76.308 986	-184.322 052	-188.254 134	-167.803 259
QZ(2 <i>d,2p</i>) MP4	-113.143 801	-40.425 820	-56.460 944	-76.319 928	-184.386 863	-188.302 813	-167.850 007
QZ(2 <i>d1f,2p1d</i>) RHF	-112.783 042	-40.214 837	-56.221 298	-76.062 297	-183.756 302	-187.714 515	-167.275 740 ^c
QZ(2 <i>d1f,2p1d</i>) MP2	-113.145 949	-40.415 340	-56.460 528	-76.329 390	-184.409 881	-188.326 983	-167.866 942 ^c
QZ(2 <i>d1f,2p1d</i>) MP3	-113.141 054	-40.433 499	-56.471 240	-76.332 669	-184.377 731	-188.308 451	-167.853 205 ^c
QZ(2 <i>d1f,2p1d</i>) MP4	-113.171 830	-40.441 279	-56.480 859	-76.343 791	-184.443 153	-188.357 538	-167.898 799 ^c
PZ(3 <i>d2f,2p1d</i>) RHF	-112.785 665	-40.215 504	-56.222 767	-76.064 601	-183.760 934	-187.719 149	...
PZ(3 <i>d2f,2p1d</i>) MP2	-113.161 503	-40.419 993	-56.468 137	-76.340 949	-184.435 160	-188.353 534	...

^aFor CO and NCO⁻, the DZ(*d,p*) CISD optimum (supermolecule) geometries in Table I were used. The remaining reference geometries were experimental *R_e* structures: CH₄, *r_e*(C-H)=1.086 Å (Ref. 212); NH₃, *r_e*(N-H)=1.0124 Å, θ_e (H-N-H)=106.7° (Ref. 157); H₂O, *r_e*(O-H)=0.9572 Å, θ_e (H-O-H)=104.52° (Ref. 156); N₂O, *r_e*(N-N)=1.1273 Å, *r_e*(N-O)=1.1851 Å (Ref. 213); and CO₂, *r_e*(C-O)=1.1600 Å (Ref. 158).

^bAdditional DZ(*d,p*) MP5 energies: CH₄(-40.394 683), NH₃(-56.415 831), and N₂O(-184.223 671).

^cAnalogous QZ(+)(2*d1f,2p1d*) results for NCO⁻: RHF(-167.277 268), MP2(-167.873 364), MP3(-167.857 126), and MP4(-167.905 357).

TABLE V. Total energies (hartree) for open-shell fragments of HNCO.^{a,b}

	$\tilde{X}^3\Sigma^-$ NH	$\tilde{X}^2\Pi$ NCO
DZ(<i>d,p</i>) RHF	-54.967 653	-167.149 777
DZ(<i>d,p</i>) UHF ^c	-54.974 772	-167.159 750
DZ(<i>d,p</i>) PUHF	-54.978 232	-167.171 295
DZ(<i>d,p</i>) UMP2	-55.078 219	-167.569 532
DZ(<i>d,p</i>) PMP2	-55.080 434	-167.578 677
DZ(<i>d,p</i>) UMP3	-55.094 291	-167.575 692
DZ(<i>d,p</i>) PMP3	-55.095 592	-167.581 529
DZ(<i>d,p</i>) UMP4	-55.098 131	-167.604 838
QZ(2 <i>d,2p</i>) RHF	-54.975 140	...
QZ(2 <i>d,2p</i>) UHF ^c	-54.982 842	-167.189 527
QZ(2 <i>d,2p</i>) PUHF	-54.986 545	-167.200 693
QZ(2 <i>d,2p</i>) UMP2	-55.110 343	-167.681 220
QZ(2 <i>d,2p</i>) PMP2	-55.112 728	-167.690 033
QZ(2 <i>d,2p</i>) UMP3	-55.126 219	-167.681 653
QZ(2 <i>d,2p</i>) PMP3	-55.127 608	-167.687 262
QZ(2 <i>d,2p</i>) UMP4	-55.131 144	-167.720 456
QZ(2 <i>d1f,2p1d</i>) UHF ^c	-54.983 246	-167.195 618
QZ(2 <i>d1f,2p1d</i>) PUHF	-54.986 981	-167.206 817
QZ(2 <i>d1f,2p1d</i>) UMP2	-55.122 917	-167.727 253
QZ(2 <i>d1f,2p1d</i>) PMP2	-55.125 314	-167.736 074
QZ(2 <i>d1f,2p1d</i>) UMP3	-55.139 080	-167.729 520
QZ(2 <i>d1f,2p1d</i>) PMP3	-55.140 451	-167.735 105
QZ(2 <i>d1f,2p1d</i>) UMP4	-55.144 146	-167.768 894
PZ(3 <i>d2f,3p2d</i>) UHF ^c	-54.984 472	-167.199 467
PZ(3 <i>d2f,3p2d</i>) UMP2	-55.129 054	-167.749 381

^aObtained at the DZ(*d,p*) CISD optimum (supermolecule) geometries in Table I.

^bTotal RHF energies of the ²S state of the H atom: DZ(*d,p*), -0.497 637; QZ(2*d,2p*), -0.499 940; QZ(2*d1f,2p1d*) and PZ(3*d2f,3p2d*), -0.499 941.

^cThe associated expectation values of S² are: DZ(*d,p*), NH(2.0148) and NCO(0.8421); QZ(2*d,2p*), NH(2.0162) and NCO(0.8371); QZ(2*d1f,2p1d*), NH(2.0161) and NCO(0.8357); PZ(3*d2f,3p2d*), NH(2.0166) and NCO(0.8360).

half of the N=C bond energy arises from electron correlation, consistent with numerous other investigations.^{87,88}

The relaxation of the restricted spin-orbital constraint on the NH reference wave functions lowers the total energy by about 5 kcal mol⁻¹ and thus reduces the RHF dissociation energy by the same amount. From the data in Table VI it is apparent that with each basis set the *E*₂ perturbation correction overshoots the exact correlation contribution to *D_e*(NH-CO), thus initiating an oscillatory series of predictions which is not fully damped even at fourth order. To wit, the MP3-MP4 shift yields a 4-6 kcal mol⁻¹ increase in *D_e*(NH-CO). The UMP_∞ estimates indicate that the UMP4 predictions may also be higher than their full CI counterparts, probably by even more than the suggested 0.4-0.6 kcal mol⁻¹.

Extensive *ab initio* studies on N₂, F₂, and other diatomic molecules have clearly shown that flexible basis sets and, in particular, high angular momentum functions are the *sine qua non* for recovering the correlation contribution to bond energies.¹⁶⁴⁻¹⁶⁶ For example, at the UMP4(SDTQ) level, an increase of 9.1 kcal mol⁻¹ in the dissociation energy of N₂ is observed upon addition of *f* functions to the 6-311G(2*d*) basis set.¹⁶⁷ Similarly the QZ(2*d,2p*) → QZ(2*d1f,2p1d*) increase in *D_e*(NH-CO) is 6.4 kcal mol⁻¹ at the MP4 level, giving an overall value of 89.8 kcal mol⁻¹. Basis set deficiencies of 2 kcal mol⁻¹ or more are likely to be present in this prediction, consistent with the QZ(2*d1f,2p1d*) and PZ(3*d2f,3p2d*) UMP2 entries in Table VI, but the resulting shift toward larger dissociation energies will be balanced by the effects of spin contamination, basis set superposition error, and higher-order perturbation energy contributions. Core-valence correlation¹⁶⁸ and relativistic effects may also be non-negligible. To obtain a net correction term for these effects, the predictions for the dissociation energy of ketene are perused. The patterns in the entries in Table VI are similar to those of HNCO, but the variations in the predictions are generally less pronounced. For example, the MP3 → MP4

TABLE VI. Dissociation energies (D_e , kcal mol⁻¹) for fragmentation of HNCO^a and CH₂CO.^b

	DZ(d,p)	QZ(2 $d,2p$)	QZ(2 $d1f,2p1d$)	PZ(3 $d2f,2p1d$)
\tilde{X}^1A' HNCO \rightarrow $\tilde{X}^3\Sigma^-$ NH + $\tilde{X}^1\Sigma^+$ CO				
RHF	45.07	46.25
UHF (PUHF)	40.60 (38.43)	41.42 (39.10)	43.25 (40.90)	43.41
UMP2 (PMP2)	87.36 (85.97)	91.40 (89.90)	97.11 (95.60)	98.11
UMP3 (PMP3)	75.15 (74.33)	77.64 (76.77)	83.74 (82.88)	...
CISD [CISD+(Q)] ^c	70.00 [73.08]	72.78 [75.90]
UMP4	79.32	83.38	89.77	...
UMP ∞ ^d	78.76	82.84	89.35	...
Method I prediction:		$D_e(\text{NH-CO}) = 92 \pm 2$ kcal mol ⁻¹		
\tilde{X}^1A' CH ₂ CO \rightarrow \tilde{X}^3B_1 CH ₂ + $\tilde{X}^1\Sigma^+$ CO				
UHF (PUHF)	40.75 (39.10)	40.96 (39.23)	42.20 (40.46)	
UMP2 (PMP2)	75.50 (74.40)	79.59 (78.44)	83.90 (82.74)	
UMP3 (PMP3)	71.12 (70.45)	73.89 (73.19)	78.42 (77.73)	
UMP4	72.12	75.95	80.78	
UMP ∞ ^d	71.71	75.54	80.46	
Experiment ^e		$D_e(\text{CH}_2\text{-CO}) = 83.0$ kcal mol ⁻¹		

^aDetermined at the optimum DZ(d,p) CISD (supermolecule) geometries in Table I.

^bThe DZ(d,p) values were determined in this study; the QZ(2 $d,2p$) and QZ(2 $d1f,2p1d$) results are from Allen and Schaefer (Ref. 214), who used slightly different polarization function exponents than those used here. The reference geometries are the optimum DZP CISD (supermolecule) structures reported in Ref. 214.

^cTotal energies for \tilde{X}^1A' HNCO: QZ(2 $d,2p$) CISD(-168.315 451), CISD+(Q) (-168.369 871). Supermolecule energies for $\tilde{X}^3\Sigma^-$ NH + $\tilde{X}^1\Sigma^+$ CO: QZ(2 $d,2p$) CISD(-168.199 469), CISD+(Q) (-168.248 917).

^dExtrapolations of the MP n series based on Eq. (16a).

^eSee the text.

increase in $D_e(\text{CH}_2\text{-CO})$ is only 2 kcal mol⁻¹ with the larger basis sets, and the effect of higher angular momentum functions is smaller, viz. 4.8 kcal mol⁻¹ at the MP4 level. Comparison of the QZ(2 $d1f,2p1d$) UMP4 result for $D_e(\text{CH}_2\text{-CO})$ with the experimental dissociation energy yields a correction term of +2.2 kcal mol⁻¹, and a final prediction of $D_e(\text{NH-CO}) = 92 \pm 2$ kcal mol⁻¹ is obtained for Method I.

The total energies involved in the application of Method II are given in Tables III and IV, and in Table VII energy differences for reaction (17) are tabulated. With the DZ(d,p) basis set, the (E_2, E_3, E_4) sets of perturbation energies (in hartree) are as follows: H₂O(-0.1968, -0.0059, -0.0060), NH₃(-0.1877, -0.0130, -0.0056),

TABLE VII. Reaction energies (ΔE_e , kcal mol⁻¹) for HNCO + H₂O \rightarrow CO₂ + NH₃.^a

	DZ(d,p)	QZ(2 $d,2p$)	QZ(2 $d1f,2p1d$)	PZ(3 $d2f,2p1d$)
$\Delta[\text{RHF}]$	-24.95	-23.98	-24.04	-23.85
$\Delta[E_2]$	+0.91	+2.08	+2.39	+2.63
$\Delta[E_3]$	+0.77	+0.70	+0.66	...
$\Delta[E_4(\text{SDTQ})]$	-1.25	-1.40	-1.34	...
$\Delta\epsilon^b$	-0.13	-0.16	-0.15	
$\Delta[\text{MP4}]$	-24.52	-22.60	-22.33	
Method II predictions:	$\Delta E_e = -21.9$ kcal mol ⁻¹			
	$\Delta H_0^{\circ}(17) = -20.1$ kcal mol ⁻¹			
	$\Delta H_{f,0}^{\circ}(\text{HNCO}) = -26.1$ kcal mol ⁻¹			
	$D_e(\text{NH-CO}) = 91.0$ kcal mol ⁻¹			

^aBased on the total energies in Tables III and IV.

^bResidual correlation error estimated as $\epsilon = \text{MP}\infty - \text{MP4}$ via Eq. (16a).

HNCO(-0.4592, +0.0053, -0.0342), and CO₂(-0.4668, +0.0136, -0.0366). The cancellations in the contributions to the reaction energy arising at each order from the isoelectronic pairs of reactants and products are very apparent. This occurrence is representative of the data for all entries in Table VII, where the net correlation contributions to ΔE_e do not exceed 2 kcal mol⁻¹. The reactants, which exhibit more highly polarized charge distributions than the products, are preferentially favored as the flexibility of the basis set is increased, and modest changes in the $\Delta[\text{RHF}]$ and $\Delta[E_2]$ results arise even from the QZ(2 $d1f,2p1d$) \rightarrow PZ(3 $d2f,2p1d$) augmentation. As in the case of the barrier to linearity, the convergence of the higher-order $\Delta[E_n]$ contributions appears to be much more rapid than for $\Delta[E_2]$. Further basis set expansion is likely to continue to reduce the reaction exoergicity, but residual correlation errors may well compensate for such shifts (n.b. the $\Delta\epsilon$ entries in Table VII). A final prediction of $\Delta E_e(17) = -21.9$ kcal mol⁻¹ is engendered by adding the nearly converged QZ(2 $d1f,2p1d$) $\Delta[E_3]$ and $\Delta[E_4]$ values to the PZ(3 $d2f,2p1d$) MP2 result.

To complete the evaluation of $\Delta H_{f,0}^{\circ}(\text{HNCO})$ and $D_0(\text{NH-CO})$ via Method II, accurate zero-point vibrational energies (ZPVEs) were determined according to the formula

$$\text{ZPVE} = \frac{1}{2} \sum_i d_i \nu_i - \frac{1}{2} \sum_i d_i \chi_{ii} \left(d_i + \frac{1}{2} \right) - \frac{1}{4} \sum_{i>j} d_i d_j \chi_{ij} - \frac{1}{2} \sum_i d_i \chi_{ii} \quad (18)$$

where ν_i and d_i represent the fundamental frequency and the degeneracy of mode i , respectively, and the χ_{ij} quantities are anharmonic constants given by standard formulas.^{132,134} The last term in Eq. (18), which appears as a result of vibrational angular momentum contributions to degenerate fundamental frequencies, is present only in the CO₂ and NH₃ cases. Terms analogous to the Y_{00} Dunham coefficient for diatomic molecules also contribute to the ZPVE as well as constants arising from vibration-rotation interaction, but the limited available evidence¹⁶⁹ indicates that these contributions tend to cancel one another and are only of the order of 20 cm⁻¹ for molecules such as those considered here. Equation (18) is particularly useful in that it allows experimental fundamental frequencies to be utilized in conjunction with χ_{ij} constants determined either empirically or theoretically. By this approach the following ZPVE values (in cm⁻¹) are found: CO₂(2531), H₂O(4634), HNCO(4675), NH₃(7410), CO(1082), and NH(1622).¹⁷⁰ Accordingly, in units of kcal mol⁻¹ the predicted ΔH_0° for reaction (17) is -20.1, and subsequently $\Delta H_{f,0}^\circ(\text{HNCO}) = -26.1$ is ascertained from the known $\Delta H_{f,0}^\circ$ values¹⁷¹ of NH₃(-9.30 ± 0.1), CO₂(-93.97 ± 0.01), and H₂O(-57.10 ± 0.01). Finally, $D_e(\text{NH-CO}) = 91.0$ kcal mol⁻¹ is found from $\Delta H_{f,0}^\circ$ of NH(86.5),¹⁵⁴ CO(-27.20 ± 0.04),¹⁷¹ and HNCO after appending a ZPVE correction of 1971 cm⁻¹. This N=C bond energy is intermediate between the observed C=C value of ketene ($D_e = 83.0$ kcal mol⁻¹, *vide supra*) and C=O value of carbon dioxide ($D_e = 129.9$ kcal mol⁻¹).¹⁷²

The $D_e(\text{NH-CO})$ values given by Methods I and II agree to 1 kcal mol⁻¹. Because the uncertainties involved in the latter case are smaller in magnitude, the Method II predictions in Table VII constitute the final proposals made here, to which error bars of ca. 1 kcal mol⁻¹ are to be associated. Thus the accuracy of the thermochemical data obtained by Spiglanin, Perry, and Chandler⁴⁰ is in large part confirmed over the earlier results of Okabe,⁴¹ although revisions in $D_e(\text{NH-CO})$ and $\Delta H_{f,0}^\circ(\text{HNCO})$ of approximately 1.5 kcal mol⁻¹ are suggested. Germane to these revisions, the threshold for NH($\tilde{a}^1\Delta$) production (41 530 cm⁻¹) obtained by Spiglanin *et al.* from an extrapolation of the HNCO photolysis efficiency curve was, in fact, 970 cm⁻¹ lower than an alternate limit given by extrapolating to zero the excess NH($\tilde{a}^1\Delta$) rotational energy appearing in photolysis up to 52 295 cm⁻¹. As mentioned in the original analysis, a resolution to this discrepancy is achieved by assuming that the lower-energy threshold is due to photolysis of rotationally and vibrationally excited molecules, since $kT \approx 200$ cm⁻¹ in the experiments and three vibrational modes of HNCO are active below 800 cm⁻¹. Therefore, the data of Spiglanin *et al.* are actually consistent with a final D_e result for \tilde{X}^1A' HNCO → $\tilde{X}^3\Sigma^-$ NH + $\tilde{X}^1\Sigma^+$ CO ranging upward from 88.5 to 91.3 kcal mol⁻¹. The *ab initio* predictions reported here favor a value near the upper limit of this range.

D. Dissociation energy for \tilde{X}^1A' HNCO → \tilde{X}^2S H + $\tilde{X}^2\Pi$ NCO

Although the NCO/NH product branching ratio for the photodissociation of isocyanic acid at 193 nm is less than 0.10, the dissociation channel HNCO → H(²S) + NCO(²Π_g) is actually favored energetically over that of NH($\tilde{a}^1\Delta$) + CO. The cyanato radical has a ²Π electronic ground state with a ²Π_{1/2}-²Π_{3/2} spin-orbit splitting parameter of 95.6 cm⁻¹; the $\tilde{A}^2\Sigma^+$ state lies adiabatically 22 754 cm⁻¹ higher in energy.¹⁷³ The value advanced by Okabe⁴¹ in 1970 for the energy required to generate NCO(²Π) via HNCO photolysis is $D_0(\text{H-NCO}) = 113.0 \pm 0.2$ kcal mol⁻¹, which is 7.0 kcal mol⁻¹ below the threshold for NH($\tilde{a}^1\Delta$) + CO production according to the revised $\Delta H_{f,0}^\circ(\text{HNCO})$ proposed here. This bond energy is, nevertheless, much greater than the corresponding bond strength in HN₃ ($D_0 = 87$ kcal mol⁻¹)¹⁷⁴ and in fact exceeds the dissociation energy in ammonia ($D_0 = 105.8$ kcal mol⁻¹).¹⁷⁵ Careful theoretical scrutiny of this quantity is warranted, particularly because it provides a means to ascertain the heat of formation of NCO. Several results for $\Delta H_{f,0}^\circ(\text{NCO})$ in the range 36–44 kcal mol⁻¹ have been considered viable in recent investigations,¹⁷⁶ and uncertainty regarding the precise value has hampered the interpretation of some experiments.¹⁷⁷

In this section the N-H bond energy in HNCO is predicted by two independent methods as before. In Method I the dissociation energy $D_e(\text{H-NCO})$ is computed directly, as in the case of $D_e(\text{HN-CO})$, whereas in Method II the energy for the isogyric process



is evaluated theoretically and then shifted using the experimental ionization potential of H (13.598 eV)¹⁷⁸ and electron affinity of NCO (3.6 ± 0.2 eV).^{179,180} The optimum DZ(d,p) CISD reference structures for the single-point energy determinations are given in Table I; the H + NCO and H⁺ + NCO⁻ supermolecule geometries are actually identical to those predicted for NCO and NCO⁻ separately, because in each case fragmentation yields only one product with correlation energy. The optimum CISD distances should represent noticeable improvements over other recent predictions. Total energies for all closed- and open-shell species of concern appear in Tables III, IV, and V and appurtenant footnotes, and the data for the dissociation energy $D_e(\text{H-NCO})$ are presented in Table VIII.

The one-particle basis set and correlation requirements for the quantitative description of a sigma bond cleavage alone are generally less severe than those encountered for multiple bonds, a fact which aids the Method I evaluation of $D_e(\text{H-NCO})$ relative to that of $D_e(\text{HN-CO})$. However, the extensive spin contamination in the UHF reference wave functions of the doublet NCO radical encumbers the procedure. The DZ(d,p) RHF → UHF lowering of $D_e(\text{H-NCO})$ is 6.3 kcal mol⁻¹, a magnitude commensurate with that observed for $D_e(\text{HN-CO})$, but the expectation value of $S^2(\text{NCO})$ is 0.09 units too high (n.b. footnote c of Table V). At the RHF, MP2, and MP3 levels, the projection

TABLE VIII. Energy differences (Δ , kcal mol⁻¹) for the dissociation \tilde{X}^1A' HNCO \rightarrow \tilde{X}^2 SH + $\tilde{X}^2\Pi$ NCO.^a

	DZ(<i>d,p</i>) ^b	QZ(2 <i>d,2p</i>)	QZ(2 <i>d1f,2p1d</i>)	PZ(3 <i>d2f,2p1d</i>)/ QZ(+)(2 <i>d1f,2p1d</i>) ^c
Method I-direct evaluation				
Δ [UHF] (δ PUHF) ^d	88.06 (-7.24)	87.60 (-7.00)	87.63 (-7.03)	87.79
Δ [<i>E</i> ₂ (UMP2)] (δ PMP2) ^d	+31.03 (-5.74)	+33.90 (-5.53)	+35.63 (-5.54)	+36.20
Δ [<i>E</i> ₃ (UMP3)] (δ PMP3) ^d	-7.20 (-3.67)	-7.74 (-3.52)	-7.73 (-3.50)	...
Δ [<i>E</i> ₄ (SDTQ)]	+3.17	+3.85	+3.82	...
$\Delta\epsilon^e$	-0.25	-0.26	-0.23	...
Δ [UMP4(SDTQ)]	115.06	117.61	119.35	...
Method II-from the isogyric reaction HNCO \rightarrow H ⁺ + NCO ⁻¹				
Δ [RHF]	122.07	120.95	120.51	119.84
Δ [MP2]	121.03	117.20	118.76	115.35
Δ [MP3]	123.62	120.61	121.08	119.12
Δ [MP4(SDTQ)]	123.96	119.47	120.99	117.47

^aDetermined at optimum DZ(*d,p*) CISD geometries in Table I. The 96 cm⁻¹ spin-orbit splitting of the ² Π states of NCO is not accounted for in the theoretical predictions.

^bAdditional DZ(*d,p*) predictions for the dissociation energy: RHF (94.32), CISD (109.16), and CISD+(Q) (110.18).

^cPZ(3*d2f,2p1d*) for Method I, and QZ(+)(2*d1f,2p1d*) for Method II.

^d δ PUHF and δ PMPn refer to the additional contributions to the bond energy arising from differential spin contamination effects. Specifically, δ PUHF = Δ [PUHF] - Δ [UHF] and δ PMPn = Δ [*E*_n(PMPn)] - Δ [*E*_n(UMPn)].

^eResidual correlation error estimated as $\epsilon = \text{MP}_\infty - \text{MP}_4$ via Eq. (16a).

^fObtained by adding an empirical shift of -230.56 kcal mol⁻¹ to the theoretical reaction energies of Eq. (19).

scheme for spin contamination in the separated NCO radical leads to reductions of $D_e(\text{H-NCO})$ in Table VIII of approximately 7.0, 5.5, and 3.5 kcal mol⁻¹, respectively. If the H+NCO system is treated as a triplet supermolecule, the analogous lowerings are 5.4, 4.3, and 2.7 kcal mol⁻¹ with the DZ(*d,p*) basis. Thus a PMP correction of roughly -2 kcal mol⁻¹ is surmised for the UMP4 predictions.

The net correlation contribution of ca. 30 kcal mol⁻¹ to the N-H bond energy constitutes about one fourth of the total value, which is 119.35 kcal mol⁻¹ at the QZ(2*d1f,2p1d*) UMP4 level. The convergence of the Δ [*E*_n] terms appears to be quite rapid in Table VIII, although the previous documentation of vagaries in the behavior of UMP expansions gives reason for caution in cases of large spin contamination.^{109,181} In this regard, comparative bond energy data for H₂O proves useful in gauging the accuracy of the $D_e(\text{H-NCO})$ predictions. With the QZ(2*d1f,2p1d*) basis set, the following contributions (kcal mol⁻¹) to $D_e(\text{H-OH})$ are found (total PMP corrections at each order in parentheses):¹⁸² Δ [UHF]=87.19 (-2.04), Δ [*E*₂]=+39.35 (-1.17), Δ [*E*₃]=-5.31 (-0.64), and Δ [*E*₄]=+2.91. The similarity of the successive Δ [*E*_n] terms for HNCO and H₂O is remarkable. The net UMP4 result for $D_e(\text{H-OH})$ is 124.14 kcal mol⁻¹, which is to be compared to the experimental bond strength of 125.9 kcal mol⁻¹. These H₂O data then suggest a 1.8 kcal mol⁻¹ increase in the QZ(2*d1f,2p1d*) UMP4 prediction for $D_e(\text{H-NCO})$ to account for basis set deficiencies and other effects mentioned in Sec. III C. However, the differential spin contamination error at fourth order between HNCO and H₂O (roughly -2 kcal mol⁻¹) largely cancels this correction. In sum, the $D_e(\text{H-NCO})$ theoretical data for Method I are consistent with a dissociation energy of 119 \pm 2 kcal mol⁻¹.

The Method II values given in Table VIII for the N-H bond energy scatter in the range 115-121 kcal mol⁻¹ for

all basis sets larger than DZ(*d,p*). The reduction of the correlated predictions for $D_e(\text{H-NCO})$ by 2.0-3.5 kcal mol⁻¹ upon the addition of diffuse functions to the QZ(2*d1f,2p1d*) basis is the most significant variation displayed in the list. As expected, the differential correlation energy effect associated with the isogyric reaction (19) is very small. The QZ(+)(2*d1f,2p1d*) MP4 result of 117.5 kcal mol⁻¹ is in good agreement with the final Method I prediction, especially considering the 4.6 kcal mol⁻¹ uncertainty present in the experimental electron affinity.

For comparison with the theoretical predictions, the $D_0(\text{H-NCO})$ value of Okabe⁴¹ must be corrected for ZPVE variations. A zero-point vibrational energy of 4675 cm⁻¹ was readily determined above for HNCO, but the corresponding value for NCO is a subtle quantity to establish because the ground electronic state exhibits not only spin-orbit coupling but also the Renner-Teller effect. According to the gas-phase spectroscopic constants of Dixon,¹⁷³ a manifold of NCO vibronic band origins between 400 and 650 cm⁻¹ arises from a single quantum of excitation in the bending mode: ² Σ^+ (441 cm⁻¹), ² $\Delta_{5/2}$ (534 cm⁻¹), ² $\Delta_{3/2}$ (628 cm⁻¹), and ² Σ^- (637 cm⁻¹). Simple models of the vibronic structure of such systems yield a ² Σ^- -² Σ^+ separation of $(4\omega_2^2\epsilon^2 + A^2)^{1/2}$, where A is the spin-orbit splitting parameter, ω_2 is the reference harmonic bending frequency, and ϵ relates ω_2 to the effective vibrational frequencies (ω_2^\pm) of the Renner-Teller split bending potentials, i.e., $\omega_2^\pm = \omega_2(1 \pm \epsilon)$. In the gas-phase analysis of Dixon, ω_2 is found to be 539 cm⁻¹, neglecting the small anharmonicity in the NCO bending mode. By approximating the ZPVE of NCO as $2^{-1}(\nu_1 + 2\omega_2 + \nu_3) - 4^{-1}(3\chi_{11} + \chi_{31} + 3\chi_{33})$, a value of 2201 cm⁻¹ is computed if the stretching fundamentals and associated anharmonic constants are taken from the matrix isolation study of Bondybey.¹⁸³ Applying the resulting ZPVE correction to the experimental N-H bond energy gives $D_e(\text{H-NCO})$

$=120.1 \pm 0.2$ kcal mol $^{-1}$. The validity of this dissociation energy is clearly confirmed by the agreement with the Method I prediction of 119 ± 2 kcal mol $^{-1}$ and the Method II limits of 117.5 ± 4.5 kcal mol $^{-1}$. Its adoption is recommended. Consequently, from our revised $\Delta H_{f,0}^\circ(\text{HNCO})$ value, 35.3 kcal mol $^{-1}$ is found for $\Delta H_{f,0}^\circ(\text{NCO})$, which lies 1–2 kcal mol $^{-1}$ below the lower set of values employed in recent studies.¹⁷⁶

E. Heats of formation of isomers of HNCO

A dearth of accurate information exists concerning the heats of formation of HOCN, HCNO, and HONC, despite many years of investigations into their chemical properties. Experimental $\Delta H_{f,0}^\circ$ values are simply not available. In the literature the relative energies predicted by levels of theory varying from 4–31G SCF to 6–31G** MRD-CI fall into the following ranges: HOCN (17–25 kcal mol $^{-1}$), HCNO (67–83 kcal mol $^{-1}$), and HONC (73–92 kcal mol $^{-1}$), assuming isocyanic acid as the reference.^{36–39,149} In this section these isomerization energies are established to within 2 kcal mol $^{-1}$, and subsequently heats of formation are proposed on the basis of our revised value of $\Delta H_{f,0}^\circ(\text{HNCO})$.

In Table III total energies of isocyanic acid and its three higher-lying isomers are given, including RHF through MP4 values for the DZ(d,p), QZ(2*d*,2*p*), and QZ(2*d*1*f*,2*p*1*d*) basis sets, RHF and MP2 results for the PZ(3*d*2*f*,2*p*1*d*) set, and QZ(2*d*1*f*,2*p*1*d*) predictions at the CCSD and CCSD(T) levels. The reference geometries for the single-point energy determinations were chosen from various sources: the DZ(d,p) CISD optimum parameters for HNCO (Table I), the 6–31G** MP2 structures of Teles *et al.*³⁶ for HOCN and HONC, and the TZ2P CCSD(T) linear geometry of Rendell and co-workers¹⁸⁴ for HCNO. In the case of fulminic acid (HCNO), the question of whether the equilibrium structure exhibits a linear or bent H–C–N angle is an area of active research. Predictions from various levels of theory, even very sophisticated ones, have differed on this issue, but the latest and most reliable data obtained with the CCSD(T) method using large atomic natural orbital basis sets strongly indicate an optimum linear configuration.¹⁸⁴ In determining $\Delta H_{f,0}^\circ(\text{HCNO})$, the point is of limited significance because the energy variations resulting from bending the H–N–C angle by up to 30° are only about 0.5 kcal mol $^{-1}$ in those cases where a nonlinear minimum is predicted.^{36,184} The flatness of the bending potential is manifested in the semi-rigid bender analysis of the rovibrational energy levels of fulminic acid by Bunker, Landsberg, and Winnewisser,¹⁸⁵ in which a prodigious bending amplitude of 34° was found in the ground vibrational state.

In Fig. 4 a plot is given of the various isomerization energies, γ_e , obtained with the QZ(2*d*1*f*,2*p*1*d*) basis. Analogous plots for the DZ(d,p) and QZ(2*d*,2*p*) basis sets can be constructed from the data in Table III, but these are not displayed here because the variations observed upon improvement of the correlation treatment are nearly identical. For HOCN and HONC the QZ(2*d*1*f*,2*p*1*d*) relative energies are generally larger than their DZ(d,p) and

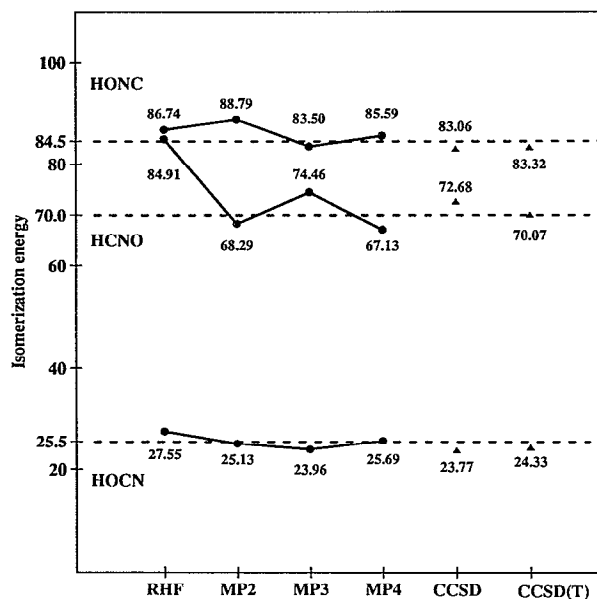


FIG. 4. A plot of the relative energies (γ_e , kcal mol $^{-1}$) of the isomers of HNCO obtained at several levels of theory with the QZ(2*d*1*f*,2*p*1*d*) basis set. In the CCSD and CCSD(T) predictions the supernumerary *s* orbitals were excluded from the *d* sets (see footnote *e* of Table III). The effect of this basis set modification on the isomerization energies is minuscule, as the resulting RHF γ_e values of 27.55, 84.87, and 86.64 kcal mol $^{-1}$ for HOCN, HCNO, and HONC, respectively, differ by 0.1 kcal mol $^{-1}$ or less from the RHF entries in the figure.

QZ(2*d*,2*p*) counterparts, while in the HCNO case the opposite is found. These trends toward larger $\gamma_e(\text{HOCN})$ and $\gamma_e(\text{HONC})$ results but smaller $\gamma_e(\text{HCNO})$ predictions appear to be maintained as the one-particle basis set limit is approached (*vide infra*). Nonetheless, all of the DZ(d,p) RHF and MP n predictions lie within 3 kcal mol $^{-1}$ of the QZ(2*d*1*f*,2*p*1*d*) values, and in the QZ(2*d*,2*p*) case the largest difference is less than 1.5 kcal mol $^{-1}$.

In Fig. 4 the convergence of the QZ(2*d*1*f*,2*p*1*d*) MP n entries for HOCN and HONC appears to be quite rapid. In units of kcal mol $^{-1}$ the variations in successive MP n values do not exceed 5.6, and in particular the respective MP4–MP3 differences for HOCN and HONC are only 1.7 and 2.1. The coupled-cluster data provide a complementary view of the higher-order correlation contributions to the relative energies. For both HOCN and HONC, the CCSD and CCSD(T) results lie below the MP4 values by 1.0–2.6 kcal mol $^{-1}$. A confluence of QZ(2*d*1*f*,2*p*1*d*) relative energy predictions near $\gamma_e(\text{HOCN})=25$ and $\gamma_e(\text{HONC})=84$ kcal mol $^{-1}$ seems likely as the full CI limit is approached. A useful indication of the remaining one-particle basis set errors contained in these results is provided by the PZ(3*d*2*f*,2*p*1*d*) RHF and MP2 relative energies, which are, in order, 27.74 and 25.60 kcal mol $^{-1}$ for HOCN, and 86.89 and 89.10 kcal mol $^{-1}$ for HONC (cf. Fig. 4). Thus basis set enlargement past QZ(2*d*1*f*,2*p*1*d*) continues to preferentially lower the energy of isocyanic acid relative to cyanic and isofulminic acid. By considering these basis set trends as well as possible geometry relaxation effects,¹⁸⁶ $\gamma_e(\text{HOCN})=25.5 \pm 1.0$ and $\gamma_e(\text{HONC})=84.5 \pm 1.5$ kcal

TABLE IX. Reaction energies (ΔE_e , kcal mol⁻¹) for HCNO + NH₃ → N₂O + CH₄.^a

	DZ(<i>d,p</i>)	QZ(2 <i>p</i> ,2 <i>p</i>)	QZ(2 <i>d</i> 1 <i>f</i> , 2 <i>p</i> 1 <i>d</i>)	PZ(3 <i>d</i> 2 <i>f</i> , 2 <i>p</i> 1 <i>d</i>)
Δ[RHF]	-30.13	-31.02	-31.34	-31.11
Δ[E ₂]	-3.04	-1.04	+0.02	+0.61
Δ[E ₃]	+3.28	+2.83	+3.03	...
Δ[E ₄ (SDTQ)]	-3.77	-4.03	-4.04	...
Δ[MP4]	-33.66	-33.26	-32.33	
Method II predictions:	$\Delta E_e = -30.2$ kcal mol ⁻¹ $\Delta H_{f,0}^{\circ}(\text{HCNO}) = 30.5 + \text{ZPVE}(\text{HCNO})$ kcal mol ⁻¹			

^aBased on the total energies in Tables III and IV.

mol⁻¹ are advanced as final proposals. Previous *ab initio* values for $\gamma_e(\text{HOCN})$ are somewhat smaller due primarily to basis set deficiencies.

From the data in Fig. 4 it is apparent that establishing a precise relative energy of fulminic acid is an arduous undertaking. The MP*n* predictions of $\gamma_e(\text{HCNO})$ exhibit large oscillations which diminish very slowly; n.b. the MP3–MP4 shift is still over 7 kcal mol⁻¹. Under these circumstances the QZ(2*d*1*f*,2*p*1*d*) CCSD(T) result of 70.07 kcal mol⁻¹, which lies almost halfway between the MP3 and MP4 values, must be regarded as the most reliable prediction. The PZ(3*d*2*f*,2*p*1*d*) RHF and MP2 relative energies of HNCO are 84.85 and 68.08 kcal mol⁻¹, respectively; hence, basis set enlargement past QZ(2*d*1*f*,2*p*1*d*) is expected to slightly lower the predicted isomerization energies of fulminic acid.

Because $\gamma_e(\text{HCNO})$ cannot be deduced reliably from the direct predictions (Method I) in Fig. 4 alone, this quantity was also evaluated indirectly (Method II) via the reaction



which consists of isoelectronic pairs of reactants and products as in the case of Eq. (17). Total energies for the auxiliary molecules involved in this reaction are given in Table IV, and the theoretical reaction energies are presented in Table IX. As seen therein, the net differential correlation effect on the exoergicity of Eq. (20) is small, even though the success of the procedure is somewhat mitigated relative to the analysis based on Eq. (17) in that the series of $\Delta[E_n]$ values is not as rapidly convergent. In particular, the cancellation of the perturbation energy contributions for the (HCNO, N₂O) isoelectronic pair is less complete, as exemplified by the corresponding DZ(*d,p*) (*E*₂, *E*₃, *E*₄) sets (in hartree): HCNO(-0.4834, 0.0138, -0.0440) and N₂O(-0.5140, 0.0259, -0.0501). Nevertheless, the $\Delta[E_3]$ and $\Delta[E_4]$ partitions of the reaction exoergicity appear to be essentially converged at the QZ(2*d*1*f*,2*p*1*d*) level, and appending these contributions to the PZ(3*d*2*f*,2*p*1*d*) MP2 result yields a preliminary value of $\Delta E_e(20) = -31.5$ kcal mol⁻¹. In this case, the exoergicity should properly be modified by a correction for correlation contributions past fourth order. Thus DZ(*d,p*) MP5 energies and [2,1] Padé approximants of MP_∞ limits

were obtained for the species in Eq. (20), giving reaction energies of -31.60 and -32.37 kcal mol⁻¹, respectively. The Padé approximants suggest that the MP4 values for $\Delta E_e(20)$ are ca. 1.3 kcal mol⁻¹ too large in magnitude, whence a final prediction of $\Delta E_e(20) = -30.2$ kcal mol⁻¹ is engendered, as shown in Table IX.

The accepted $\Delta H_{f,0}^{\circ}$ values of N₂O, CH₄, and NH₃ are 20.43 ± 0.1, -15.99 ± 0.08, and -9.30 ± 0.1 kcal mol⁻¹, respectively,¹⁷¹ and the zero-point vibrational energies given by Eq. (18) for these molecules are (in cm⁻¹) N₂O(2365),¹⁸⁷ CH₄(9758),¹⁸⁸ and NH₃(7410).¹⁷⁰ Using these data in conjunction with the predicted $\Delta E_e(20)$, the following relation for the heat of formation of fulminic acid is found: $\Delta H_{f,0}^{\circ}(\text{HCNO}) = 30.5$ kcal mol⁻¹ + ZPVE(HCNO). Subsequently, from $\Delta H_{f,0}^{\circ}(\text{HNCO}) = -26.1$ kcal mol⁻¹ and ZPVE(HNCO) = 4675 cm⁻¹ (*vide supra*), one arrives at $\gamma_e(\text{HCNO}) = 70.0$ kcal mol⁻¹, a value in excellent agreement with the directly determined QZ(2*d*1*f*,2*p*1*d*) CCSD(T) result of 70.1 kcal mol⁻¹. In summary, a final $\gamma_e(\text{HCNO})$ energy of 70 ± 2 kcal mol⁻¹ is proposed as a value consistent not only with the directly determined CCSD(T) result but also with the thermochemical analysis based on Eq. (20).

There are insufficient data at present to determine precise zero-point vibrational contributions to the isomerization energies of HNCO, because the set of gas-phase fundamental frequencies is not complete and complexities arise in the case of HCNO due to the quasilinear nature of the bending vibrations. However, from the 6-31G** MP2 harmonic frequencies of Teles *et al.*,³⁶ ZPVE corrections of -0.14, -0.93, and -0.73 kcal mol⁻¹ are predicted for $\gamma_e(\text{HOCN})$, $\gamma_e(\text{HCNO})$, and $\gamma_e(\text{HONC})$, respectively. The ZPVE effects on the isomerization energies thus appear to be quite small, and the 6-31G** MP2 estimates should be of sufficient accuracy to allow heats of formation to be evaluated. The isomerization energies recommended above then lead to the following $\Delta H_{f,0}^{\circ}$ values in kcal mol⁻¹: HOCN (-0.7 ± 1.0), HCNO (43.0 ± 2), and HONC (57.6 ± 1.5), for which uncertainty in the reference value, $\Delta H_{f,0}^{\circ}(\text{HNCO}) = -26.1$ kcal mol⁻¹, is not included in the error estimates.

The final thermochemical data obtained here for the CHNO isomers are summarized in Fig. 5 and characterized therein by comparison with the heats of formation of numerous low-lying fragmentation products. All four of the CHNO isomers are seen to lie below the most thermodynamically stable pair of fragments, NH(³Σ⁻) + CO, in the case of HONC by less than 2 kcal mol⁻¹, however. The most favorable direct dissociation channel of both HNCO and HOCN is to H + NCO(²Π), requiring 113 and 87 kcal mol⁻¹, respectively. In the case of fulminic acid, the N–O bond dissociation products HCN + O(³P) lie only 48 kcal mol⁻¹ higher in energy than the parent molecule, but the analogous spin-conserving process yielding HCN + O(¹D) involves 94 kcal mol⁻¹. Unlike the other three isomers, the preferred direct dissociation pathway of iso-fulminic acid involves two diatomic fragments, OH(²Π) + CN(²Σ⁺), which are 55 kcal mol⁻¹ higher in energy. Finally, in characterizing the ground-state surface on

Heats of Formation ($\Delta H_{f,0}^\circ$) of CHNO Isomers and Associated Fragments		
C(3P) + HNO	(+194.5)	
H + CNO($^2\Pi$)	(ca. 154.)	CH($^2\Pi$) + NO($^2\Pi$) (+163.0)
H + NCO($^2\Sigma^+$)	(+151.9)	
O(1D) + HNC	(+151.1)	
O(1D) + HCN	(+136.7)	
N(4S) + HCO($^2A'$)	(+122.7)	NH($^1\Sigma^+$) + CO (+119)
O(3P) + HNC	(+105.8)	OH($^2\Pi$) + CN($^2\Pi$) (+112.4)
O(3P) + HCN	(+91.4)	NH($^1\Delta$) + CO (+94.1)
H + NCO($^2\Pi$)	(+86.8)	
	HONC (+57.5)	NH($^3\Sigma^-$) + CO (+58.1)
	HCNO (+42.9)	
	HO CN (-0.3)	
	HNCO (-26.2)	

FIG. 5. Thermochemical data for CHNO species. The entries for the tetraatomic molecules are derived in the text. The $\Delta H_{f,0}^\circ$ values for the ground electronic states of HCN, HCO, HNO, CO, NO, OH, CH, O, C, N were taken from Ref. 171. Additional data sources were used to obtain ground-state heats of formation for NH (Ref. 154), HNC (Refs. 217, 218), CN (Ref. 45), and CNO (Ref. 180). The relative energies for excited-state species were computed from established T_0 values for O(1D) (Ref. 178), NH($^1\Delta, ^1\Sigma^+$) (Ref. 152), CN($^2\Pi$) (Ref. 152), and NCO($^2\Sigma^+$) (Ref. 173).

which the CHNO isomers lie, it is noteworthy that the barriers to isomerization are quite large, as found in the early, extensive *ab initio* investigation by Poppinger, Radom, and Pople³⁷ and more recently by Yokoyama *et al.*³⁹ The two most viable pathways connecting cyanic acid and fulminic acid to HNCO both involve a half-ring, oxazirine structure ($\overline{\text{HCON}}$), which appears to be a legitimate intermediate separated by a barrier of less than 5 kcal mol⁻¹ from the HNCO minimum lying 80 kcal mol⁻¹ lower in energy. The transition state involving the 1,2-hydrogen migration of HO CN to this intermediate is 100 kcal mol⁻¹ above isocyanic acid, whereas the critical configuration connecting HCNO to the oxazirine structure has the character of a loose complex of HCN + O(1D), perhaps 130 kcal mol⁻¹ higher than HNCO according to Fig. 5. The isomerizations of HONC involve an initial rearrangement to cyanic acid over a barrier of ca. 25 kcal mol⁻¹,³⁷ after which the interconversion pathways of HO CN become effective. The reverse of this process may contribute to the production of CN and OH fragments from the "direct" decomposition of HNCO at high temperatures.¹⁸⁹

F. Fundamental vibrational frequencies and anharmonic force fields of HNCO

The observed rotational constants of HNCO in the ground vibrational state are $A_0 = 30.638$ cm⁻¹, $B_0 = 0.3693$ cm⁻¹, and $C_0 = 0.3639$ cm⁻¹,⁴⁶ and thus this C_s symmetry

molecule lies very near the prolate symmetric-top limit. Consequently, the rovibrational energy levels can be expressed to a first approximation as

$$E^0(\mathbf{v}; K, J) = \sum_i \omega_i \left(v_i + \frac{1}{2} \right) + \sum_{i>j} \chi_{ij} \left(v_i + \frac{1}{2} \right) \left(v_j + \frac{1}{2} \right) + A^{\text{eff}}(\mathbf{v}, K) K^2 + B^{\text{eff}}(\mathbf{v}, K, \sigma) J(J+1), \quad (21)$$

where standard spectroscopic notation is assumed. The effective rotational constants appearing in this equation are given by

$$A^{\text{eff}}(\mathbf{v}, K) = A(\mathbf{v}, K) - \frac{1}{2} [B(\mathbf{v}, K) + C(\mathbf{v}, K)] \quad (22)$$

and

$$B^{\text{eff}}(\mathbf{v}, K, \sigma) = \frac{1}{2} [B(\mathbf{v}, K) + C(\mathbf{v}, K)] + \frac{1}{4} \delta_{K,1} \sigma [B(\mathbf{v}, K) - C(\mathbf{v}, K)], \quad (23)$$

in which the quantity σ is set to ± 1 depending on which levels of the asymmetrically split K doublets are of concern. Because the $A^{\text{eff}}(\mathbf{v}, K)$ constants for the HNCO molecule are unusually large, as K increases the separation between successive rotational levels rapidly becomes comparable to vibrational energy level spacings. Therefore, the energy states of this quasilinear molecule are best categorized as (\mathbf{v}, K) manifolds stacked with rotational levels $J \gg K$ which are characterized by a K -dependent rotational constant, B^{eff} , whose value is near 0.36 cm⁻¹.

The origins of the low-lying (\mathbf{v}, K) manifolds for HNCO, as reported by Yamada,⁵³ are depicted in Fig. 6. The general selection rules for electric-dipole transitions among the rovibrational levels in these stacks are $\Delta J = 0, \pm 1$ and $\Delta K = 0, \pm 1$, which are augmented by parity selection rules within the K doublets. At room temperature the populations of the rotational levels in the vibrational ground state up to $(K, J) = (6, 34)$ are sufficient to produce detectable absorptions in the infrared spectrum. The large number of allowed combination differences yields a morass of overlapping K subbands in the region of the low-frequency bending vibrations, and the complete bending fundamental bands span the ranges (in cm⁻¹) ν_4 (671–1057), ν_5 (433–598), and ν_6 (627–900). The infrared spectrum in the 400–1100 cm⁻¹ region is complicated further by strong Coriolis mixing of the zeroth-order wave functions $\psi(r; J, K, \sigma)$ for the fundamental levels ν_r , which can be analyzed approximately via the interaction matrix^{51,54}

	$\psi(4; J, K, \sigma)$	$\psi(5; J, K, \sigma)$	$\psi(6; J, K, \sigma')$
$\psi(4; J, K, \sigma)$	$E^0(4; K, J)$	0	$\xi_{46} K$
$\psi(5; J, K, \sigma)$	0	$E^0(5; K, J)$	$\xi_{56} K$
$\psi(6; J, K, \sigma')$	$\xi_{46} K$	$\xi_{56} K$	$E^0(6; K, J)$

(24)

The diagonal elements therein are given by Eq. (21), and the off-diagonal terms are related to the Coriolis constants, $\xi_{i6}^{(a)}$, for a -axis interaction according to

$$-\xi_{i6}^{(a)} = A_0 \xi_{i6}^{(a)} \left[\left(\frac{\omega_i}{\omega_6} \right)^{1/2} + \left(\frac{\omega_6}{\omega_i} \right)^{1/2} \right] \quad (25)$$

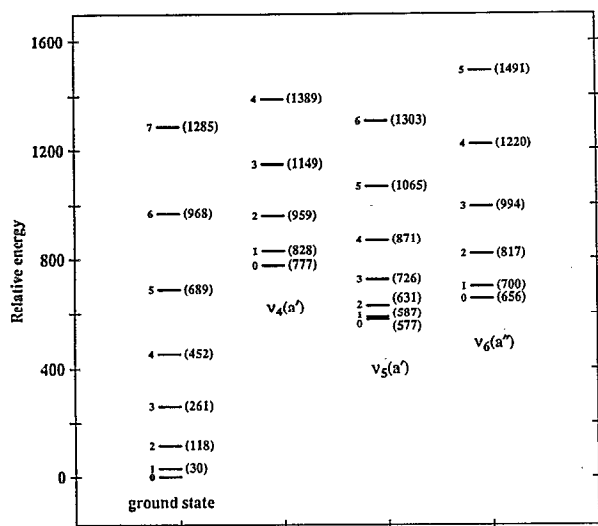


FIG. 6. Relative energies (cm^{-1}) for the origins of the low-lying (ν,K) manifolds of HNCO. Both the ground-state and bending fundamental stacks are depicted, as tabulated by Yamada (Ref. 53).

for $i=4$ and 5. Given the complexity of the 400–1100 cm^{-1} region, it is not surprising that there is a history of incorrect band assignments, as summarized in Table I of Ref. 51. Nevertheless, the band origins $\nu_4(a')=776.623 \text{ cm}^{-1}$ and $\nu_5(a')=577.346 \text{ cm}^{-1}$ are now well established as a consequence of the work by Steiner and co-workers.⁵¹ For ν_6 , these authors identified oQ_K subband centers only for $K=1-5$, and thus did not ascertain a precise value for the out-of-plane bending fundamental. Yet from the term value of 699.731 cm^{-1} determined by Yamada⁵³ for the $(J,K)=(1,1)$ level of the $\nu_6=1$ vibrational state as well as the $^R R_0$ pure rotational subband origin (43.444 cm^{-1}) for this excited state deduced by Fusina *et al.*⁵⁶ from far-infrared measurements, $\nu_6(a'')=656.287 \text{ cm}^{-1}$ is reliably calculated.¹⁹⁰

The fundamental absorption of isocyanic acid due to the N–C–O antisymmetric stretching mode, $\nu_2(a')$, appears as an intense band centered at 2268.89 cm^{-1} in the gas phase,^{191,192} while the analogous symmetric stretching fundamental, $\nu_3(a')$, occurs as a very weak band near 1327 cm^{-1} .⁵⁷ As in the case of CO_2 , the symmetric stretching fundamental is surely perturbed to some extent by Fermi resonance interactions with near-lying excited bending levels, specifically, $2\nu_6$ and $\nu_4+\nu_5$, although a detailed experimental analysis of this region has not been accomplished heretofore. For the N–H stretching fundamental, $\nu_1(a')$, the most recent data are those reported in 1990 by Yamada *et al.*,⁴⁶ who recorded over 700 transitions in the 3450–3700 cm^{-1} region and ascertained a definitive band origin of $3538.2498 \text{ cm}^{-1}$. The aforementioned K structure is prominent in the spectrum, and the data were analyzed by fits to individual K'_a substates from 0 to 5. The $K'_a=2$ and 4 sublevels of the $\nu_1=1$ manifold are doubled as a consequence of resonance interactions with two unidentified vibrational states. Thus a global fit of the data could not be achieved even with a Watson S -reduced effective rotational

Hamiltonian that included centrifugal distortion terms through fourteenth order.

A concerted effort to establish the anharmonic force field of HNCO and to address unresolved spectroscopic issues has been undertaken here. Quadratic, cubic, and quartic force constants were determined at various levels of theory with the $\text{DZ}(d,p)$ basis at both the corresponding optimum theoretical geometries and the experimental R_e structure. The latter was ascertained from empirical rotational constants with the aid of the *ab initio* cubic force fields (see Sec. III H below); the associated geometrical parameters are those listed in Table I for R_e structure I. Recent work by Allen and Császár¹⁹³ and previous studies by several other investigators^{194–196} have shown that the “correlation contribution” to higher-order force constants is almost entirely a geometry effect, i.e., the residual errors in uncorrelated higher-order force constants generally become minuscule when the reference geometry is shifted from the Hartree–Fock minimum to the proper experimental R_e structure. This observation can be exploited to obtain correlation-quality force fields using Hartree–Fock wave functions alone.

The principal drawback to this approach is that a subtle coordinate dependence is imparted to the potential energy surface on which the anharmonic force field is formally based whenever the reference structure is not a stationary point at the level of theory employed. This coordinate dependence is elucidated if the stepwise procedure for determining anharmonic spectroscopic constants at a nonstationary point is precisely defined: (1) The complete theoretical quartic force field is determined using an arbitrary set of internal coordinates at the selected reference geometry; (2) A nonlinear transformation of all potential energy derivatives from first to fourth order is performed to a specific set of internal coordinates on which the analysis is formally based. (3) The first derivatives of the potential energy surface are neglected in the chosen representation, while the quadratic, cubic, and quartic force constants are analytically transformed to the Cartesian space. (4) A normal coordinate analysis is carried out in the Cartesian space, and subsequently a final, linear transformation of the quartic force field to a reduced normal coordinate representation is performed. (5) Spectroscopic constants based on this normal coordinate force field are evaluated using standard formulas from second-order perturbation theory. The coordinate dependence in the procedure arises in Steps 2 and 3. In order to avert anomalies, the internal coordinates for the analysis must be chosen perspicaciously; specifically, a chemically meaningful set is required which does not exhibit singularities within the nuclear configuration space of concern.¹⁹³

For an open-chain tetratomic system $ABCD$, the most straightforward choice of internal coordinates consists of the three bond distances, the two valence bond angles, and the $A-B-C-D$ torsional angle. A singularity develops in this set, however, if either of the bond angles approaches 180° . The N–C–O framework in the equilibrium configuration of isocyanic acid deviates from linearity by 8° , which does not preclude the use of this coordinate set in Step 1 of

the procedure but makes this choice inappropriate for Steps 2 and 3. Therefore, the anharmonic analysis was based on the following internal coordinates: $S_1=r(\text{N-H})$, $S_2=2^{-1/2}[r(\text{C-O})-r(\text{N-C})]$, $S_3=2^{-1/2}[r(\text{C-O})+r(\text{N-C})]$, $S_4=\theta(\text{H-N-C})$, $S_5=\alpha_y(\text{N-C-O})$, and $S_6=\alpha_x(\text{N-C-O})$. In this improved set, α_x and α_y are the x and y components of the unit vector directed from C to O in the coordinate system in which the N-C bond defines the z axis and the H atom lies in the yz plane along the $+y$ direction. As such, α_x and α_y are dimensionless, N-C-O linear bending coordinates for which the bending planes are defined instantaneously by the molecular framework. Because both coordinates change sign in a continuous manner in traversing linear N-C-O configurations, singularities are eliminated. The geometrical derivatives of these coordinates required for nonlinear transformations of the associated force fields to other coordinate sets were derived using the relations $(\alpha_x, \alpha_y) = (\sin \rho \sin \tau, \sin \rho \cos \tau)$, where ρ denotes the N-C-O valence angle and τ the H-N-C-O torsional angle.

The quadratic force constants and harmonic frequencies obtained in this study by various methods are listed in Table X. The complete set of RHF cubic and quartic force constants are given in Tables XI and XII, as evaluated at both the RHF optimum geometry and the experimental R_e structure, these sets being denoted as RHF//RHF and RHF//expt., respectively. As expected, the RHF//RHF harmonic frequencies lie 8%–12% above the experimental fundamentals, except in the case of ω_5 , which is only 2.1% larger than the observed ν_5 band origin. The CISD//CISD frequencies ω_1 – ω_4 lie 3%–9% above their empirical ν_i counterparts, whereas ω_5 and ω_6 are within 5 cm^{-1} of the observed fundamentals. The RHF//RHF quartic force field given in Tables X–XII and the resulting χ_{ij} constants yield the following anharmonicity estimates ($\Delta_p \text{ cm}^{-1}$) for the fundamental vibrational frequencies: $\Delta_1 = -151$, $\Delta_2 = -36$, $\Delta_3 = -20$, $\Delta_4 = -37$, $\Delta_5 = -4$, and $\Delta_6 = +23$. Appending these values to the CISD//CISD harmonic frequencies produces more uniform agreement with experiment; in particular, the percent errors in ν_1 – ν_6 become 3.9, 3.7, 1.7, 4.6, -1.4 , and 2.9, respectively. The ν_5 error actually shifts to $+0.6\%$ if the improved Δ_5 prediction found below ($+8 \text{ cm}^{-1}$) is used. In brief, the agreement between the CISD//CISD vibrational frequencies and the observed band origins is not only good but also characteristic of this level of theory, and none of the experimental assignments appear to be suspect. With regard to other recent *ab initio* predictions, the 6–31G** MP2 harmonic frequencies of Teles *et al.*³⁶ are uniformly smaller than the CISD//CISD values, such that the RHF//RHF anharmonic corrections listed above place ν_3 – ν_6 between 2% and 3% below experiment while ν_1 and ν_2 become 3% overestimations.

In shifting the reference geometry to the experimental structure, the RHF ω_1 – ω_6 predictions are changed by -77 , -120 , -57 , -3 , -1 , and -18 cm^{-1} , respectively, in each case improving the agreement with experiment. The correlation contributions to the harmonic frequencies at the experimental structure as given by the CCSD method are $+8$, $+108$, -1 , -34 , -11 , and -42 cm^{-1} ,

respectively. Thus for ω_1 , ω_3 , and ω_5 the CCSD correlation treatment produces very little change, in contrast to the remarkably large *positive* contribution given for the N-C-O antisymmetric stretching frequency. This positive shift in ω_2 is evident from the values of the F_{22} force constant in Table X, wherein the CCSD//expt. result is substantially larger than both the RHF//expt. and CISD//CISD entries but slightly smaller than the RHF//RHF prediction. Generally the variations in the other quadratic constants are small, particularly among the entries in the last three columns of the table. The two diagonal constants for N-C-O linear bending, F_{55} and F_{66} , are nearly equivalent and are downshifted more strongly by legitimate correlation effects than by the choice of reference geometry. Finally, the F_{44} constant for H-N-C bending, which lies near 0.34 aJ rad^{-2} , is approximately three times smaller than its counterpart in methyleneimine, for example, and thus reflects the broad, flat bending potential which precipitates the quasilinear behavior in the bending vibrations of HNCO.

As shown in Tables XI and XII, the cubic and quartic constants obtained by the RHF//RHF and RHF//expt. procedures compare favorably. In accord with previous observations,^{193,196} the dominant stretching constants are significantly reduced in magnitude by the geometry shift, but the variations in the remaining constants are generally not substantial. The F_{555} cubic constant, which increases in magnitude by 45% due to the geometry shift, constitutes a notable exception to this general trend. The reliability of the RHF//expt. predictions is vividly demonstrated by a comparison with the diagonal and semidiagonal cubic constants resulting from the CCSD//expt. finite-difference evaluations of the quadratic force field. In the original set of internal coordinates used for the numerical differentiation, namely $a=r(\text{N-H})$, $b=r(\text{C-O})$, $c=r(\text{N-C})$, $d=\theta(\text{H-N-C})$, $e=\rho(\text{N-C-O})$, and $f=\tau(\text{H-N-C-O})$, some representative pairs of RHF//expt. and CCSD//expt. cubic force constants are $f_{aaa}(-51.2, -51.7)$, $f_{bbb}(-125.9, -124.0)$, $f_{ccc}(-99.0, -97.7)$, $f_{ddd}(-0.82, -0.70)$, $f_{eee}(-0.15, -0.15)$, $f_{cbb}(-2.3, -2.1)$, $f_{eec}(-1.1, -1.1)$, $f_{dda}(-0.42, -0.36)$, and $f_{ffe}(-0.09, -0.10)$, in the same units used in Table XI. On the basis of the high level of agreement observed among these values, the RHF//expt. higher-order force constants may be regarded as comparable in quality to correlated predictions.

Even though the quality of the theoretical cubic and quartic force constants for HNCO is expected to be high, the accuracy of the spectroscopic data derived from them may be vitiated if deficiencies exist in the quadratic force field, because the vibrational anharmonic constants (χ_{ij}) given by second-order perturbation theory are quite sensitive to the spacings and absolute positions of the zeroth-order energy levels. To circumvent such problems, the scaled quantum mechanical force field (SQM) procedure^{195–197} was implemented in conjunction with anharmonic vibrational analyses to obtain an improved quadratic force field as follows: (1) Anharmonicities of the vibrational fundamentals were predicted via perturbation

TABLE X. Quadratic force constants and harmonic vibrational frequencies (cm^{-1}) for HNCO^a

F_{ij}	RHF// RHF	CASSCF// CASSCF	RHF// expt. ^b	CISD// CISD	CCSD// expt. ^b	SQM(CCSD)// expt.
11	8.476	8.550	8.147	8.060	8.178	7.637
21	-0.019	0.015	-0.017	0.012	0.017	0.015
22	15.471	15.629	14.004	14.549	15.370	13.577
31	-0.208	-0.198	-0.203	-0.196	-0.210	-0.196
32	1.543	1.447	1.220	1.282	1.347	1.221
33	19.317	17.801	17.768	17.252	17.747	16.501
41	0.277	0.250	0.279	0.275	0.265	0.257
42	-0.770	-0.707	-0.758	-0.716	-0.705	-0.664
43	0.539	0.515	0.536	0.513	0.502	0.485
44	0.327	0.359	0.345	0.344	0.335	0.335
51	0.024	0.026	0.024	0.035	0.040	0.037
52	-0.241	-0.237	-0.239	-0.230	-0.232	-0.212
53	0.240	0.492	0.291	0.261	0.284	0.267
54	0.058	0.006	0.061	0.051	0.037	0.036
55	0.962	0.768	0.948	0.848	0.833	0.790
66	0.948	0.702	0.920	0.827	0.811	0.769
$\omega_1(a')$	3919	3937	3842	3821	3850	3720
$\omega_2(a')$	2471	2478	2351	2394	2459	2312
$\omega_3(a')$	1447	1391	1390	1369	1389	1339
$\omega_4(a')$	871	827	868	848	834	827
$\omega_5(a')$	589	582	588	573	577	567
$\omega_6(a'')$	713	610	695	657	653	636

Internal coordinate set: $S_1=r(\text{N-H})$, $S_2=2^{-1/2}[r(\text{C-O})-r(\text{N-C})]$, $S_3=2^{-1/2}[r(\text{C-O})+r(\text{N-C})]$,
 $S_4=\theta(\text{H-N-C})$, $S_5=\alpha_x(\text{N-C-O})=\sin \rho \sin \tau$, $S_6=\alpha_y(\text{N-C-O})=\sin \rho \cos \tau$,
 $\rho=\theta(\text{N-C-O})$, $\tau=\tau(\text{H-N-C-O})$

^aObtained with the $\text{DZ}(d,p)$ basis set. The units of the force constants are consistent with energy in aJ, bond lengths in Å, and bond angles in radians. The experimental reference geometry used in three of the cases is R_e structure I of Table I.

^bTo fully specify the force field for mathematical transformations, the first derivatives (F_i) at the experimental reference structure must be specified. The F_i values are RHF 1(0.0451), 2(0.0665), 3(0.3157), 4(0.0042), 5(-0.0294); and CCSD 1(-0.0569), 2(-0.0471), 3(-0.3243), 4(0.0006), 5(-0.0052). See footnote a for units.

TABLE XI. Cubic force constants of isocyanic acid.^a

ijk	F_{ijk}		$\phi_{ijk}(\text{HNCO})$		$\phi_{ijk}(\text{DNCO})$		ijk	F_{ijk}		$\phi_{ijk}(\text{HNCO})$		$\phi_{ijk}(\text{DNCO})$	
	RHF//RHF	RHF//expt.	RHF//expt.	RHF//expt.	RHF//expt.	RHF//expt.		RHF//RHF	RHF//expt.	RHF//expt.	RHF//expt.	RHF//expt.	RHF//expt.
111	-53.042	-51.187	-2428.2	-1411.2	511	-0.023	-0.021	-106.0	-124.7				
211	0.107	0.116	104.8	302.6	521	0.020	0.021	-2.1	-26.0				
221	-0.547	-0.537	16.7	-32.0	522	0.218	0.296	-9.9	-3.9				
222	-10.486	-8.979	-161.0	-195.0	531	-0.099	-0.101	35.1	102.5				
311	0.043	0.036	-108.2	-179.6	532	0.034	0.042	33.7	29.2				
321	0.323	0.325	-28.1	-92.0	533	-0.307	-0.397	-28.4	-21.5				
322	-83.511	-78.053	-516.5	-494.9	541	-0.048	-0.044	-840.3	-352.4				
331	-0.105	-0.118	21.5	52.3	542	-0.158	-0.171	60.0	134.6				
332	-11.187	-9.697	33.4	45.3	543	0.095	0.105	47.1	21.6				
333	-89.425	-83.809	-277.3	-277.8	544	-0.343	-0.342	185.4	154.6				
411	0.079	0.068	196.3	110.9	551	-0.033	-0.039	861.0	810.7				
421	0.222	0.242	31.4	39.7	552	0.025	0.026	15.4	-111.1				
422	0.021	0.005	81.5	34.9	553	-1.697	-1.689	118.1	117.1				
431	-0.253	-0.274	-55.6	-70.7	554	0.063	0.060	-40.8	-112.6				
432	-0.034	-0.025	-109.1	-62.4	555	-0.394	-0.571	-33.9	33.1				
433	0.162	0.139	51.1	16.5	661	-0.039	-0.042	64.4	-11.1				
441	-0.412	-0.415	762.8	119.0	662	0.174	0.176	42.9	68.1				
442	-0.401	-0.462	-57.5	-44.2	663	-1.935	-1.906	137.8	137.7				
443	0.001	0.029	64.5	124.8	664	0.051	0.049	21.9	4.5				
444	-0.820	-0.823	-458.2	-164.8	665	-0.153	-0.211	-14.3	-6.7				

^aThe internal coordinate set for the F_{ijk} values is that defined in Table X. See also footnotes a and b of Table X. The ϕ_{ijk} constants in reduced normal coordinate representations are given in cm^{-1} .

TABLE XII. Quartic force constants of isocyanic acid.^a

<i>ijkl</i>	F_{ijkl}		ϕ_{ijkl} (HNCO)		ϕ_{ijkl} (DNCO)		F_{ijkl}		ϕ_{ijkl} (HNCO)		ϕ_{ijkl} (DNCO)		F_{ijkl}		ϕ_{ijkl} (HNCO)		ϕ_{ijkl} (DNCO)	
	RHF// RHF	RHF// expt.	RHF// expt.	RHF// expt.	<i>ijkl</i>	RHF// RHF	RHF// expt.	RHF// expt.	RHF// expt.	RHF// expt.	<i>ijkl</i>	RHF// RHF	RHF// expt.	RHF// expt.	RHF// expt.	RHF// expt.		
1111	299.52	288.82	1343.3	658.5	4432	-0.760	-0.726	-1.6	2.1	5531	-0.005	0.010	-32.5	-72.4				
2111	1.126	1.070	-50.4	-126.5	4433	0.763	0.737	-9.8	-29.2	5532	-0.555	-0.506	-10.9	-7.9				
2211	-0.282	-0.242	2.3	33.1	4441	0.621	0.666	263.5	37.0	5533	2.465	2.447	-29.3	-6.0				
2221	1.450	1.467	10.8	28.7	4442	2.406	2.309	39.3	-16.0	5541	-0.043	-0.046	130.0	106.2				
2222	321.87	298.69	166.7	157.8	4443	-1.093	-1.066	-28.6	3.1	5542	0.011	0.028	5.2	22.0				
3111	-1.353	-1.311	56.4	67.7	4444	0.046	-0.031	497.7	47.2	5543	-0.106	-0.115	-31.7	-45.9				
3211	0.124	0.087	-3.1	-16.3	5111	-0.038	-0.033	100.7	85.3	5544	0.098	0.101	604.0	163.0				
3221	0.105	0.105	-5.0	-4.5	5211	0.053	0.058	-19.0	-4.2	5551	0.177	0.177	-76.1	-133.1				
3222	59.04	52.11	17.1	20.3	5221	-0.142	-0.146	3.5	-3.1	5552	-0.391	-0.402	12.9	-13.3				
3311	-0.078	-0.043	2.4	6.5	5222	0.925	0.849	-3.7	-10.8	5553	0.878	1.205	23.3	91.7				
3321	0.416	0.370	5.9	18.6	5311	-0.073	-0.083	-17.1	-54.3	5554	0.005	0.004	-592.1	-334.3				
3322	312.81	290.14	75.7	71.0	5321	0.038	0.040	-1.9	12.3	5555	5.572	5.741	664.5	796.2				
3331	-0.725	-0.586	-4.3	-10.9	5322	-0.115	-0.131	1.5	2.0	6611	-0.064	-0.061	-73.3	-11.8				
3332	55.99	49.23	-9.1	-12.2	5331	0.116	0.130	-0.2	-13.3	6621	0.100	0.101	-0.7	-22.7				
3333	321.54	299.76	40.2	41.0	5332	-0.755	-0.803	-3.4	-5.4	6622	-2.510	-2.468	-111.8	-114.5				
4111	-1.064	-1.077	-148.8	-53.5	5333	-0.185	-0.001	5.2	7.6	6631	-0.078	-0.068	-0.3	5.7				
4211	-0.226	-0.209	21.8	10.0	5411	0.021	0.016	753.8	276.6	6632	0.059	0.126	-7.0	-7.7				
4221	-0.225	-0.276	3.9	10.7	5421	-0.195	-0.199	-32.3	-66.7	6633	2.322	2.274	-45.2	-47.0				
4222	-0.940	-0.845	35.3	24.0	5422	0.395	0.382	-49.8	-42.6	6641	-0.005	-0.009	-6.9	-6.9				
4311	-0.009	-0.008	13.4	19.6	5431	0.282	0.279	35.3	37.4	6642	-0.007	0.005	-18.7	-12.0				
4321	0.384	0.411	-3.3	-11.2	5432	-0.348	-0.356	-0.6	-9.9	6643	0.024	0.009	5.6	3.0				
4322	0.491	0.393	-12.6	-4.4	5433	0.290	0.277	-25.2	-25.2	6644	0.034	0.037	6.8	11.5				
4331	-0.300	-0.323	-3.9	11.2	5441	0.174	0.167	-198.6	-76.9	6651	0.060	0.061	4.4	5.4				
4332	-0.899	-0.833	17.5	11.3	5442	0.528	0.491	-48.0	-20.7	6652	-0.098	-0.098	5.7	7.5				
4333	0.027	-0.193	-8.4	-3.2	5443	-0.068	-0.015	41.4	17.2	6653	0.264	0.373	-1.9	-3.7				
4411	0.285	0.279	-740.1	-132.7	5444	-0.235	-0.227	-540.6	-35.7	6654	0.036	0.036	2.4	16.2				
4421	-0.707	-0.732	21.6	9.4	5511	-0.133	-0.123	-766.9	-605.7	6655	1.833	1.840	28.2	2.0				
4422	0.698	0.612	-35.0	-73.2	5521	0.048	0.047	28.5	115.3	6666	5.421	5.305	69.5	70.7				
4431	0.515	0.550	-28.6	-11.6	5522	-2.390	-2.425	-81.6	-65.4									

^aSee footnotes a and b of Table X.

theory from the CCSD//expt. quadratic force field and the RHF//expt. cubic and quartic force constants. (2) These anharmonic corrections were applied to the experimental band origins to obtain a set of empirically based harmonic vibrational frequencies. (3) Optimum scale factors for the CCSD//expt. quadratic force constants were found via a least-squares fit to the experimental harmonic frequency estimates according to the SQM scheme. (4) The refined quadratic force field was used in conjunction with the unmodified RHF//expt. cubic and quartic constants to predict a new set of vibrational anharmonicities. (5) Steps 2–4 were performed iteratively until self-consistency was achieved, i.e., the vibrational anharmonicities used in Step 2 to obtain the input harmonic frequencies for the SQM fit were the same as those determined in Step 4 using the resulting SQM force field. The definitions of the internal coordinates used in the analysis are reiterated in Table X. Based on physical considerations, separate scale factors were used for coordinates S_1 – S_4 , while both linear bending coordinates in the set, S_5 and S_6 , were assigned to the same factor.¹⁹⁸ The reference data set included all six of the gas-phase fundamental frequencies of HNCO (see Fig. 2) as well as the stretching fundamentals of gaseous DNCO, viz. $\nu_1=2637\text{ cm}^{-1}$, $\nu_2=2235\text{ cm}^{-1}$, and $\nu_3=1310\text{ cm}^{-1}$. Bending frequencies of DNCO were not included in the

SQM procedure because, as detailed below, confusion remains over the assignment of these bands.

The final quadratic force field and the associated harmonic frequencies, denoted as SQM(CCSD)//expt., are tabulated in Table X along with the results presented previously. These improved predictions largely supplant the partial empirical force field derived in 1981 by Fusina and Mills.⁵⁵ The optimum scale factors (with standard errors in parentheses) relating the SQM force constants to the CCSD//expt. data are $f_1=0.934$ (0.002), $f_2=0.883$ (0.002), $f_3=0.930$ (0.003), $f_4=1.002$ (0.009), and $f_5=f_6=0.949$ (0.006), all of which lie in the expected range. The insignificant deviation of the $\theta(\text{H-N-C})$ factor above 1.00 is a consequence of the diminutive F_{44} value and the strong correlation of f_4 and f_5 resulting from the extensive mixing of the H–N–C and N–C–O bending motions in ν_4 and ν_5 . Note in Table X that the scaled F_{55} and F_{66} constants are larger than those predicted by the π -space CASSCF method, a level of theory which might be expected *a priori* to underestimate the curvature of the N–C–O bending potential due to the overestimation of $\pi \rightarrow \pi^*$ diradical character in the wave function.

The RHF//expt. third and fourth derivatives combined with the SQM(CCSD) quadratic force field yield the ϕ_{ijk} and ϕ_{ijkl} force constants in the reduced normal coordinates.

TABLE XIII. Vibrational anharmonic constants χ_{ij} (cm^{-1}) for HNCO and DNCO.^a

<i>ij</i>	HNCO			DNCO				
	χ_{ij}^a	Σ_1	Σ_2	Σ_3	χ_{ij}^a	Σ_1	Σ_2	Σ_3
11	-91.04	(-165.11,	83.96,	-9.88)	-48.09	(-75.63,	41.16,	-13.62)
21	-9.46	(-10.60,	1.15,	0.00)	-15.56	(-7.80,	-7.76,	0.00)
22	-15.51	(-1.17,	10.42,	-24.76)	-14.25	(-1.73,	9.86,	-22.38)
31	-4.92	(-6.21,	1.30,	0.00)	-2.55	(-4.65,	2.09,	0.02)
32	-16.42	(-8.62,	-7.80,	0.00)	-20.51	(-7.39,	-13.12,	0.00)
33	-4.02	(-5.98,	2.51,	-0.55)	-4.61	(-6.09,	2.56,	-1.08)
41	16.52	(-22.75,	38.20,	1.07)	10.62	(4.28,	5.77,	0.57)
42	18.51	(7.70,	10.38,	0.42)	-0.32	(-4.94,	3.98,	0.64)
43	-10.34	(9.39,	-19.74,	0.01)	-14.50	(1.61,	-16.13,	0.01)
44	-34.52	(-26.42,	31.11,	-39.20)	-6.93	(-3.80,	2.95,	-6.08)
51	-6.79	(-48.18,	40.50,	0.89)	-0.79	(-33.11,	31.22,	1.10)
52	-7.08	(-8.87,	0.79,	1.00)	-0.76	(-3.99,	2.46,	0.77)
53	-0.34	(-2.31,	1.98,	0.00)	3.45	(2.34,	1.10,	0.01)
54	-3.45	(102.65,	-106.10,	0.00)	-24.91	(19.68,	-44.59,	0.00)
55	-1.06	(-0.21,	41.53,	-42.38)	-1.34	(-0.24,	49.76,	-50.86)
61	-2.95	(-7.48,	0.11,	4.42)	-2.09	(-2.56,	0.01,	0.46)
62	-12.92	(-14.59,	0.16,	1.51)	-12.62	(-14.37,	0.39,	1.35)
63	29.51	(-4.93,	34.29,	0.15)	26.44	(-4.88,	31.20,	0.12)
64	16.48	(1.20,	-0.16,	15.45)	22.50	(0.87,	-0.01,	21.63)
65	39.88	(0.28,	-0.05,	39.65)	10.27	(-0.60,	-0.01,	10.89)
66	-6.93	(0.00,	4.34,	-11.27)	-6.10	(0.00,	4.42,	-10.51)

^aBased on the SQM(CCSD)+RHF//expt. quartic force field. In parentheses the decomposition of the χ_{ij} values is shown into the three successive terms (Σ_1 , Σ_2 , and Σ_3) in braces in Eqs. (26) and (27).

dinate space which are listed in Tables XI and XII for both HNCO and DNCO. The expressions for the vibrational anharmonic constants χ_{ij} in terms of these force constants are^{132,134}

$$\chi_{ii} = \left\{ -\frac{5}{48} \frac{\phi_{iii}^2}{\omega_i} \right\} + \left\{ \frac{1}{16} \phi_{iii} \right\} + \left\{ -\frac{1}{16} \sum_j \frac{\phi_{ijj}^2 (8\omega_i^2 - 3\omega_j^2)}{\omega_i (4\omega_i^2 - \omega_j^2)} \right\} \quad (26)$$

and

$$\chi_{ij} = \left\{ -\frac{1}{4} \sum_k \frac{\phi_{iik} \phi_{kjj}}{\omega_k} + \frac{1}{4} \phi_{ijj} \right\} + \left\{ -\frac{1}{2} \sum_k \frac{\phi_{ijk}^2 \omega_k (\omega_k^2 - \omega_i^2 - \omega_j^2)}{[(\omega_i + \omega_j)^2 - \omega_k^2][(\omega_i - \omega_j)^2 - \omega_k^2]} \right\} + \left\{ [A_e(\xi_{ij}^a)^2 + B_e(\xi_{ij}^b)^2 + C_e(\xi_{ij}^c)^2] \left(\frac{\omega_i}{\omega_j} + \frac{\omega_j}{\omega_i} \right) \right\}, \quad (27)$$

where the ξ_{ij} quantities are Coriolis coupling constants for rotations about the principal axes *a*, *b*, and *c*, and the prime on the summation in Eq. (26) indicates the exclusion of the *i*=*j* term. The predicted χ_{ij} values for HNCO and DNCO are given in Table XIII, wherein the decomposition of these constants into the three separate terms (Σ_1 , Σ_2 , and Σ_3) enclosed in braces in Eqs. (26) and (27) is shown to facilitate their interpretation. Assuming a 50 cm^{-1} cut-off criterion for zeroth-order energy level spacings, it was necessary to exclude only one resonance denominator in the χ_{ij} evaluations, specifically $\omega_1 \approx \omega_2 + \omega_5$ for DNCO in the second term in Eq. (27).

A summary of the vibrational analyses for HNCO and DNCO appears in Table XIV. The calculated stretching frequencies for HNCO reproduce the experimental band origins within 5 cm^{-1} , and the residuals for the bending fundamentals are less than 2 cm^{-1} . The anharmonicity of the N-H stretching vibration (-186 cm^{-1}) is of exceptional size and is attended by values of ω_1 (3720 cm^{-1}) and D_e (120.0 kcal mol⁻¹) which are unusually large for an N-H sigma bond.¹⁹⁹ However, the off-diagonal components to Δ_1 are primarily responsible for its unusually large magnitude, as the first two terms for χ_{11} in Eq. (26) yield a diagonal contribution of $2\chi_{11}^* = -162.3 \text{ cm}^{-1}$, which is not far removed from the $-2\omega_e x_e = -156.7 \text{ cm}^{-1}$ anharmonicity observed for NH(³ Σ^-).¹⁵² The Δ_2 value for the N-C-O antisymmetric stretching mode (-44.7 cm^{-1}) is very similar to the anharmonicity for ν_3 of CO₂ (-47.4 cm^{-1}),²⁰⁰ but Fermi resonance interactions spoil the corresponding comparison for the symmetric stretching fundamentals of the two molecules. For HNCO, the ϕ_{543} cubic constant is 47.1 cm^{-1} , and the $\omega_3 \approx \omega_4 + \omega_5$ resonance term contributes only -5.2 and -5.1 cm^{-1} to χ_{43} and χ_{53} , respectively. The $\omega_3 - 2\omega_6$ term in χ_{63} is more substantial (+34.1 cm^{-1}) because $\phi_{663} = 137.8 \text{ cm}^{-1}$, but the treatment of this interaction by a perturbation approach can still be justified. In contrast, for carbon dioxide the cubic constant ϕ_{221} (150.5 cm^{-1})²⁰¹ contributes +353 cm^{-1} to χ_{12} upon inclusion of the $\omega_1 - 2\omega_2$ resonance term,¹³⁸ and thus this interaction must instead be treated via a secular equation in first order. The anharmonicities of the bending fundamentals of HNCO vary widely. The total energy distributions (TEDs) in Table XIV reveal that the ν_4 mode is composed of 70% H-N-C bend and 30% N-C-O linear

bend combined in phase. Therefore, the normal mode for ν_4 connects the equilibrium *trans*-bent structure to the linear transition state, which lies only 6 kcal mol⁻¹ higher in energy, thus explaining the large negative anharmonicity (-50.2 cm⁻¹) of this vibration. By comparison, the anharmonicities of ν_5 and ν_6 are dominated by the Coriolis terms in Eq. (27), as shown by the Δ' entries in Table XIV; accordingly, positive values of Δ_5 and Δ_6 are engendered.

With the aid of the final vibrational anharmonic constants, it is possible to elaborate on several spectroscopic issues which have been raised in the literature. First, Carloti *et al.*²⁰² have determined the second overtone of the N-H stretch to lie at 10 145.79 cm⁻¹. According to Eq. (21) the band origin of this overtone is given by

$$3\nu_1 = 3\omega_1 + 12\chi_{11} + \frac{3}{2} \sum_{i \neq 1} \chi_{i1}, \quad (28)$$

which predicts $3\nu_1 = 10\,056$ cm⁻¹. Alternatively, if the $\nu_1 = 3$ level is predominantly of local mode character, then $3\nu_1 = 3\omega_1 + 12\chi_{11}^* = 10\,185$ cm⁻¹, where χ_{11}^* (-81.1 cm⁻¹) involves the diagonal component of the ν_1 anharmonicity mentioned above. These predictions bracket the observed band origin, but the local mode description appears to be preferred. Second, Teles *et al.*³⁶ have proposed the $\nu_2 + \nu_4 + \nu_5$ combination level to be the most likely candidate for the observed resonance with the $\nu_1 = 1$, $K_a = 2$ substate at 3639 cm⁻¹. The analysis presented here places $\nu_2 + \nu_4 + \nu_5$ at 3630 cm⁻¹, and thus supports this assignment strongly. Other possibilities in the 3575–3700 cm⁻¹ region are $\nu_2 + \nu_3 = 3582$, $\nu_3 + 4\nu_5 = 3622$, $\nu_4 + 5\nu_5 = 3621$, and $6\nu_4 = 3630$ cm⁻¹. For the perturbation of the $\nu_1 = 1$, $K_a = 4$ substate at 3953 cm⁻¹, there are 15 resonance candidates in the 3900–4000 cm⁻¹ region. Those with a total excitation level less than five are $\nu_2 + 3\nu_5 = 3969$, $2\nu_3 + \nu_4 + \nu_5 = 3982$, $2\nu_3 + \nu_5 + \nu_6 = 3984$, and $3\nu_3 = 3967$ cm⁻¹. Third, Steiner and co-workers⁵¹ have assigned an infrared absorption at 507.715 cm⁻¹ to the $(2\nu_5) - \nu_5$ difference band. From Eq. (21) the expression for the origin of this band is

$$(2\nu_5) - \nu_5 = \omega_5 + 4\chi_{55} + \frac{1}{2} \sum_{i \neq 5} \chi_{i5}, \quad (29)$$

whence $(2\nu_5) - \nu_5 = 573.9$ cm⁻¹ is found. In brief, the small, net anharmonicity predicted for the ν_5 mode makes the experimental assignment of the 507.715 cm⁻¹ absorption dubious. Finally, in the matrix isolation experiments of Teles *et al.*,³⁶ infrared absorptions at 1315.0, 1307.7, and 1303.6 were observed for HNCO, HN¹³CO, and H¹⁵NCO, respectively. Based on 6–31G** MP2 harmonic frequency predictions, these workers concluded that the observed isotopic shifts are not consistent with the assignment of these bands to the ν_3 fundamental and thus ascribed them to the $\nu_4 + \nu_5$ combination level. The $\nu_4 + \nu_5$ vibrational levels for the HNCO isotopomers given by the current analysis lie 30–40 cm⁻¹ higher than the bands in question, a disparity which is probably too large to be attributed to matrix shifts. Moreover, the inclusion here of anharmonic terms in the vibrational analysis reverses the argument based on isotopic shifts. The theoretical ν_3 fundamentals for HNCO,

HN¹³CO, and H¹⁵NCO are 1330.3, 1322.3, 1315.8 cm⁻¹, respectively, whereas the corresponding $\nu_4 + \nu_5$ values for these isotopomers are 1350.4, 1336.2, and 1344.0 cm⁻¹. Therefore, the theoretical ¹³C and ¹⁵N isotopic shifts for ν_3 are, in order, -8.0 and -14.5 cm⁻¹, and those for $\nu_4 + \nu_5$ are -14.2 and -6.5 cm⁻¹. By comparison, the ¹³C and ¹⁵N argon-matrix shifts are -7.3 and -11.4 cm⁻¹, respectively, which favors the assignment of the observed bands to ν_3 rather than $\nu_4 + \nu_5$.

G. Fundamental vibrational frequencies of DNCO

In a recent compilation of vibrational frequencies,²⁰³ the fundamentals of DNCO are listed as follows: $\nu_1(a') = 2637.20$ cm⁻¹, $\nu_2(a') = 2235$ cm⁻¹, $\nu_3(a') = 1310$ cm⁻¹, $\nu_4(a') = 578.6$ cm⁻¹, $\nu_5(a') = 475.4$ cm⁻¹, and $\nu_6(a'') = 602.9$ cm⁻¹; the ν_4 and ν_5 values are argon-matrix results while the other frequencies are gas-phase observations. For the stretching fundamentals $\nu_1 - \nu_3$, preliminary theoretical predictions obtained here based on the CISD/CISD quadratic force field and the RHF//RHF anharmonicities gave isotopic shifts upon deuteration of -936 , -31 , and -24 cm⁻¹, respectively. The listed experimental values yield corresponding shifts of -901 , -34 , and -17 cm⁻¹, and thus the previous assignments for the stretching fundamentals were included above in the final SQM(CCSD) determination of the quadratic force field. The broad confirmation of the stretching frequencies notwithstanding, the ν_2 and ν_3 values, which are from the 1966 investigation of Ashby and Werner,⁴⁸ are likely to be refined somewhat by future studies. Rotational band analyses were not possible from the recorded spectra, and the band origins were merely estimated from the observed contours. In particular, the ν_3 band only appeared as a very weak shoulder in an absorption region dominated by residual HNCO.

All three bending fundamental assignments of DNCO appear to be questionable on the basis of the theoretical data obtained here. Ashby and Werner⁴⁸ attributed to the lowest-frequency a' vibration a parallel band in the gas phase whose center was estimated to lie at 460 cm⁻¹. A similar value (460.1 cm⁻¹) was assigned by Bondybey and co-workers²⁰⁴ from isolation experiments in a neon matrix. However, the $\nu_5 = 475.4$ cm⁻¹ result listed above is from the argon-matrix work of Teles *et al.*,³⁶ who state that the Ashby and Werner gas-phase assignment is "probably incorrect." As shown in Table XIV, the theoretical fundamental is located at 458 cm⁻¹, and thus there appears to be little reason to question the gas-phase assignment $\nu_5 = 460$ cm⁻¹. Spectral absorptions due to $\nu_6(a'')$ of DNCO were not observed in any of the aforementioned matrix-isolation experiments, and thus the early data from Ashby and Werner are the only results available in the literature. Series of $R(J)$ and $P(J)$ lines for $J = 1-32$ were recorded in the 580–640 cm⁻¹ region, while three Q -type band heads were measured at 604.9, 610.6, and 619.1 cm⁻¹. These Q -type bands were presumed to originate from $K_a'' = 1, 2$, and 3, respectively, whence a band origin of 602.9 cm⁻¹ was deduced for ν_6 . Two objections can be raised regarding

TABLE XIV. Summary of final vibrational analysis for HNCO and DNCO.^a

Mode	Description	ω	Δ	Δ'	ν	Expt.	Infrared intensity	TED ^b
HNCO								
$\nu_1(a')$	N-H stretch	3720	-185.9	+3.2	3534	3538.25 ^c	173.6	$S_1(99)$
$\nu_2(a')$	N-C-O asym. stretch	2312	-44.7	+1.5	2268	2268.89 ^{d,e}	905.9	$S_2(98)$
$\nu_3(a')$	N-C-O sym. stretch	1340	-9.3	+0.1	1330	1327 ^f	0.08	$S_3(100)$
$\nu_4(a')$	sym. in-plane bend	828	-50.2	+8.5	778	776.62 ^g	216.1	$S_5(30) + S_4(70)$
$\nu_5(a')$	asym. in-plane bend	567	+9.0	+20.8	576	577.35 ^g	98.7	$S_5(70) - S_4(30)$
$\nu_6(a'')$	N-C-O out-of-plane bend	636	+21.1	+30.6	657	656.29 ^{g,h}	7.9	$S_6(100)$
DNCO								
$\nu_1(a')$	N-D stretch	2743	-101.4	+1.1	2642	2637.20 ⁱ	222.4	$S_1(94) + S_2(5)$
$\nu_2(a')$	N-C-O asym. stretch	2290	-53.4	+1.4	2236	2235 ^j	850.2	$S_2(94) - S_1(4)$
$\nu_3(a')$	N-C-O sym. stretch	1320	-13.1	+0.1	1307	1310 ^j	1.8	$S_3(99)$
$\nu_4(a')$	sym. in-plane bend	744	-17.2	+11.4	727	(722.4) ^k	84.5	$S_5(63) + S_4(38)$
$\nu_5(a')$	asym. in-plane bend	467	-9.1	+6.4	458	460 ^j	95.4	$S_5(37) - S_4(64)$
$\nu_6(a'')$	N-C-O out-of-plane bend	623	+10.1	+17.2	633	...	19.4	$S_6(100)$

^aSQM(CCSD)+RHF//expt. values (in cm^{-1}) are given for the harmonic frequencies (ω_i), the total anharmonicities (Δ_i), the Coriolis contribution to the anharmonicity (Δ'_i), and the fundamental vibrational frequencies (ν_i). The infrared intensities (in km mol^{-1}) are $DZ(d,p)$ CISD// $DZ(d,p)$ CISD double-harmonic predictions.

^bTotal energy distributions among the internal coordinates S_i for each normal mode K , as given by the SQM(CCSD) force field. Each entry is listed as $S_i(n)$, where $n=100$ [TED] _{i} ^k (see Ref. 197). The signs preceding these entries denote the relative phases of the internal coordinates in the normal-mode eigenvectors.

^cReference 46.

^dReference 191.

^eReference 192.

^fReference 57.

^gReference 51.

^hReference 56.

ⁱReference 220.

^jReference 48.

^kMatrix-isolation value from Ref. 204.

this assignment on the basis of the theoretical results presented here. First, the predicted isotopic shifts upon deuteration for ω_6 and ν_6 are -13 and -24 cm^{-1} (see Table XIV), which are much smaller than the -53.4 cm^{-1} shift exhibited by the experimental values. In fact, Ashby and Werner previously used product rule considerations to justify the $\nu_6(\text{DNCO})=602.9$ cm^{-1} assignment under the incorrect assumption that $\nu_6(\text{HNCO})$ lies only slightly higher at 610 cm^{-1} ! Second, the spacing of the observed Q -type subband origins suggests an effective vibration-rotation interaction constant of $\alpha_6^A \approx -1.9$ cm^{-1} (see Table XVIII below). However, the α_6^A constant for DNCO predicted by the RHF//expt. cubic force constants and the SQM(CCSD) harmonic frequencies is $+3.55$ cm^{-1} . In summary, $\nu_6(\text{DNCO})=633$ cm^{-1} is predicted here, and a discrepancy of 30 cm^{-1} appears between theory and experiment which has yet to be resolved. In this regard it is noteworthy that a prominent, unassigned band near 637 cm^{-1} appears in the spectral plot given by Ashby and Werner which is a viable candidate for the reassignment of $\nu_6(\text{DNCO})$.

The source of most contention in the low-frequency infrared spectrum of DNCO is $\nu_4(a')$. The associated normal mode is the in-phase combination of the two in-plane bending coordinates, but unlike HNCO its character is predominantly N-C-O rather than H-N-C bending motion (cf. the TEDs in Table XIV). Ashby and Werner⁴⁸ ana-

lyzed an extensive series of gas-phase rovibrational transitions in the 650 – 950 cm^{-1} region and arrived at a ν_4 band origin of 766.8 cm^{-1} . The work of Bondybey and co-workers²⁰⁴ brought this assignment into question, as an absorption at 722.4 cm^{-1} was ascribed to $\nu_4(\text{DNCO})$ in a neon matrix at 4 K. Influenced by the observation of a weak band at 1036.6 cm^{-1} which was interpreted as $\nu_4 + \nu_5$, Teles and co-workers³⁶ proposed an argon-matrix result of $\nu_4=578.6$ cm^{-1} , which is the value cited in Ref. 203. The theoretical results summarized in Table XIV give $\omega_4=744$ and $\nu_4=727$ cm^{-1} . These frequencies are incompatible with the assignment of Teles *et al.* and raise the possibility that the observed 578.6 cm^{-1} band is attributable to DCN, whose bending fundamental in the gas phase lies at 570.3 cm^{-1} .²⁰⁵ As a curious contradistinction, Teles *et al.* claim that the band found by Bondybey and co-workers near 722 cm^{-1} "certainly belongs to hydrogen cyanide." In resolving this issue, it is asserted here that a $\nu_4(\text{DNCO})$ fundamental frequency near 722 cm^{-1} is completely consistent not only with the theoretical predictions appearing in Table XIV, but also with the original gas-phase data of Ashby and Werner, provided several reassignments of the observed K -subband origins are made.

The proposed reassignments of the K subbands for the ν_4 fundamental are collected in Table XV. The Q -type absorptions measured by Ashby and Werner lie at 755.5 , 782.6 , 810.6 , and 838.0 cm^{-1} , and the bands with P or R

TABLE XV. Proposed reassignments of the gas-phase subband origins (cm^{-1}) of the ν_4 fundamental of DNCO.^a

K	${}^R Q_K$	${}^Q Q_K$	${}^P Q_K$	${}^R Q_K - {}^Q Q_{K+1}$	${}^Q Q_K - {}^P Q_{K+1}$
0	749.5	[722.3]	...	[17.8]	[17.8]
1	[805.0]	[731.7]	704.5	(49.50)	(49.50)
2	863.6	755.5	682.2	81.0	81.0
3	921.0	782.6	674.5	110.4	110.1
4	[975.7]	810.6	672.5	(137.66)	(137.66)
5	...	838.0	[672.9]

^aBased on the data appearing in Table II of Ref. 48. The values in brackets are calculated from the observed subband origins. The combination differences in parentheses are firmly established results from far-infrared rotational spectroscopy (Ref. 49).

character are centered at 672.5, 674.5, 682.2, 704.5, 749.5, 863.6, and 921.0 cm^{-1} . The task is to construct the reassignment of these bands by assuming that $\nu_4 \approx 722 \text{ cm}^{-1}$. The A_0 rotational constant for the ground vibrational state of DNCO is 17.0442 cm^{-1} . The corresponding constant in the $\nu_4=1$ excited state differs from A_0 by an effective vibration-rotation interaction constant α_{eff} . For small values of K , α_{eff} should be close to the $\alpha_4^A(\text{DNCO})$ value of -7.22 cm^{-1} appearing below in Table XVIII. The ${}^R Q_0$ and ${}^P Q_1$ subband origins should be shifted from the ν_4 origin by roughly $(A_0 - \alpha_{\text{eff}})$ and $-A_0$, respectively, and thus the assignments ${}^R Q_0=749.5$ and ${}^P Q_1=704.5 \text{ cm}^{-1}$ are established. Next, ${}^P Q_2$ should differ from ${}^P Q_1$ by roughly $(2A_0 + \alpha_{\text{eff}})$, whence the association ${}^P Q_2=682.2 \text{ cm}^{-1}$ is revealed. The separation of the $(J'', K'') = (2, 1)$ and $(2, 2)$ levels in the ground vibrational state, which is equivalent to ${}^R Q_1 - {}^Q Q_2$, is known to be 49.50 cm^{-1} from far-infrared absorption spectroscopy.⁴⁹ From the assigned ${}^P Q_2$ subband origin, it is then deduced that ${}^Q Q_1=731.7 \text{ cm}^{-1}$. By subtracting ${}^Q Q_1$ from ${}^R Q_0$, it is found that the $(J'', K'') = (1, 0)$ and $(1, 1)$ levels are separated by 17.8 cm^{-1} , which is reasonably close to the anticipated value of 16.75 cm^{-1} , i.e., the magnitude of $A_0 - B_0$. From ${}^P Q_1=704.5 \text{ cm}^{-1}$ and the ${}^R Q_0 - {}^Q Q_1$ difference, a more precise ν_4 origin of ${}^Q Q_0=722.3 \text{ cm}^{-1}$ is suggested. As a check of this estimate, $\alpha_{\text{eff}} = {}^Q Q_0 - {}^Q Q_1$ is surmised to be -9.4 cm^{-1} , in accord with the predicted $\alpha_4^A(\text{DNCO})$. Noting that ${}^Q Q_2 \approx {}^Q Q_1 - 3\alpha_{\text{eff}}$, the assignment ${}^Q Q_2=755.5 \text{ cm}^{-1}$ results. Having ascertained the value of ${}^Q Q_2$, the remaining ${}^Q Q_K$ subband origins in Table XV, which are uniformly spaced 27–28 cm^{-1} apart, are readily interpreted. The $(3, 2)$ – $(3, 3)$ and $(4, 3)$ – $(4, 4)$ (J'', K'') separations, 80.90 and 110.32 cm^{-1} , respectively, have also been determined directly from the far-infrared spectrum of DNCO.⁴⁹ These energy differences in the ground vibrational state allow the assignments of the R - and P -type subbands to be completed on the basis of the ${}^Q Q_K$ series, as detailed in Table XV. The combination differences resulting from the tabulated reassignments are essentially the same as those extracted from the band analysis by Ashby and Werner of the N–D stretching fundamental (see Table I therein⁴⁸). The overall consistency of the assignments in Table XV is indeed remarkable. In summary, the acceptance of a gas-phase frequency for ν_4 near 722 cm^{-1} is advocated strongly on the basis of the current theoretical analysis.

H. The R_e structure and vibration-rotation interaction constants of HNCO

The planarity of the equilibrium structure of isocyanic acid dictates that the nuclear coordinates along the c inertial axis are identically zero. The remaining Cartesian coordinates in the principal axis system, a_i and b_i , can be ascertained from isotopic-substitution data by means of the Kraitchman equations,^{63,64} in particular,

$$a_i^2 = \left(\frac{\hbar}{4\pi c} \right) \left(\frac{1}{\Delta m_i} + \frac{1}{M} \right) \left(\frac{A_e^\circ}{B_e^\circ} \right) \left(1 - \frac{B_e^\circ}{B_e^i} \right) \left(1 - \frac{B_e^\circ}{A_e^i} \right) \times (B_e^\circ - A_e^\circ)^{-1} \quad (30)$$

and

$$b_i^2 = \left(\frac{\hbar}{4\pi c} \right) \left(\frac{1}{\Delta m_i} + \frac{1}{M} \right) \left(\frac{B_e^\circ}{A_e^\circ} \right) \left(1 - \frac{A_e^\circ}{A_e^i} \right) \left(1 - \frac{A_e^\circ}{B_e^i} \right) \times (A_e^\circ - B_e^\circ)^{-1}, \quad (31)$$

where A_e° and B_e° are rotational constants (in cm^{-1}) of the parent HNCO molecule, A_e^i and B_e^i are analogous constants resulting from isotopic substitution at nucleus i , Δm_i is the change in molecular mass upon substitution, and M is the total mass of the parent species. By using experimental A_0 and B_0 constants in Eqs. (30) and (31), empirical R_s structures of HNCO can be extracted. However, a_C , b_C , b_N , and b_O are poorly determined by the procedure in this case because the carbon nucleus lies very close to the center of mass of the system, and the NCO chain is almost coincident with the a axis. In fact, in the previous spectroscopic studies of Yamada⁵² and Hocking *et al.*,⁶² imaginary values of the a_C coordinate were obtained as a consequence of zero-point vibrational effects and uncertainties in the input data. Such problems can be mitigated by utilizing three first- and second-moment conditions to evaluate a_C , b_C , b_N , and b_O ,

$$\sum_i m_i a_i = 0, \quad (32)$$

$$\sum_i m_i b_i = 0, \quad (33)$$

and

$$\sum_i m_i a_i b_i = 0. \quad (34)$$

The linearity of the NCO chain was assumed as the fourth constraint by Hocking *et al.* in their R_s structure determination; in contrast, Yamada was able to construct a complete set of R_s parameters by requiring the I_a moment of inertia computed after invoking Eqs. (32)–(34) to be the same as that given directly by the unconstrained Kraitchman a_i and b_i coordinates. In yet another approach, an empirical R_s structure of HNCO was computed by Fusina and Mills⁵⁵ from a least-squares fit to a set of modified rotational constants under isotopic-shift constraints given by trial anharmonic force fields.

The experimental R_s and R_z structures of HNCO are given above in Table I. The bond distances and bond angles

are generally consistent not only with the optimum theoretical parameters predicted here but also with several previous *ab initio* structures.^{36,206–208} Comparisons of the various C–O bond distances are representative of those possible within the data set. Specifically, the available RHF equilibrium distances with polarized basis sets range from the 6–311G** value (1.139 Å) of Glidewell and Thomson²⁰⁷ to the DZ(*d,p*) result (1.150 Å) obtained here, i.e., from 0.027 to 0.017 Å below the experimental R_s distance. On the other hand, the 6–31G** MP2 distance (1.183 Å) of Teles *et al.*³⁶ and the 6–31G** MP4 (SDTQ) distance (1.91 Å) of Mack and Oberhammer²⁰⁸ are 0.017 and 0.025 Å longer than experiment, respectively. These observations are consonant with the propensity of the RHF method to underestimate lengths of multiple bonds and the MP2 and MP4 methods to overcompensate for this deficiency. A cancellation of basis set and correlation errors makes the DZ(*d,p*) CISD prediction (1.169 Å) of $r_e(\text{C–O})$ the most accurate, as evidenced by the actual deterioration of the DZ(*d,p*) results upon improvement of the correlation treatment; to wit, both the DZ(*d,p*) CCSD distance found here (1.177 Å) and the DZP CISD + (Q) result (1.178 Å) of DeFrees *et al.*²⁰⁶ are farther removed from experiment than the DZ(*d,p*) CISD value. Mack and Oberhammer also report 6–31G** CISD optimum geometric parameters quite similar to our DZ(*d,p*) CISD results. Further comparisons reveal that the experimental $r_s(\text{N–H})$ and $r_z(\text{N–H})$ values, 0.9946 and 1.0127 Å, respectively, are poor approximations to the equilibrium N–H distance. At variance with expected trends, the former result is 0.0024 Å shorter than the DZ(*d,p*) RHF bond length, whereas the latter value is 0.0012 Å longer than the DZ(*d,p*) CCSD distance. For NH($^3\Sigma^-$) the DZ(*d,p*) RHF and CISD bond lengths bracket the experimental distance, suggesting that $r_e(\text{N–H}) \approx 1.004$ Å for HNCO by interpolation of analogous predictions.

In this section a precise R_e structure for isocyanic acid is determined via Eqs. (30) and (31) after correcting the experimental Watson S -reduced $A_0^{(S)}$, $B_0^{(S)}$, and $C_0^{(S)}$ rotational constants for HNCO, DNCO, H¹⁵NCO, HN¹³CO, and HNC¹⁸O for zero-point vibrational corrections; these corrections were approximated as one-half the sums of theoretical vibration–rotation interaction constants (α_i). The empirical rotational constants were derived in a comprehensive analysis⁵² wherein the far-infrared data measured directly by Yamada⁵² in 1980 were combined with the microwave and millimeter wave transitions of Hocking *et al.*⁶² as well as the earlier far-infrared absorption lines of Krakow, Lord, and Neely.⁴⁹ In our first determination of the R_e structure, the α_i constants were evaluated from the RHF//RHF cubic force field given in Tables X and XI. The form of the standard expression for these vibration–rotation interaction constants is^{132,134}

$$\alpha_i^B = - \left(\frac{2B_e^2}{\omega_i} \right) \left[\sum_{\gamma} \frac{3(a_i^{b\gamma})^2}{4I_{\gamma\gamma}} + \sum_j \frac{(\zeta_{ij}^b)^2(3\omega_i^2 + \omega_j^2)}{\omega_i^2 - \omega_j^2} + \pi \left(\frac{c}{h} \right)^{1/2} \sum_j \phi_{ij} a_j^{bb} \left(\frac{\omega_i}{\omega_j^{3/2}} \right) \right], \quad (35)$$

where the quantities $a_i^{b\gamma} \equiv (\partial I_{B\gamma} / \partial Q_i)_e$ are inertial derivatives and the prime on the second summation indicates the exclusion of the $i=j$ term as before. For HNCO the computed α_i^A constants for the bending vibrations are immense due to the $\omega_4 - \omega_6$ and $\omega_5 - \omega_6$ Coriolis resonance terms, and the perturbation treatment of this interaction implicit in Eq. (35) is invalid. Ostensibly the associated vibrational correction to the A_0 constant becomes anomalous, but in fact the resonance interactions in Eq. (35) cancel when summed. In brief, the $A_e - A_0$ difference is unaffected by Coriolis resonances in that the net Coriolis contribution to this vibrational correction is of the form

$$A_e^2 \sum_{i>j} \frac{(\zeta_{ij}^a)^2(\omega_i - \omega_j)^2}{\omega_i \omega_j (\omega_i + \omega_j)}, \quad (36)$$

which is devoid of resonance denominators. For this reason the use of α_i constants from Eq. (35) in the determination of the experimental R_e structure is justified.

The RHF//RHF vibrational correction terms are tabulated in Table XVI for each isotopomer along with the associated $A_0^{(S)}$, $B_0^{(S)}$, and $C_0^{(S)}$ constants. When employed in Eqs. (30) and (31), the resulting A_e and B_e quantities still yield small imaginary values for a_c and b_o . The procedure of Yamada⁵² based on the conditions of Eqs. (32)–(34) was used to circumvent this problem, giving the empirically derived R_e structural parameters in Table XVII. Because the inertial defect among the corrected rotational constants is nonvanishing, the nuclear coordinates obtained from the (A_e, B_e) pair are slightly different from those given by the (A_e, C_e) and (B_e, C_e) pairs and the planarity relation $A_e^{-1} + B_e^{-1} = C_e^{-1}$. Both the experimental uncertainties in the $A_0^{(S)}$ constants and the $A_e - A_0$ corrections are larger than those for the $B_0^{(S)}$ and $C_0^{(S)}$ constants. Consequently, the final R_e structure (I) listed in Table XVII was obtained somewhat arbitrarily by averaging the (A_e, B_e) , (A_e, C_e) , and (B_e, C_e) results using weighting factors of 1/4, 1/4, and 1/2, respectively.

The R_e structure (I) derived from the RHF//RHF data is the reference geometry used above to establish an improved anharmonic force field comprised of SQM(CCSD)//expt. quadratic force constants and RHF//expt. higher-order derivatives. Using this improved force field to re-evaluate the α_i constants, a refined R_e structure (II) was determined. It should be recognized that the effective rotational constants in the Watson S -reduced rotational Hamiltonian, i.e., $A_0^{(S)}$, $B_0^{(S)}$, and $C_0^{(S)}$, are not precisely equivalent to A_0 , B_0 , and C_0 . The pertinent relationships are^{135,137}

$$A_0 = A_0^{(S)} - 6R_6 + 5\sigma^{-1}R_5 - 4^{-1}(3\tau_{bcbc} - 2\tau_{caca} - 2\tau_{abab}), \quad (37)$$

$$B_0 = B_0^{(S)} + 4R_6 - 2(2 + \sigma^{-1})R_5 - 4^{-1}(3\tau_{caca} - 2\tau_{abab} - 2\tau_{bcbc}), \quad (38)$$

and

$$C_0 = C_0^{(S)} + 4R_6 + 2(2 - \sigma^{-1})R_5 - 4^{-1}(3\tau_{abab} - 2\tau_{bcbc} - 2\tau_{caca}), \quad (39)$$

TABLE XVI. Data for the determination of A_e , B_e , and C_e for the isotopomers of isocyanic acid.^a

	HNCO	DNCO	H ¹⁵ NCO	HN ¹³ CO	HNC ¹⁸ O
Experimental rotational constants ^b					
$A_0^{(S)}$	30.638 01	17.094 24	30.319 92	30.564 27	30.635 08
$B_0^{(S)}$	0.369 289 08	0.344 028 44	0.358 175 47	0.369 304 81	0.349 271 48
$C_0^{(S)}$	0.363 937 63	0.336 221 80	0.353 093 12	0.363 942 80	0.344 479 72
RHF//RHF vibrational corrections					
$A_e - A_0$	-2.178 35	-0.949 34	-2.147 95	-2.177 21	-2.175 20
$B_e - B_0$	0.001 062	0.000 976	0.001 010	0.001 047	0.001 001
$C_e - C_0$	0.001 488	0.001 451	0.001 413	0.001 473	0.001 385
SQM(CCSD) + RHF//expt. vibrational and centrifugal distortion corrections					
$A_e - A_0$	-1.822 04	-0.798 26	-1.797 07	-1.823 10	-1.820 78
$B_e - B_0$	0.001 407	0.001 265	0.001 344	0.001 388	0.001 322
$C_e - C_0$	0.001 821	0.001 732	0.001 735	0.001 801	0.001 695
$A_0^{(S)} - A_0$	0.000 067	0.000 050	0.000 064	0.000 066	0.000 060
$B_0^{(S)} - B_0$	4×10^{-7}	4.9×10^{-6}	1×10^{-7}	3×10^{-7}	3×10^{-7}
$C_0^{(S)} - C_0$	-0.000 067	-0.000 053	-0.000 063	-0.000 067	-0.000 060
Δ_e^c	0.020 305	0.017 301	0.020 367	0.020 325	0.020 271

^aAll rotation constant data in cm^{-1} .

^bReference 52.

^cInertial defect ($\text{amu} \text{ \AA}^2$) remaining in the equilibrium rotational constants derived from the SQM(CCSD) + RHF//expt. force field.

where R_5 , R_6 , and the $\tau_{\alpha\beta\alpha\beta}$ quantities are quartic centrifugal distortion constants, and $\sigma^{-1} = (B'_0 - C'_0)(2A'_0 - B'_0 - C'_0)^{-1}$ is the inverse asymmetry parameter computed from the effective rotational constants appearing in the Kivelson and Wilson formalism.²⁰⁹ The theoretical $A_0^{(S)} - A_0$, $B_0^{(S)} - B_0$, and $C_0^{(S)} - C_0$ differences, which are very small, are listed in Table XVI along with the $A_e - A_0$, $B_e - B_0$, and $C_e - C_0$ vibrational correction terms from the SQM(CCSD) + RHF//expt. force field. In principle, the only remaining source of error in the equilibrium rotational constants resulting from the vibrational and centrifugal distortion corrections is that due to the coupling of electronic orbital angular momentum with the rotation of the nuclear framework.^{134,210} For closed-shell systems containing π electrons, the effect of this phenomenon on the inertial defect of planar molecules can be significant, and in the case of HNCO it is probably greater than the centrif-

ugal distortion contribution.²¹⁰ However, uncertainties already present in the experimental $A_0^{(S)}$ constants and in the theoretical vibrational corrections are expected to be much larger than electronic contributions to the inertial defect, and thus no effort was made incorporate electronic effects into the final determination of the R_e structure.

The improved accuracy of the A_e , B_e , and C_e constants obtained from the SQM(CCSD) + RHF//expt. force field clearly becomes evident in the Kraitchman analysis. All imaginary roots are eliminated, and the coordinates determined directly from Eqs. (30) and (31) are in good agreement with those obtained from the procedure of Yamada.⁵² Thus the refined R_e parameters in Table XVII were extracted from the Kraitchman conditions without constraint, except that the center of mass conditions, i.e., Eqs. (31) and (32), were employed to evaluate the minute a_C and b_O values, both of which are less than 0.005 \AA in magnitude in the final structure. The differences between R_e structures (I) and (II) are all insignificant. The recommended structure (II) values were computed as weighted averages as before, and the listed uncertainties were estimated from the ranges of the data in Table XVII. The $r_e(\text{N-H})$ distance of 1.0030 \AA is in remarkable agreement with the 1.004 \AA estimate mentioned above, and this parameter is now much more firmly established than before. The agreement between the empirically derived R_e parameters and the DZ(d,p) CISD predictions is particularly good. The theoretical bond lengths are uniformly $0.003\text{--}0.006 \text{ \AA}$ longer than experiment, and the bond angles agree to within 1.3° .

The complete set of vibration-rotation interaction constants and quartic centrifugal distortion parameters for HNCO and DNCO is tabulated in Table XVIII. The contributions to the α_i constants from each of the three summations in Eq. (35) are also listed in order to identify the physical basis for each value. All Coriolis terms were in-

TABLE XVII. R_e structural parameters for isocyanic acid derived from empirical rotational constants.^a

	$r(\text{N-H})$	$r(\text{N-C})$	$r(\text{C-O})$	$\theta(\text{H-N-C})$	$\theta(\text{N-C-O})$
Structure (I) (RHF//RHF)					
(A,B)	1.004 90	1.215 07	1.163 67	123.212	172.337
(A,C)	1.004 13	1.214 97	1.163 77	123.161	172.333
(B,C)	1.002 01	1.214 99	1.163 65	123.394	172.407
Final ^b	1.003 3	1.215 0	1.163 7	123.29	172.37
Structure (II) [SQM(CCSD) + RHF//expt.]					
(A,B)	1.003 89	1.214 50	1.163 42	123.325	172.236
(A,C)	1.003 33	1.214 50	1.163 44	123.289	172.236
(B,C)	1.002 43	1.214 57	1.163 41	123.366	172.209
Final ^b	1.003 0(20)	1.214 5(6)	1.163 4(4)	123.34(20)	172.32(20)

^aBond distances in \AA and bond angles in deg. Structures (I) and (II) were derived from the RHF//RHF and SQM(CCSD) + RHF//expt. cubic force fields, respectively, as described in the text.

^bWeighted averages of the parameters resulting from the (A,B), (A,C), and (B,C) pairs of rotational constants; the respective weighting factors were chosen as 1/4, 1/4, and 1/2.

TABLE XVIII. Vibration-rotation interaction constants (α_i) and quartic centrifugal distortion constants for HNCO and DNCO.^a

HNCO				DNCO			
α_1^A	2 436	(-688, -34, 3158)	1223	(-287, -4, 1514)			
α_2^A	572	(-1, -2, 574)	201	(-13, 0, 214)			
α_3^A	411	(-7, -10, 428)	161	(-26, -5, 192)			
α_4^A	-10 473	(-2774, -4422, -3777)	-7219	(-384, -5700, -1135)			
α_5^A	30 923	(-536, 32 160, -700)	491.0	(-931, 2201, -778)			
α_6^A	-27 512	(0, -27619, 107)	3546	(0, 3532, 15)			
α_1^B	0.403	(-0.093, -0.002, 0.498)	0.129	(-0.122, -0.004, 0.255)			
α_2^B	2.841	(-0.008, -0.385, 3.235)	2.453	(-0.001, -0.338, 2.791)			
α_3^B	1.092	(-0.611, -0.000, 1.704)	0.937	(-0.527, -0.001, 1.464)			
α_4^B	-0.08	(-0.326, -0.014, 0.258)	0.228	(-0.142, -0.008, 0.378)			
α_5^B	-1.014	(-0.322, 0.072, -0.763)	-0.860	(-0.589, 0.018, -0.289)			
α_6^B	-0.427	(0.000, 0.506, -0.933)	-0.357	(0, 0.490, -0.847)			
α_1^C	0.796	(-0.003, -0.225, 1.024)	0.650	(-0.004, -0.264, 0.917)			
α_2^C	2.860	(-0.001, -0.388, 3.249)	2.437	(-0.000, -0.333, 2.770)			
α_3^C	1.129	(-0.588, -0.016, 1.732)	0.983	(-0.499, -0.007, 1.488)			
α_4^C	0.042	(-0.001, 0.437, -0.394)	0.277	(-0.011, 0.431, -0.142)			
α_5^C	-0.294	(-0.000, 0.569, -0.863)	-0.077	(-0.010, 0.556, -0.623)			
α_6^C	-0.891	(0.000, 0.000, -0.891)	-0.805	(0, 0, -0.805)			
D_J	1.11×10^{-4}		1.04×10^{-4}				
D_{JK}	0.026 86		-0.002 56				
D_K	70.98		27.49				
d_1	-1.86×10^{-6}		-5.84×10^{-6}				
d_2	-4.07×10^{-7}		-8.81×10^{-7}				

^aObtained from the SQM(CCSD)+RHF//expt. force field. All constants are in units of 10^{-3} cm^{-1} .

cluded in the evaluation of the α_i quantities from the ξ_{ij} constants in Table XIX. For the stretching modes the anharmonic components of the α_i constants are preponderate for every rotational constant, whereas the Coriolis contribution becomes large for the bending fundamentals. As expected, the Coriolis interaction is dominant for α_5^A and α_6^A and is comparable to the anharmonic term for α_4^A , α_4^C , α_5^C , and α_6^B . In fact, the strong $\omega_4 - \omega_6$ and $\omega_5 - \omega_6$ Coriolis interactions engender α_5^A and α_6^A constants as large as A_e itself, and thus a catastrophic breakdown of perturbation theory is observed. The directions and magnitudes of the vibrational shifts indicated by the α_5^A and α_6^A constants are qualitatively correct, however, in that the empirical rotational constants for the ν_5 and ν_6 fundamental levels are shifted +19.15 and -5.98 cm^{-1} , respectively, from A_0 .⁵¹ For α_4^A all three contributions in Eq. (35) are sizeable, and the predicted vibrational shift is in surprisingly good agreement with the observed -10.94 cm^{-1} .⁵¹ In general the α_i^B and α_i^C constants are of the expected magnitude and should

be amenable to prediction by perturbation theory, but the values listed in Table XIX are only broadly consistent with the meager experimental data available in the literature. The agreement between theory and experiment for the quartic centrifugal distortion parameters is better. Although Yamada, Winnewisser, and Johns⁴⁶ have very recently revised the centrifugal distortion constants for the ground vibrational state of HNCO, an earlier set of results obtained by Fusina *et al.*⁵⁶ (Set II of Table I therein) is a more proper choice for comparison with the current predictions because the planarity condition on the quartic constants was imposed in the analysis. In units of 10^3 cm^{-1} , the empirical values in question are $D_J = 1.17 \times 10^{-4}$, $D_{JK} = 0.0313$, $D_K = 198.0$, $d_1 = -2.45 \times 10^{-6}$, and $d_2 = -6.18 \times 10^{-7}$. The D_K value differs by a factor of 2.8 from that in Table XIX because this quantity is associated with the \hat{J}_a operator, but the agreement for the remaining constants is quite satisfactory.

TABLE XIX. Coriolis coupling constants for HNCO and DNCO.^a

HNCO				DNCO			
ij (ξ_{ij}^a)	ij (ξ_{ij}^b)	ij (ξ_{ij}^c)	ij (ξ_{ij}^d)	ij (ξ_{ij}^e)	ij (ξ_{ij}^f)	ij (ξ_{ij}^g)	ij (ξ_{ij}^h)
61 (0.162)	61 (0.098)	21 (0.052)	43 (0.119)	61 (-0.077)	61 (0.118)	21 (-0.004)	43 (0.106)
62 (-0.030)	62 (-0.988)	31 (0.015)	51 (0.603)	62 (0.018)	62 (0.989)	31 (0.134)	51 (0.735)
63 (-0.046)	63 (0.027)	32 (0.036)	52 (-0.795)	63 (0.053)	63 (-0.029)	32 (0.026)	52 (-0.667)
64 (0.516) ^b	64 (0.069)	41 (-0.787)	53 (-0.039)	64 (-0.815)	64 (-0.045)	41 (-0.651)	53 (-0.084)
65 (0.839) ^b	65 (0.095)	42 (-0.603)	54 (-0.055)	65 (0.571)	65 (-0.076)	42 (-0.744)	54 (0.004)

^aComputed from the SQM(CCSD)//expt. quadratic force field.

^bThese values compare well with the $\xi_{64}^a = 0.554$ and $\xi_{65}^a = 0.801$ results derived from an empirical fit in Ref. 51.

ACKNOWLEDGMENTS

The research presented here was partially supported by the U.S. National Science Foundation, Grant No. CHEM-8821737 and also by computer time grants from Academic Information Resources at Stanford University. Dr. Brian F. Yates of the University of Tasmania is thanked for helpful discussions during his 1991 visit to Stanford.

- ¹ *Man's Impact on the Global Environment, Report of the Study of Critical Environmental Problems (SCEP)*, (M. I. T., Cambridge, Mass., 1970).
- ² H. Johnston, *Science* **173**, 517 (1971).
- ³ T. Godish, *Air Quality*, 2nd ed. (Lewis, Chelsea, Michigan, 1991).
- ⁴ I. Glassman, *Combustion*, 2nd ed. (Academic, Orlando, 1987).
- ⁵ K. Wark and C. F. Warner, *Air Pollution: Its Origin and Control*, 2nd ed. (Harper & Row, New York, 1981).
- ⁶ R. K. Hanson and S. Salimian, in *Combustion Chemistry*, edited by W. C. Gardiner, Jr. (Springer, New York, 1984), p. 361.
- ⁷ R. K. Lyon, *Method for the Reduction of the Concentration of NO in Combustion Effluents Using Ammonia*, U.S. Patent No. 3,900,554 (1975).
- ⁸ M. A. Kimball-Linne and R. K. Hanson, *Combust. Flame* **64**, 337 (1986).
- ⁹ R. K. Lyon, *Kinetics and Mechanism of Thermal DeNO_x: A Review*, 194th Annual ACS Meeting, Division of Fuel Chemistry **32**, 433 (1987).
- ¹⁰ J. A. Miller and C. T. Bowman, *Int. J. Chem. Kinet.* **23**, 289 (1991).
- ¹¹ S. P. Walch, R. J. Duchovic, and C. M. Rohlfling, *J. Chem. Phys.* **90**, 3230 (1989).
- ¹² S. P. Walch, *J. Chem. Phys.* **93**, 2384 (1990).
- ¹³ H. Koizuma, G. C. Schatz, and S. P. Walch, *J. Chem. Phys.* **95**, 4130 (1991).
- ¹⁴ R. A. Perry and D. L. Siebers, *Nature (London)* **324**, 657 (1986).
- ¹⁵ D. L. Siebers and J. A. Caton, *Reduction of Nitrogen Oxides by the RAPRENO_x Process*, Sandia National Laboratories Report SAND88-8713B (1988).
- ¹⁶ R. K. Lyon and J. A. Cole, *Combust. Flame* **82**, 435 (1990).
- ¹⁷ M. P. Heap, S. L. Chen, J. C. Kramlich, J. M. McCarthy, and D. W. Pershing, *Nature (London)* **335**, 620 (1988).
- ¹⁸ B. G. Wicke, K. A. Grady, and J. W. Ratcliffe, *Combust. Flame* **78**, 249 (1989).
- ¹⁹ D. L. Siebers and J. A. Caton, *Combust. Flame* **79**, 31 (1990).
- ²⁰ J. A. Caton and D. L. Siebers, *Combust. Sci. Technol.* **65**, 277 (1989).
- ²¹ F. P. Tully, R. A. Perry, L. R. Thorne, and M. D. Allendorf, *Twenty-Second Symposium (International) on Combustion*, The Combustion Institute, Pittsburgh (1989), p. 1101.
- ²² J. A. Miller and C. T. Bowman, *Prog. Energy Combust. Sci.* **15**, 287 (1989).
- ²³ D. J. Belson and A. N. Strachan, *Chem. Soc. Rev.* **11**, 41 (1982).
- ²⁴ J. D. Mertens, A. Y. Chang, R. K. Hanson, and C. T. Bowman, *Int. J. Chem. Kinet.* **24**, 279 (1992).
- ²⁵ X. Liu, N. P. Machara, and R. D. Coombe, *J. Phys. Chem.* **95**, 4983 (1991).
- ²⁶ J. D. Mertens, K. Kohse-Hoinghaus, R. K. Hanson, and C. T. Bowman, *Int. J. Chem. Kinet.* **23**, 655 (1991).
- ²⁷ J. D. Mertens, A. Y. Chang, R. K. Hanson, and C. T. Bowman, *Int. J. Chem. Kinet.* **21**, 1049 (1989).
- ²⁸ Y. He, X. Liu, M. C. Lin, and C. F. Melius, *Int. J. Chem. Kinet.* **23**, 1129 (1991).
- ²⁹ W. Beck and K. Feldl, *Angew. Chem. Internat. Ed.* **5**, 722 (1966).
- ³⁰ W. Beck, P. Swoboda, K. Feldl, and R. S. Tobias, *Chem. Ber.* **104**, 533 (1971).
- ³¹ W. Beck, E. Schuierer, and K. Feldl, *Angew. Chem. Internat. Ed.* **4**, 698 (1965).
- ³² B. P. Winnewisser, M. Winnewisser, and F. Winther, *J. Mol. Spectrosc.* **51**, 65 (1974).
- ³³ M. Winnewisser and H. K. Bodenseh, *Z. Naturforsch. Teil A* **22**, 1724 (1967).
- ³⁴ H. K. Bodenseh and M. Winnewisser, *Z. Naturforsch. Teil A* **24**, 1966 (1969).
- ³⁵ H. K. Bodenseh and M. Winnewisser, *Z. Naturforsch. Teil A* **24**, 1973 (1969).
- ³⁶ J. H. Teles, G. Maier, B. A. Hess, Jr., L. J. Schaad, M. Winnewisser, and B. P. Winnewisser, *Chem. Ber.* **122**, 753 (1989).
- ³⁷ D. Poppinger, L. Radom, and J. A. Pople, *J. Am. Chem. Soc.* **99**, 7806 (1977).
- ³⁸ A. D. McLean, G. H. Loew, and D. S. Berkowitz, *J. Mol. Spectrosc.* **64**, 184 (1977).
- ³⁹ K. Yokoyama, S. Takane, and T. Fueno, *Bull. Chem. Soc. Jpn.* **64**, 2230 (1991).
- ⁴⁰ T. A. Spiglanin, R. A. Perry, and D. W. Chandler, *J. Phys. Chem.* **90**, 6184 (1986).
- ⁴¹ H. Okabe, *J. Chem. Phys.* **53**, 3507 (1970).
- ⁴² J. Breulet and J. Lievin, *Theor. Chim. Acta* **61**, 59 (1982).
- ⁴³ I. Tokue and Y. Ito, *Chem. Phys.* **89**, 51 (1984).
- ⁴⁴ T. Hikida, Y. Maruyama, Y. Saito, and Y. Mori, *Chem. Phys.* **121**, 63 (1988).
- ⁴⁵ E. Quiñones, J. Chen, and P. J. Dagdigan, *Chem. Phys. Lett.* **174**, 65 (1990).
- ⁴⁶ K. M. T. Yamada, M. Winnewisser, and J. W. C. Johns, *J. Mol. Spectrosc.* **140**, 353 (1990).
- ⁴⁷ R. A. Ashby and R. L. Werner, *J. Mol. Spectrosc.* **18**, 184 (1965).
- ⁴⁸ R. A. Ashby and R. L. Werner, *Spectrochim. Acta* **22**, 1345 (1966).
- ⁴⁹ B. Krakow, R. C. Lord, and G. O. Neely, *J. Mol. Spectrosc.* **27**, 148 (1968).
- ⁵⁰ G. O. Neely, *J. Mol. Spectrosc.* **27**, 177 (1968).
- ⁵¹ D. A. Steiner, K. A. Wishah, S. R. Polo, and T. K. McCubbin, Jr., *J. Mol. Spectrosc.* **76**, 341 (1979).
- ⁵² K. Yamada, *J. Mol. Spectrosc.* **79**, 323 (1980).
- ⁵³ K. Yamada, *J. Mol. Spectrosc.* **81**, 139 (1980).
- ⁵⁴ K. Yamada, *J. Mol. Spectrosc.* **68**, 423 (1977).
- ⁵⁵ L. Fusina and I. M. Mills, *J. Mol. Spectrosc.* **86**, 488 (1981).
- ⁵⁶ L. Fusina, M. Carlotti, and B. Carli, *Can. J. Phys.* **62**, 1452 (1984).
- ⁵⁷ G. Herzberg and C. Reid, *Discuss. Faraday Soc.* **9**, 92 (1950).
- ⁵⁸ P. Botschwina, E. Nachbaur, and B. M. Rode, *Chem. Phys. Lett.* **41**, 486 (1976).
- ⁵⁹ D. Buhl, L. E. Snyder, and J. Edrich, *Astrophys. J.* **177**, 625 (1972).
- ⁶⁰ D. Buhl, L. E. Snyder, P. R. Schwartz, and J. Edrich, *Nature (London)* **243**, 513 (1973).
- ⁶¹ P. M. Solomon, A. A. Penzias, K. B. Jefferts, and R. W. Wilson, *Astrophys. J. Lett.* **185**, L63 (1973).
- ⁶² W. H. Hocking, M. C. L. Gerry, and G. Winnewisser, *Can. J. Phys.* **53**, 1869 (1975).
- ⁶³ J. Kraitchman, *Am. J. Phys.* **21**, 17 (1953).
- ⁶⁴ C. C. Costain, *J. Chem. Phys.* **29**, 864 (1958).
- ⁶⁵ J. W. Rabalais, J. R. McDonald, and S. P. McGlynn, *J. Chem. Phys.* **51**, 5103 (1969).
- ⁶⁶ R. N. Dixon and G. H. Kirby, *Trans. Faraday Soc.* **64**, 2002 (1968).
- ⁶⁷ J. Y. P. Mui and R. A. Back, *Can. J. Chem.* **41**, 826 (1963).
- ⁶⁸ R. A. Back, *J. Chem. Phys.* **40**, 3493 (1964).
- ⁶⁹ J. L. Brash and R. A. Back, *Can. J. Chem.* **43**, 1778 (1965).
- ⁷⁰ R. A. Back and R. Ketcheson, *Can. J. Chem.* **46**, 531 (1968).
- ⁷¹ N. J. Friswell and R. A. Back, *Can. J. Chem.* **46**, 527 (1968).
- ⁷² W. D. Woolley and R. A. Back, *Can. J. Chem.* **46**, 295 (1968).
- ⁷³ T. A. Spiglanin, R. A. Perry, and D. W. Chandler, *J. Chem. Phys.* **87**, 1568 (1987).
- ⁷⁴ T. A. Spiglanin and D. W. Chandler, *J. Chem. Phys.* **87**, 1577 (1987).
- ⁷⁵ T. A. Spiglanin and D. W. Chandler, *Chem. Phys. Lett.* **141**, 428 (1987).
- ⁷⁶ The descriptors DZ (double-zeta), QZ (quadruple-zeta), and PZ (penta-zeta) are derived specifically from the number of contracted *p* shells in the valence region of the heavy-atom basis sets.
- ⁷⁷ S. Huzinaga, *J. Chem. Phys.* **42**, 1293 (1965).
- ⁷⁸ T. H. Dunning, Jr., *J. Chem. Phys.* **53**, 2823 (1970).
- ⁷⁹ T. H. Dunning, Jr., *J. Chem. Phys.* **55**, 716 (1971).
- ⁸⁰ W. D. Allen and H. F. Schaefer III, *Chem. Phys.* **108**, 243 (1986).
- ⁸¹ The orbital exponents of the diffuse functions are $\alpha_s(\text{O})=0.084\ 58$, $\alpha_p(\text{O})=0.056\ 54$, $\alpha_s(\text{N})=0.063\ 76$, $\alpha_p(\text{N})=0.048\ 61$, $\alpha_s(\text{C})=0.045\ 61$, and $\alpha_p(\text{C})=0.033\ 44$.
- ⁸² H. Partridge, *Near Hartree-Fock Quality Gaussian Type Orbital Basis Sets for the First- and Third-Row Atoms*, NASA Technical Memorandum 101044 (1989).

- ⁸³M. W. Wong, P. M. W. Gill, R. H. Nobes, and L. Radom, *J. Phys. Chem.* **92**, 4875 (1988).
- ⁸⁴T. H. Dunning, Jr., *J. Chem. Phys.* **90**, 1007 (1989).
- ⁸⁵C. C. J. Roothaan, *Rev. Mod. Phys.* **23**, 69 (1951).
- ⁸⁶J. A. Pople and R. K. Nesbet, *J. Chem. Phys.* **22**, 571 (1954).
- ⁸⁷W. J. Hehre, L. Radom, P. v. R. Schleyer, and J. A. Pople, *Ab initio Molecular Orbital Theory* (Wiley-Interscience, New York, 1986).
- ⁸⁸A. Szabo and N. S. Ostlund, *Modern Quantum Chemistry* (McGraw-Hill, New York, 1989).
- ⁸⁹B. O. Roos, in *Ab Initio Methods in Quantum Chemistry*, edited by K. P. Lawley (Wiley, 1987), Vol. III, p. 399.
- ⁹⁰I. Shavitt, in *Modern Theoretical Chemistry*, edited by H. F. Schaefer III (Plenum, New York, 1977), Vol. 3, p. 189.
- ⁹¹B. R. Brooks and H. F. Schaefer III, *J. Chem. Phys.* **70**, 5391 (1979).
- ⁹²P. Saxe, D. J. Fox, H. F. Schaefer III, and N. C. Handy, *J. Chem. Phys.* **77**, (1982).
- ⁹³S. R. Langhoff and E. R. Davidson, *Int. J. Quantum Chem.* **8**, 61 (1974).
- ⁹⁴C. Møller and M. S. Plesset, *Phys. Rev.* **46**, 618 (1934).
- ⁹⁵J. A. Pople, J. S. Binkley, and R. Seeger, *Int. J. Quantum Chem. Symp.* **10**, 1 (1976).
- ⁹⁶R. Krishnan and J. A. Pople, *Int. J. Quantum Chem.* **14**, 91 (1978).
- ⁹⁷R. Krishnan, M. J. Frisch, and J. A. Pople, *J. Chem. Phys.* **72**, 4244 (1980).
- ⁹⁸K. Raghavachari, J. A. Pople, E. S. Replogle, and M. Head-Gordon, *J. Phys. Chem.* **94**, 5579 (1990).
- ⁹⁹S. W. Kucharski and R. J. Bartlett, *Adv. Quantum Chem.* **18**, 281 (1986).
- ¹⁰⁰R. J. Bartlett, *Annu. Rev. Phys. Chem.* **32**, 359 (1981).
- ¹⁰¹G. D. Purvis and R. J. Bartlett, *J. Chem. Phys.* **76**, 1910 (1982).
- ¹⁰²J. Paldus, in *New Horizons of Quantum Chemistry*, edited by P.-O. Löwdin and B. Pullman (Reidel, Dordrecht, 1983), p. 31.
- ¹⁰³R. J. Bartlett, C. E. Dykstra, and J. Paldus, in *Advanced Theories and Computational Approaches to the Electronic Structure of Molecules*, edited by C. E. Dykstra (Reidel, Dordrecht, 1984), p. 127.
- ¹⁰⁴G. E. Scuseria, A. C. Scheiner, T. J. Lee, J. E. Rice, and H. F. Schaefer III, *J. Chem. Phys.* **86**, 2881 (1987).
- ¹⁰⁵A. C. Scheiner, G. E. Scuseria, J. E. Rice, T. J. Lee, and H. F. Schaefer III, *J. Chem. Phys.* **87**, 5361 (1987).
- ¹⁰⁶K. Raghavachari, G. W. Trucks, J. A. Pople, and M. Head-Gordon, *Chem. Phys. Lett.* **157**, 479 (1989).
- ¹⁰⁷G. E. Scuseria and T. J. Lee, *J. Chem. Phys.* **93**, 5851 (1990).
- ¹⁰⁸J. A. Pople, M. J. Frisch, B. T. Luke, and J. S. Binkley, *Int. J. Quantum Chem. Symp.* **17**, 307 (1983).
- ¹⁰⁹N. C. Handy, P. J. Knowles, and K. Somasundram, *Theor. Chim. Acta* **68**, 87 (1985).
- ¹¹⁰R. J. Bartlett and I. Shavitt, *Chem. Phys. Lett.* **50**, 190 (1977).
- ¹¹¹W. D. Laidig, G. Fitzgerald, and R. J. Bartlett, *Chem. Phys. Lett.* **113**, 151 (1985).
- ¹¹²H. B. Schlegel, *J. Chem. Phys.* **84**, 4530 (1986).
- ¹¹³H. B. Schlegel, *J. Phys. Chem.* **92**, 3075 (1988).
- ¹¹⁴PSI 1.0 (PSITECH Inc., Watkinsville, Georgia, 1989).
- ¹¹⁵R. D. Amos and J. E. Rice, *CADPAC: The Cambridge Analytic Derivative Package* (Cambridge University, Cambridge, 1987).
- ¹¹⁶M. J. Frisch, M. Head-Gordon, G. W. Trucks, J. B. Foresman, H. B. Schlegel, K. Raghavachari, M. A. Robb, J. S. Binkley, C. Gonzalez, D. J. Defrees, D. J. Fox, R. A. Whiteside, R. Seeger, C. F. Melius, J. Baker, R. Martin, L. R. Kahn, J. J. P. Stewart, S. Topiol, and J. A. Pople, *GAUSSIAN 90* (Gaussian, Inc., Pittsburgh, 1990).
- ¹¹⁷J. F. Gaw and N. C. Handy, *Ann. Rept. R. Soc. Chem. C* **291** (1984).
- ¹¹⁸H. F. Schaefer III and Y. Yamaguchi, *J. Mol. Struct. THEOCHEM* **135**, 369 (1986).
- ¹¹⁹*Geometrical Derivatives of Energy Surfaces and Molecular Properties*, edited by P. Jørgensen and J. Simons (Reidel, Dordrecht, 1986).
- ¹²⁰P. Pulay, *Mol. Phys.* **17**, 197 (1969).
- ¹²¹P. Pulay, in *Modern Theoretical Chemistry*, edited by H. F. Schaefer III, (Plenum, New York, 1977), Vol. 4, p. 153.
- ¹²²B. R. Brooks, W. D. Laidig, P. Saxe, M. A. Vincent, J. F. Gaw, and H. F. Schaefer III, *J. Chem. Phys.* **72**, 4652 (1980).
- ¹²³J. E. Rice, R. D. Amos, N. C. Handy, T. J. Lee, and H. F. Schaefer III, *J. Chem. Phys.* **85**, 963 (1986).
- ¹²⁴A. P. Rendell and T. J. Lee, *J. Chem. Phys.* **94**, 6219 (1991).
- ¹²⁵Y. Osamura, Y. Yamaguchi, P. Saxe, M. A. Vincent, J. F. Gaw, and H. F. Schaefer III, *Chem. Phys.* **72**, 131 (1982).
- ¹²⁶Y. Osamura, Y. Yamaguchi, P. Saxe, D. J. Fox, M. A. Vincent, and H. F. Schaefer III, *J. Mol. Struct. THEOCHEM* **103**, 183 (1983).
- ¹²⁷P. Pulay and F. Török, *Acta Chim. Hung.* **44**, 287 (1965).
- ¹²⁸J. Overend, in *Infrared Spectroscopy and Molecular Structure*, edited by M. Davies (Elsevier, Amsterdam, 1963), p. 345.
- ¹²⁹G. Zerbi, in *Vibrational Intensities in Infrared and Raman Spectroscopy*, edited by W. B. Person and G. Zerbi (Elsevier, Amsterdam, 1982).
- ¹³⁰J. F. Gaw, Y. Yamaguchi, and H. F. Schaefer III, *J. Chem. Phys.* **81**, 6395 (1984).
- ¹³¹J. F. Gaw, Y. Yamaguchi, H. F. Schaefer III, and N. C. Handy, *J. Chem. Phys.* **85**, 5132 (1986).
- ¹³²I. M. Mills, in *Molecular Spectroscopy: Modern Research*, edited by K. N. Rao and C. W. Mathews (Academic, New York, 1972), Vol. 1, p. 115.
- ¹³³H. H. Nielsen, *Rev. Mod. Phys.* **23**, 90 (1951).
- ¹³⁴D. Papoušek and M. R. Aliev, *Molecular Vibrational-Rotational Spectra* (Elsevier, Amsterdam, 1982).
- ¹³⁵J. K. G. Watson, in *Vibrational Spectra and Structure*, edited by J. R. Durig (Elsevier, Amsterdam, 1977), Vol. 6, p. 1.
- ¹³⁶J. K. G. Watson, *J. Chem. Phys.* **48**, 4517 (1968).
- ¹³⁷D. A. Clabo, Jr., W. D. Allen, R. B. Remington, Y. Yamaguchi, and H. F. Schaefer III, *Chem. Phys.* **123**, 187 (1988).
- ¹³⁸W. D. Allen, Y. Yamaguchi, A. G. Császár, D. A. Clabo, Jr., R. B. Remington, and H. F. Schaefer III, *Chem. Phys.* **145**, 427 (1990).
- ¹³⁹The Hessian index formally denotes the total number of negative eigenvalues resulting from the vibrational secular equations involving the quadratic force field. However, the out-of-plane block of the secular problem is excluded from consideration here.
- ¹⁴⁰The FNNF molecule is representative of such systems. See T. J. Lee, J. E. Rice, G. E. Scuseria, and H. F. Schaefer III, *Theor. Chim. Acta* **75**, 81 (1989).
- ¹⁴¹See, for example, P. Valtazanos and K. Ruedenberg, *Theor. Chim. Acta* **69**, 281 (1986).
- ¹⁴²R. J. Buenker and S. D. Peyerimhoff, *Chem. Rev.* **74**, 127 (1974).
- ¹⁴³A. D. Walsh, *J. Chem. Soc., Part. III*, 2260 (1953), and articles which immediately follow.
- ¹⁴⁴Note from the data given in the caption of Fig. 3 that the inclusion of the 1s core orbitals in the sum actually reverses the sign of the net orbital energy first derivative, indicating an erroneous preference for *cis* bending.
- ¹⁴⁵The directions of the shifts in the net atomic charges are confirmed by calculations using larger basis sets. For example, at the DZ(*d,p*) CISD optimum structures, the QZ(2*d*1*f*,2*p*1*d*) SCF net charges are linear, $q(O) = -0.307$, $q(C) = 0.534$, $q(N) = -0.532$, and $q(H) = 0.305$; and *trans* bent, $q(O) = -0.262$, $q(C) = 0.473$, $q(N) = -0.422$, and $q(H) = 0.212$.
- ¹⁴⁶At the DZ(*d,p*) CISD geometry, the following RHF dipole moments (in D) are obtained: DZ(*d,p*), 2.344; QZ(2*d*,2*p*), 2.256; and PZ(3*d*2*f*,2*p*1*d*), 2.236. Moreover, the DZ(*d,p*) CCSD//DZ(*d,p*) CCSD value is 2.154 D.
- ¹⁴⁷The empirical estimate of $|\mu_b| = 1.35 \pm 0.10$ D is actually smaller than the corresponding μ_a component, at variance with the CISD prediction. To the degree that $\theta(H-N-C)$ is shifted toward linearity upon vibrational averaging, the equilibrium μ_a and μ_b values should be smaller and larger in magnitude, respectively, than the observed components. Thus zero-point vibrational effects may account for much of the disparity in the relative ordering of $|\mu_a|$ and $|\mu_b|$.
- ¹⁴⁸T. J. Lee and P. R. Taylor, *Int. J. Quantum Chem. Symp.* **23**, 199 (1989).
- ¹⁴⁹A. D. McLean, G. H. Loew, and D. S. Berkowitz, *J. Mol. Spectrosc.* **72**, 430 (1978).
- ¹⁵⁰C. Glidewell and C. Thomson, *J. Mol. Struct. THEOCHEM* **104**, 287 (1983).
- ¹⁵¹T. J. Lee, R. B. Remington, Y. Yamaguchi, and H. F. Schaefer III, *J. Chem. Phys.* **89**, 408 (1988).
- ¹⁵²K. P. Huber and G. Herzberg, *Constants of Diatomic Molecules* (Van Nostrand, Princeton, 1979).
- ¹⁵³W. R. Anderson, *J. Phys. Chem.* **93**, 530 (1989).
- ¹⁵⁴C. W. Bauschlicher, Jr. and S. R. Langhoff, *Chem. Phys. Lett.* **135**, 67 (1987).
- ¹⁵⁵A similar result of 86.7 ± 0.5 kcal mol⁻¹ was recently obtained via large-basis MP4 and CCSD(T) studies of pertinent isodesmic reac-

- tions; N. Oliphant, M. Rosenkrantz, and D. Konowalow (personal communication, 1992).
- ¹⁵⁶ A. R. Hoy, I. M. Mills, and G. Strey, *Mol. Phys.* **24**, 1265 (1972).
- ¹⁵⁷ W. S. Benedict and E. K. Plyler, *Can. J. Phys.* **35**, 1235 (1957).
- ¹⁵⁸ I. Suzuki, *J. Mol. Spectrosc.* **25**, 479 (1968).
- ¹⁵⁹ I.-C. Chen, W. H. Green, Jr., and C. B. Moore, *J. Chem. Phys.* **89**, 314 (1988).
- ¹⁶⁰ P. R. Bunker, P. Jensen, W. P. Kraemer, and R. Beardsworth, *J. Chem. Phys.* **85**, 3724 (1986).
- ¹⁶¹ C. B. Moore and G. C. Pimentel, *J. Chem. Phys.* **38**, 2816 (1963).
- ¹⁶² A. D. McLean, P. R. Bunker, R. M. Escibano, and P. Jensen, *J. Chem. Phys.* **87**, 2166 (1987).
- ¹⁶³ M. D. Marshall and A. R. W. McKellar, *J. Chem. Phys.* **85**, 3716 (1986).
- ¹⁶⁴ C. W. Bauschlicher, Jr., S. R. Langhoff, and P. R. Taylor, *Chem. Phys. Lett.* **135**, 543 (1987); *Adv. Chem. Phys.* **77**, 103 (1990).
- ¹⁶⁵ H. Partridge, S. R. Langhoff, C. W. Bauschlicher, Jr., and D. W. Schwenke, *J. Chem. Phys.* **88**, 3174 (1988).
- ¹⁶⁶ K. Jankowski, R. Becherer, P. Scharf, H. Schiffer, and R. Ahlrichs, *J. Chem. Phys.* **82**, 1413 (1985).
- ¹⁶⁷ M. J. Frisch, J. A. Pople, and J. S. Binkley, *J. Chem. Phys.* **80**, 3265 (1984).
- ¹⁶⁸ R. S. Grev and H. F. Schaefer III, *J. Chem. Phys.* (submitted for publication).
- ¹⁶⁹ M. Wolfsberg, A. A. Massa, and J. W. Pyper, *J. Chem. Phys.* **53**, 3138 (1970).
- ¹⁷⁰ Experimental ν_i and χ_{ij} values were employed for CO₂, H₂O, CO, and NH (Refs. 200, 221, and 152, respectively). For HNCO the observed fundamental frequencies appearing in Fig. 2 were utilized in conjunction with the SQM(CCSD)+RHF//expt. anharmonic constants given in Table XIII (*vide infra*). For NH₃ the χ_{ij} and χ_{ij} values were theoretical DZ+d SCF results from Ref. 216 except those which were affected by Fermi resonance. The remaining anharmonic constants and the fundamental frequencies of NH₃ are experimental results (Refs. 157, 215).
- ¹⁷¹ *JANAF Thermochemical Tables*, 3rd ed., J. Phys. Chem. Ref. Data **14**, Supp. No. 1 (1985).
- ¹⁷² Evaluated from the heats of formation and the ZPVE corrections of CO and CO₂ given in the text, as well as $\Delta H_{f,0}^\circ = 58.98$ kcal mol⁻¹ for O(³P) (Ref. 171).
- ¹⁷³ R. N. Dixon, *Philos. Trans. R. Soc. London Ser. A* **252**, 165 (1960).
- ¹⁷⁴ From the heats of formation (kcal mol⁻¹) listed in Ref. 171 for N₂ (188), H(216.0), and HN₃(300.5), as well as the electron affinity of N₃ reported in R. L. Jackson, M. J. Pellerite, and J. I. Brauman, *J. Am. Chem. Soc.* **103**, 1802 (1981).
- ¹⁷⁵ Obtained from the heats of formation of NH₂, H, and NH₃ given in Ref. 171.
- ¹⁷⁶ See the discussion in Refs. 45 and 177.
- ¹⁷⁷ K.-Y. Du and D. W. Setser, *Chem. Phys. Lett.* **153**, 393 (1988).
- ¹⁷⁸ C. E. Moore, *Atomic Energy Levels*, Office of Standard Reference Data, National Bureau of Standards (U.S. GPO, Washington, D.C., 1971), Vol. 1.
- ¹⁷⁹ From Ref. 211. The Raman fundamental frequencies of the cyanate anion in a host of solid KBr have been reported as $\nu_1(\sigma) = 1207$, $\nu_2(\pi) = 630$, and $\nu_3(\sigma) = 2173$ cm⁻¹ (Ref. 219). For NCO, $\nu_1(\sigma) = 1272$, $\nu_2(\pi) = 530$, and $\nu_3(\sigma) = 1923$ cm⁻¹ have been found in an argon matrix (Ref. 183). These data yield a ZPVE correction to the electron affinity of +0.024 eV, which is much less than the uncertainty quoted by Ref. 211. Thus the cited value of 3.6 eV is taken as the vibrationless electron affinity.
- ¹⁸⁰ W. Koch and G. Frenking, *J. Phys. Chem.* **91**, 49 (1987).
- ¹⁸¹ P. M. W. Gill and L. Radom, *Chem. Phys. Lett.* **132**, 16 (1986).
- ¹⁸² QZ(2d1f,2p1d) total energies for OH (²II) at $r_e(\text{O-H}) = 0.96966$ Å (Ref. 152): UHF(-75.423 406), UMP2(-75.627 790), UMP3(-75.639 528), and UMP4(-75.646 016). See Table IV and footnote b of Table V for the total energies of H₂O and H.
- ¹⁸³ V. E. Bondybey and J. H. English, *J. Chem. Phys.* **67**, 2868 (1977).
- ¹⁸⁴ A. P. Rendell, T. J. Lee, and R. Lindh, *Chem. Phys. Lett.* **194**, 84 (1992).
- ¹⁸⁵ P. R. Bunker, B. M. Landsberg, and B. P. Winnewisser, *J. Mol. Spectrosc.* **74**, 9 (1979).
- ¹⁸⁶ The C-N distances in the 6-31G** MP2 reference structures (Ref. 36) of HOCN and HONC are probably 0.02–0.03 Å too long, as gauged from analogous results for HCN. Deficiencies of this size are not present in the DZ(d,p) CISD geometry of HNCO. Thus geometry relaxation effects are likely to decrease the relative energies of HOCN and HONC and partially offset the basis set trends.
- ¹⁸⁷ The experimental ν_i and χ_{ij} constants used in Eq. (18) for N₂O appear in Ref. 213.
- ¹⁸⁸ The experimental ν_i and χ_{ij} values of Ref. 212 were utilized for CH₄. The application of Eq. (18) is valid if one equates $\chi_{1/3} = 2G_{33}$ and $\chi_{1/4} = 2G_{44}$.
- ¹⁸⁹ The observation of sizeable amounts of CN radicals in the shock-heated decomposition of HNCO in the 2500–3500 K region was attributed in Ref. 39 to the fragmentation of HOCN. The degree to which the HOCN $\xrightarrow{\text{direct}}$ HONC \rightarrow HO + CN pathway is competitive is unclear, however.
- ¹⁹⁰ Ashby and Werner (Ref. 47) give 659.8 cm⁻¹ for the ν_6 band origin.
- ¹⁹¹ B. Lemoine, K. Yamada, and G. Winnewisser, *Ber. Bunsenges. Phys. Chem.* **86**, 795 (1982).
- ¹⁹² D. A. Steiner, S. R. Polo, T. K. McCubbin, Jr., and K. A. Wishah, *J. Mol. Spectrosc.* **98**, 453 (1983).
- ¹⁹³ W. D. Allen and A. G. Császár, *J. Chem. Phys.* **98** (1992), in press. See also W. D. Allen, A. L. L. East, and A. G. Császár, in *Structures and Conformations of Non-Rigid Molecules*, edited by J. Laane and M. Dakkouri (Kluwer, Dordrecht, 1993), in press.
- ¹⁹⁴ P. Pulay, W. Meyer, and J. E. Boggs, *J. Chem. Phys.* **68**, 5077 (1978).
- ¹⁹⁵ P. Pulay, G. Fogarasi, G. Pongor, J. E. Boggs, and A. Vargha, *J. Am. Chem. Soc.* **105**, 7037 (1983).
- ¹⁹⁶ G. Fogarasi and P. Pulay, in *Vibrational Spectra and Structure*, edited by J. R. Durig (Elsevier, Amsterdam, 1985), Vol. 14, p. 125.
- ¹⁹⁷ W. D. Allen, A. G. Császár, and D. A. Horner, *J. Am. Chem. Soc.* **114**, 6834 (1992).
- ¹⁹⁸ Relaxation of the constraint of α_x and α_y to the same scale factor was observed to yield optimum values separated by less than 0.015.
- ¹⁹⁹ For example, the harmonic stretching frequency (cm⁻¹) for NH(³Σ⁻) is 3282.27 and those for NH₃ are 3506 and 3577 (Ref. 157). The hydrogen stretching anharmonicities of some common species (cm⁻¹) are: HF (-177) (Ref. 152); H₂O ($\Delta_1 = -176$, $\Delta_3 = -187$) (Ref. 221); NH₃ ($\Delta_1 = -170$, $\Delta_3 = -133$) (Ref. 157); and CH₄ ($\Delta_1 = -105$, $\Delta_3 = -134$) (Ref. 212). Note that the Δ_1 value for HNCO given by the RHF//RHF procedure (-151 cm⁻¹) is significantly smaller than the SQM(CCSD)+RHF//expt. result, primarily due to the increased magnitude of the underlying F_{11} force constant.
- ²⁰⁰ A. Chédin, *J. Mol. Spectrosc.* **76**, 430 (1979).
- ²⁰¹ R. B. Wattson and L. S. Rothman, *J. Mol. Spectrosc.* **119**, 83 (1986).
- ²⁰² M. Carlotti, G. di Lonardo, G. Galloni, and A. Trombetti, *J. Mol. Spectrosc.* **62**, 192 (1976).
- ²⁰³ M. E. Jacox, *J. Phys. Chem. Ref. Data* **19**, 1387 (1990).
- ²⁰⁴ V. E. Bondybey, J. H. English, C. W. Mathews, and R. J. Contolini, *J. Mol. Spectrosc.* **92**, 431 (1982).
- ²⁰⁵ I. Suzuki, M. A. Pariseau, and J. Overend, *J. Chem. Phys.* **44**, 3561 (1966).
- ²⁰⁶ D. J. DeFrees, G. H. Loew, and A. D. McLean, *Astrophys. J.* **254**, 405 (1982).
- ²⁰⁷ C. Glidewell and C. Thomson, *Chem. Phys. Lett.* **86**, 340 (1982).
- ²⁰⁸ H.-G. Mack and H. Oberhammer, *Chem. Phys. Lett.* **157**, 436 (1989).
- ²⁰⁹ D. Kivelson and E. B. Wilson, *J. Chem. Phys.* **20**, 1575 (1952). See also p. 193 of Ref. 137.
- ²¹⁰ T. Oka and Y. Morino, *J. Mol. Spectrosc.* **6**, 472 (1961).
- ²¹¹ C. A. Wight and J. L. Beauchamp, *J. Am. Chem. Soc.* **84**, 2503 (1980).
- ²¹² D. L. Gray and A. G. Robiette, *Mol. Phys.* **37**, 1901 (1979).
- ²¹³ J.-L. Teffo and A. Chédin, *J. Mol. Spectrosc.* **135**, 389 (1989).
- ²¹⁴ W. D. Allen and H. F. Schaefer III, *J. Chem. Phys.* **89**, 329 (1988).
- ²¹⁵ Y. Morino, K. Kuchitsu, and S. Yamamoto, *Spectrochim. Acta A* **24**, 3353 (1968).
- ²¹⁶ J. F. Gaw and N. C. Handy, *Chem. Phys. Lett.* **121**, 321 (1985).
- ²¹⁷ C.-F. Pau and W. J. Hehre, *J. Phys. Chem.* **86**, 321 (1982).
- ²¹⁸ T. J. Lee and A. P. Rendell, *Chem. Phys. Lett.* **177**, 491 (1991).
- ²¹⁹ H. Fleurent, W. Joosen, and D. Schoemaker, *Phys. Rev. B* **39**, 10409 (1989).
- ²²⁰ D. A. Steiner, S. R. Polo, T. K. McCubbin, and K. A. Wishah, *Can. J. Phys.* **59**, 1313 (1981).
- ²²¹ J. Pliva, V. Špirko, and D. Papoušek, *J. Mol. Spectrosc.* **23**, 331 (1967).